DISSERTATION

DEMOGRAPHIC CONSEQUENCES OF AGRICULTURAL PRACTICES ON A LONG-LIVED AVIAN PREDATOR

Submitted by

Christopher Ryan Vennum

Department of Fish, Wildlife, and Conservation Biology

In partial fulfillment of the requirements

For the degree of Doctor of Philosophy

Colorado State University

Fort Collins, Colorado

Fall 2022

Doctoral Committee:

Advisor: David N. Koons

Liba Pejchar
Bill Kendall
Randall Boone

ABSTRACT

DEMOGRAPHIC CONSEQUENCES OF AGRICULTURAL PRACTICES ON A LONG-LIVED AVIAN PREDATOR

Within this dissertation we investigate the biological and demographic aspects of the entire life cycle of a hemispheric migrant and top avian predator - the Swainson's hawk (*Buteo swainsoni*). The individual chapters progress in age-related steps from early life development to lifetime fitness metrics. Several chapters utilize individual-based data to estimate major demographic milestones (e.g., recruitment, lifetime fitness) while accounting for different sources of uncertainty, both in biological states and imperfect field observations. While the statistical and hierarchical accounting of observational uncertainty within demographic models allows for accurate inference, these models provide insight into ecological processes and are applied here to understand the influence of anthropogenic land use and agricultural habitats on Swainson's hawk demography. To do this we utilize an individual based mark-resight project from 1985-2020 on a population of Swainson's hawks breeding in an agricultural valley along the northern border of the state of California, USA.

In chapter one we build a morphometric tool for classifying the sex of nestlings. Sex determination can be particularly challenging with species that don't display external sex-linked plumage differences, have overlapping structural morphologies, and especially when examining individuals still undergoing ontogenetic development, but is a fundamental aspect to understanding organismal biology. We develop a morphological model that uses tarsus width and mass (with 91.5% accuracy) for determining sex in developing Swainson's hawks that

incorporates the natural variation among broods and hatch order status based on a custom developmental index for stunting. This morphometric tool allowed us to investigate sex-specific demography – the focus of chapter three.

Chapter two covers the development and results of remote sensing efforts to obtain habitat data relevant to nearly four decades of demographic data. Understanding land alterations motivated by agriculture is important as croplands constitute over 20% of total land in the conterminous United States. Quantifying the cumulative transitions of anthropogenic habit change is important for understanding wildlife populations co-habiting these areas, as species may be slow or incapable of adapting. Here we develop an integrated workflow design using Google's Earth Engine API platform and Program R to implement a supervised classification model using machine learning algorithms to identify crop types at the individual field level. Incorporating historical imagery we assess long-term changes in anthropogenic land use. This model is applied to Landsat imagery spanning over three decades (1985-2020) and encompasses three satellite generations (Landsat 5, 7, and 8). The supervised landcover classification model achieved an 85% accuracy rate, providing compositional and proximity characterization of Swainson's hawk territories, and showed a clear increase in irrigated alfalfa across the study period.

Chapter three uses the morphometric sexing tool developed in chapter one to examine recruitment dynamics in relation to intrinsic (i.e., size and brood) and extrinsic (i.e., territory habitat) variables. For territorial species occurring within agricultural environments, habitat alteration can occur frequently and have dramatic effects on offspring ontogeny and early life demographics. We utilize over a decade (2009-2020) of mark-resight and landcover classification data to estimate age- and sex-specific demographic rates across a range of possible

recruitment ages using a hidden multi-state model with initial state (sex) uncertainties. Females proportionally recruited at earlier ages than males, and the study population had a slight bias in favor of female offspring production. We found that large structural size, large natal brood size, and earlier hatch dates were all associated with high apparent survival for males in their first year of life after fledging, and higher chances of recruiting later in life, while later hatch dates explained increased apparent survival of females in their first year. Surprisingly, no compositional or proximity measures of natal habitat type influenced early life demographics, but we did find evidence of density-dependence in the early life demography of both sexes. Density-dependent processes could therefore be masking direct relationships between habitat and early life demographics, which are important relationships to identify for management schemes, especially in intensive agroecosystems.

Finally, in chapter four we examine the relationship between territory habitat composition, inter-annual effects of habitat on reproductive outcomes, and overall lifetime fitness. Utilizing data from 1985-2020 and tracking individually marked females across their lifespans, we estimate lifetime reproductive success (LRS) metrics of a long-lived raptor breeding within a non-stationary agroecosystem. Regardless of age, individuals that failed to reproduce in a given year experienced lower survival probabilities, a feature exacerbated by a strong probability that once an individual failed to successfully reproduce, they were likely to consecutively fail again. Results show substantial variation in LRS, with a large percentage (40.3%) of monitored females fledging four or fewer offspring over their entire life span, a quantity that can potentially be achieved in a single reproductive attempt for this species. In our attempts to examine agricultural effects (breeding territory habitat composition and proximities of nests to specific types of agricultural fields) on annual transitions between differing levels of

reproductive success, we failed to find a relationship between the measured habitat variables, including measures of population density, and therefore a lack of any relationship with LRS. Our lack of results may therefore lend more credibility to the role of stochasticity on individual dynamics and life history outcomes than differences in features of habitat selection that natural selection can act upon.

ACKNOWLEDGEMENTS

This dissertation would not have been possible without the decades of combined efforts from an uncountable number of volunteers, biologists, technicians, and private landowners. It's taken an army of people passionate about raptors to keep this project running. Over half of the nests monitored on this project exist on private land, making this project impossible without land access granted from the farmers and ranchers of Butte Valley. Special thanks in particular goes to the Prather Ranch, Don-Lo Ranch, and Red Rock Valley Ranch (which keeps changing names). Diana Engle was one of the first people I met in Butte Valley, and she continued to help and support our efforts for many years. Jim Williams has also been a long-time supporter of the project, providing housing at times and connecting us with other landowners.

The USFS Goosenest Ranger District has supported the project for decades on many different levels. During my time in Butte Valley, they provided a free space for our project trailer, and I enjoyed my time with the annual owl crews. Debra Freeling was a new biologist on the district when I started, and I was thankful for her continued support, and quite saddened when she passed recently.

Badge Run Rehabilitation, helmed by Liz Burton, was always just a phone call away. Liz and her crew successfully rehabbed several injured SWHAs from our project, and even found a home in New York for an individual that was permanently injured. The services of Ewok, Luke, Leia, Sir Hammy, Ernesto, and Champ helped us get a lot of birds marked. Loaf - you were the best!

The Butte Valley Swainson's hawk project dates it's origin back to 1979, with the first surveying and banding efforts by Pete Bloom. I appreciated the time we shared over the

summers, our discussions, and especially banding the “Airport” territory together (one of the true original SWHA territories in the valley.

Brian Woodbridge really deserves credit for laying the bedrock of this project. What I achieved and built was only possible to what came before me. Brian, Jan, and Bucho not only adopted me but opened your home to me. I still miss sitting next to the koi pond in Yreka, and Jan’s food, although the new pond in Corvallis isn’t too bad.

To my many friends who’ve supported me physically and emotional across the eight years spent working in Butte Valley thank you! My FOCO crew Abbey Fueka, Brian Avila, Audrey Harris, Nathan Han, Bennett Hardy, Emma Henslowe (I was blessed to have too many to name). My fellow “raptorpiles” Ben Dudek and Teresa Ely who made the annual pilgrimage for July banding – thank you. My fellow “Loons” and duck lab members, Kristin Ellis, Casey Setash, Mike Johnson, and Caroline Blommel – thanks for all the coffee breaks, failed and successful bird hunts, conversations, shared beers, and being all around a great bunch.

To our fearless lab leader and my advisor Dave Koons, you were always there when I needed you – something few graduate students can claim. You are truly superhuman when it comes to reviewing and editing, among many other talents. You’ve supported me without pause and made it possible for me to chase my dreams – I will always be grateful.

Kelsey Navarre you’ve been a rock and my best friend through all of this. We may have met on a rock pile, became friends while sharing a cooking yurt, and bonded over a mix of brant and tequila, but I wouldn’t have it any other way.

Chris “Senior” Briggs has had my back since day one. I still remember my initial technician interview back in 2013, from a snowy cabin at the end of highway 20. You’ve stuck with me all these years and apparently want to keep going….I can’t wait.

I have one of the most supportive families, I truly love you all, and couldn't imagine life without you. To my younger brother, Andy, thanks for putting up with my bird nerd life, and you'll be at my next job interview to negotiate salary. I blame many of my life choices and career decisions on my father Mike. You showed me the world and all it contains at such a young age and fueled my passion for wildlife – you set me on this path. To my mother Kathy, you've been there every hour I've ever needed you. Your love, energy, and support have kept me on my path and helped me achieve all my dreams- there is no better gift.

Lastly, I'd like to thank myself - it was a grind.

TABLE OF CONTENTS

LIST OF TABLES

LIST OF FIGURES

Chapter 1

PREDICTING SEX OF NESTLING BIRDS WITH MORPHOMETRICS

Introduction

In the case of dimorphic species, the larger sex requires greater investment of resources and time to adequately develop, establishing sex-linked differences early in the life cycle (Trivers & Willard 1973; Newton 1978). Understanding this dynamic is a fundamental part of avian ecology and requires the ability to accurately classify offspring sex (Sheldon 1998). However, sex determination can be particularly challenging with species that don't display external sex-linked plumage differences, have overlapping structural morphologies, and especially when examining individuals that are still undergoing biological development. The accurate discrimination of offspring sex is significant to avian research in that it allows us to establish and advance our understanding of sex-based differences in survivorship (Hernández-Matías et al. 2011), natal and breeding dispersal distances (Newton & Marquiss 1983; Newton 2001), and migration patterns (Hull et al. 2012) while broadening our understanding of life-history ecology and ideally the conservation of a species (Muriel et al. 2010; Batbayar et al. 2014). Sex-linked differences may be particularly strong across raptorial species, as most are sexually dimorphic (i.e., females are larger than males; McClure et al. 2019).

Globally, there are still many species of raptor where little is documented about life histories and basic ecology (Buechley et al. 2019). Methods for accurately measuring individual sex prior to fledging could enhance our understanding of sex-specific developmental growth rates, intra-brood dynamics, survivorship, and other key life history traits (Bortolotti 1984), attributes that can carry over into older life stages (Van De Pol et al. 2006). Assigning sex labels

at the earliest points in life, a fixed individual trait, allows for a fuller understanding of life-histories. To understand basic biology and successfully conserve raptor species, it is therefore necessary to develop a functional and cost-effective method for determining offspring sex prior to fledging. Molecular methods are commonly used to determine sex and can be necessary for monomorphic species (i.e., Cinereous Vultures (*Aegypius monachus*) Batbayar et al. 2014). While exceptionally reliable, the use of molecular genetics can be costly, difficult to perform on site (exceptions see Koch et al. 2019), and time consuming. In contrast, the use of morphometrics can be performed cheaply, is easily performed on site, and is less time consuming if a reliable sexually-dimorphic trait during development can be identified (Dykstra et al. 2012).

Within sexually dimorphic species the degree of dimorphism can vary between sexes and morphological structures, even in fully developed adults (López-López et al. 2011). This potential for morphometric range overlap is greater among rapidly growing nestlings, particularly with the added complexities of hatching asynchrony and varying brood sizes (Moss 1979). These factors tied with individual hatch order create complex interactions when sex-based differences in growth trajectory and terminal size exist (McDonald 2003). Variation in morphometric trait size can arise from multiple sources (i.e., environmental or genetic factors) and should be expected, but outliers will always exist and a means to identify these can be challenging. For example, female nestlings that hatch first versus third may obtain slightly different terminal structural size. Due to the exceptionally unpredictable nature of these effects on any one particular brood, sorting outlying individuals presents a multifaceted problem only made more difficult by the common practice of only visiting a nest once to collect data and minimize disturbance.

The timing of nest visits presents another issue as the age of nestlings during data collection is crucial, as increased age and thus development will likely influence assignment accuracy and determine which traits are useful for discrimination. For example, traits such as mass or wing length may continue to change even after obtaining the ability to fly. While "hard" morphometric structures such as tarsus size stop growing much earlier in the development process. Thus the timing of nest visitation can be influential in determining the accuracy of morphometric predictors, whereas molecular approaches are not impacted by an individual's age. Yet the utility of morphometric discriminates across life stages (e.g. nestling, juvenile, adult) is not guaranteed and may not be identical (Dykstra et al. 2012).

This study aims to develop a morphological model for determining sex in developing Swainson's hawks that incorporates the natural variation between and among broods and hatch order status. Variation across these brood dynamics can confound or impede accurate sex classification, but are not unique to this study and are expected to be issues for all related studies. Nestlings represent a life-stage with unique challenges to our goal, which can be summarized under a central analytical question, how to determine which individuals should be included in the predictive model? As brood size increases, the potential for reduced resource allocation also increases. Swainson's hawks have also shown the potential for stunting as a survival mechanism (unpublished; Vennum). Within the nestling period (e.g., hatch to flight), the potential interactions and complexities that influence sex-based development in a dimorphic species are difficult for which to account. A rapid field-based tool for classifying offspring sex of raptors, that is accurate across an entire brood, will ultimately provide value and utility.

Methods

Study Species

Swainson's hawks are a relatively common species with knowledge gaps remaining in their life history, particularly during earlier life stages prior to breeding. They are sexually monomorphic in plumage; yet like most birds of prey display reverse sexual dimorphism in physical size. All age classes undergo an annual migration to South America with the majority wintering in central Argentina (exceptions see Airola et al. 2019). Recent evidence from satellite tracking revealed that juveniles may take up to at least 5 years to recruit and are difficult to observe during this time due to nomadic behaviors (Vennum unpublished). This represents a significant period for selective forces to shape population dynamics, particularly when considering that first-year survival rates of raptorial species are low (Newton et al. 2016) and mortality rates often increase during migratory periods (Klaassen et al. 2014). For many avian species, but especially migratory ones, the developmental period prior to fledging represents the best viable period for data collection, highlighting the importance of scientific methods that improve biological inference.

Study Area

Butte Valley, California (United States) is a heterogeneous landscape (415 km^2) comprised of high elevation (1,280 m to 1,340 m) sagebrush steppe, managed wetland, and groundwater-irrigated agriculture (Woodbridge 1991). Located in Siskiyou County, California (41˚ 49'N, 122˚ 0'W) the northern study boundary parallels the California/Oregon state border and extends south to include Red Rock Valley (41˚ 45' 42''N, 121˚ 48' 22''W). Breeding Swainson's hawks (SWHA) primarily nest on the valley bottom of this arid juniper and sagebrush steppe, but higher nesting densities are associated with ground-water irrigated hay

fields (i.e., alfalfa). The dominant crop type and primary foraging habitat, alfalfa, provides consistent and high prey densities. Belding's ground squirrels (*Urocitellus beldingi*) are the dominant prey species for the first half of the breeding season, until they locally estivate in late June, after which prey composition diversifies to include pocket gophers (*Thomomys* spp.), voles (*Microtus* spp.), reptiles, small bird species, and insects (Woodbridge 1991).

General Field & Morphometric Data Collection

Genetic samples and morphometric measurements were collected across multiple years (2014, 2017, and 2018) as part of an ongoing long-term demographic study. During these years a subset of nests were visited twice to collect growth-related measurements (2015 and 2016 field protocols didn't require double entries), prior to nestlings leaving the nest. These included nestling mass (grams), lengths of several hard structures (tarsus width, tarsus length, footpad, culmen, hallux), and lengths of soft structures (unflattened wing cord, 7^{th} primary, and tail length). Definitions of each measurement are provided in (Ch.1) Appendix A. Project guidelines delay nest visitation until offspring reach at least three weeks of age to reduce the probability of nest abandonment by parents. This minimum age of three weeks also represents the youngest age at which bands can safely be fitted to nestlings, a natural starting point to examine the ability to distinguish nestling sex in the field.

All nestlings were fitted with a United States Geologic Survey aluminum band during the first nest visit and a unique alphanumeric color band upon the second. During the second nest visit developing pin feathers were collected for the purpose of DNA extraction and molecular sexing. Nestling age at time of all sampling ranged from 21-44 days old. We purposely sampled nestlings as young as 21 days old as this is generally the youngest age bands can be safely attached, allowing us to examine how classification accuracy changed with age. Our two nest

visit study design divided our repeated measure samples into two age groups, a younger age class of 21-30 days old and an older 32-44 day old class. The natural growth pattern of feathers for Swainson's hawks leaves the head for last with pin feathers typically becoming visible at 32 days of age (Gossett & Makela 2005). This biological age feature corresponds well with our two age classes and represents the easiest feature to observe when trying to age nestlings from a distance, prior to nest visitation. Field protocols were therefore established to visit each nest before and after this "32 day" age mark. Although fledging age can vary by a few days, we assume mean fledging age was 45 days of age (Bechard et al. 2020).

This study was conducted as part of a long-term, multi-decadal mark-resight project on the breeding ecology of SWHA. As a benefit from prolonged data collection, a secondary 11-year (2009-2019) dataset of color-banded nestlings that survived the juvenile stage and were observed again as recruited breeders into the study population was available. These individuals were measured only once, but overlapped in age with our "older" group when measured, providing a non-overlapping validation dataset (hereafter, "recruited" dataset).

Genetic Analysis – DNA Collection and Extraction

Three developing feathers were plucked from each nestling's breast between 32-44 days of age, and generally contained visible blood vessel(s) in the field at time of collection. Feathers were stored in individual envelopes at room temperature (24° C) for up to five (2014-2019) years before extraction. Genomic DNA was extracted from one dry breast feather per nestling (n=82). A 5mm piece from the tip of the calamus was removed, cut lengthwise and then one half was used for extraction. We extracted feather samples using the DNeasy Blood and Tissue Kit (Qiagen), according to manufacturer protocol, but with the following modifications to increase yield: (1) added a total of 40ul proteinase K to each sample during digestion, (2) extended

digestion time to 48hrs at 56° C, and (3) eluted DNA into 100ul AE buffer (instead of 200ul), to increase DNA concentration. We extracted feathers in batches of ~24, with a negative control included for each batch to detect any contamination. We assessed the DNA quantity in a subset of samples (n=5), including the oldest and newest feathers collected, using Qubit Florimeter HS reagents. DNA quantities ranged from 3.6-14.1 ηg/μl, a sufficient quantity to proceed with PCR amplification.

Molecular Sexing

Molecular sexing of all nestlings was conducted by polymerase chain reaction (PCR) amplification of sexually diagnostic CHD1 alleles, using 2550F/2718R primers (Fridolfsson & Ellegren 1999). Reactions were amplified in volumes of 25μl, using 2μl template DNA, 0.25 μl each F and R primers, 22.5 μl water, and one Illustra PuReTaq Ready-To-Go PCR bead (GE Healthcare Life Sciences, Marlborough, MA, USA) per reaction. Negative extraction controls were amplified alongside nestling samples. We used PCR conditions as outlined in Woolaver et al. (2013): first, a 2-min denaturing step at 94° C; 30 cycles of 30 sec at 94° C for denaturing, 30 sec at 50° C for annealing, and 30 sec at 72° C for extension; and last, a final 5 min extension at 72° C. For a subset of samples that did not amplify the first time, presumably due to low starting concentrations of DNA, we used a nested protocol. For these reactions, we repeated the PCR conditions above, but with 2 μl of PCR product instead of template DNA for the nested amplification round.

Amplified CHD1 alleles were visualized on 2% agarose gels, stained with 10ul GelRed Nucleic Acid Gel Stain (Biotium, Inc., Hayward, CA, USA), under ultraviolet light. At least one negative control was included on each gel; none of the negative controls yielded detectable amplification. From our recruited dataset of known-sex individuals we used six individuals of

(n=3 males, n=3 females) to confirm that our CHD1 amplification generated 1 band for males (ZZ) and 2 bands for females (ZW). All six correctly amplified. Male Swainson's hawks showed a single band at ~600bp, while female Swainson's hawks showed the 600bp band plus another at 450bp. Allelic dropout can be a problem in DNA samples with low starting quantities, and would cause us to mis-assign females (2 bands) as males (1 band). We checked for allelic dropout by re-running 10 males - all males were confirmed.

Biological Outliers

Central to the development of an effective field-based tool is a protocol that outlines the age and developmental ranges that can be accurately incorporated. While we acknowledge that increased nest visitation (i.e., greater than two) would provide the clearest understanding of growth trajectories, most morphometric sex-predictor studies appear to only perform a single nest visit. We combined two methods for identifying biological outliers, one method that can be used if only a single nest visit is possible and a second option for repeated nest visits. Individuals were excluded from the analysis if growth (i.e., change in mass) between the two visits was negligible, a simple but useful means if multiple nest visits are performed. For single nest visit studies, however, we suggest the application of a "development index." This index is as follows. Swainson's hawk nestlings hatch between 1-2 days apart (Fitzner 1980), thus feather development should lag accordingly as one examines nestlings from oldest to youngest within a brood. To produce our development index score we aged all nestlings using a photographic guide and feather development (Gossett & Makela 2005). An individual nestlings' score is simply its assigned age subtracted from the age of the oldest nestling. For example, in a three brood nest under ideal conditions we'd expect the development index for each nestling to be: oldest (0 days), middle (-1 or -2 days) and the youngest (-3 or -4 days, see Appendix A). Individuals that exceeded this (i.e., have larger negative index values then expected by rank in nest) were

excluded as their score indicates outward physical signs of abnormally slow or reduced development (i.e., stunted). These two benchmarks for exclusion provide biological reasoning for studies that conduct multiple visits and those that do not.

Statistical Analysis

All plotting and statistical analyses were conducted in R v. 4.1.0 (R Core Team 2021). Initial plotting of morphometric trait data revealed that all soft structures, unflattened wing cord, 7th primary, and tail length(s) were still growing at the time of fledging (45 days old). These structures overlapped completely between the sexes and were thus excluded from the analysis as no discriminatory power existed (Ch.1 Appendix B). The remaining five variables included in our predictive model were: tarsus length, tarsus width, hallux, culmen, and body mass. All predictor variables were evaluated for multicollinearity using Pearson's correlation analysis, for normality with Shapiro-Wilk tests, and for homogeneity of variance using the Fligner-Killeen test (R package *stat,* R Core Team 2021). No data transformations were required and all predictors were standardized (mean = 0, s.d. = 1). Additionally, we tested for multivariate normality with the Shapiro-Wilk Multivariate Normality test (R package *mvnormtest*, Jarek 2015) and checked for multivariate outliers by calculating Mahalanobis distances (R package *stat,* R Core Team 2021). We evaluated differences in morphometrics between the two age groups using a two-way multivariate analysis of variance (MANOVA). These two age groups represent approximate development stages of 50-70% and 70-100%, with the latter group containing the 80% development point that is commonly applied in raptor demographic studies as a reliable milestone, where one can assume an individual will successfully fledge from the nest. The morphometric data for the "recruited" dataset was compared against the older group for statistical differences using a MANOVA. We combined all three years of morphometric data,

ignoring year-to-year variation, as we felt this variation was necessary for developing an effective classification scheme that incorporated annual environmental variability. In addition to our five main predictors we felt obligated to examine the predictive power of footpad length, as it is commonly included in related studies. However, this metric was only collected in 2017 and 2018 reducing the sample size (n = 57), so we generated separate models for this reduced dataset. Overall classification models were built using two different statistical approaches following related studies; recursive partitioning (Dykstra et al. 2012) and linear discriminatory function analysis (DFA; Pay et al. 2021).

Recursive partitioning is a statistical method for incorporating multiple variables, classifying, and splitting samples into subgroups in a dichotomous manner (Strobl et al. 2009). Our recursive partitioning tree was generated with the *rpart* package v 4.1-15 (Therneau et al. 2019). Our comparative and second statistical analysis, a stepwise DFA, was performed using the *klaR* package v 1.7-0 (Roever et al. 2022). This stepwise procedure identified the minimum number of predictors, where inclusion or removal of a parameter for classification improvement was based on a significance level of 0.05. We validated the resulting stepwise model, our global model that included all predictors, and all morphometrics in singular form using a leave-one-out (jack-knife) procedure to produce posterior assignment probabilities and model accuracy scores (Pay et al. 2021). Summary statistics for each measurement and computed values of dimorphism between sexes were calculated as $100*[(X_{male}/X_{female}) - 1]$ (Krüger 2005). Finally, confidence intervals on assignment were calculated using a bootstrapped leave-one-out model (Hartman et al. 2016).

Results

For the older age group both statistical methods (i.e., recursive partitioning and linear discriminatory function analysis) identified the same morphometric predictors as best discriminating between the nestling sexes, specifically tarsus width and mass. Of the 82 nestlings included in the older age group 36 were scored male (ZZ) and 39 as female (ZW) correctly, with 7 individuals (3 males, 4 females) individuals being misclassified. Both methods generated the same overall accuracy of 91.5% (DFA, CI 0.83-0.96; Figure 1-1B.). For this older age group, a two-tiered tree for weight and tarsus width was generated (Figure 1-1A.), with morphometric cutoffs greater than 820g (mass) and 9.4mm (tarsus width) indicating female, with males below these values. The alternative older age model that included footpad length, with a reduced sample size (n=57) produced the same result as our primary model. Mahalanobis distance values identified no multivariate outliers for the older age class.

Our classification results for the younger age class (n = 76) did not match between statistical methods, as occurred with the older age group. The stepwise DFA identified tarsus width as the sole and best predictor with an overall accuracy of 76.3% (f=8, m=10; CI 0.65-0.85; Figure 1-2B.), with 18 individuals being misclassified. This contrasts with the recursive partition analysis where only 10 individuals were misclassified (f=8, m=2) and an overall accuracy of 86.8% (f=31, m=35 correct). The recursive partition determined that a three-tiered tree including weight, tarsus length, and culmen as the best predictors (Figure 1-2A.). Mahalanobis distance values identified no multivariate outliers for the younger age class as well.

The recruit dataset (n=103; male = 52, female = 51) originally planned for validation procedures, consisted of individuals marked as nestlings between 2009-2019. However, t-test comparisons showed that the recruited individuals were structurally larger as nestlings than the

random PCR sample. Weight did not differ between recruited females (Mean= 897g SD=80g) and those from our randomized PCR sample (Mean=877g, SD=83g, $t(88) = -1.19$, $p = .236$), however between recruited males (Mean = 744g SD = 61g) and non-recruited males (Mean=717g, SD=67g, $t(78) = -1.98$, $p = 0.050$) there was a difference. In addition, tarsus width was different between groups with recruited females (Mean = 10.02mm SD = 0.63mm) being larger than non-recruits (Mean=9.65mm, SD=0.55mm, $t(91) = -3.02$, $p = .003$) and recruited males (Mean=9.12mm SD=0.46mm) being larger than non-recruits (Mean=8.72mm, SD=0.47mm, $t(80) = -4.10$, $p < .001$). Mean age at time of measurement were identical (recruit=37.75days, PCR=37.76days) between groups. These differences show a morphometric size bias between nestlings known to survive and those never observed again.

Discussion

We determined that it is possible to accurately distinguish the sex of nestling Swainson's hawks to a reasonably young age with utility for field-base studies. Results from two different statistical approaches both identified tarsus width and mass as the best combination of morphometric predictors for our older age class. That individuals from our recruited dataset are structurally larger (females = 3.69%, males = 4.39%; tarsus width) than our random sample of nestlings is not surprising given larger offspring have been shown to have greater juvenile survival rates across avian taxa (passerine, Magrath 1991; waterfowl, Sedinger et al. 1995; raptors, McDonald et al. 2005) and are thus available to recruit. It is possible that increased structural size provides an advantage in regard to intrasexual competition for territorial space and vacancies, providing an additional selective force that could have shaped our dataset of recruited individuals. Determining an appropriate methodology for whether an individual should be included in our predictive model set required two nest visits, something many studies don't

perform, and an overall means of identifying brood quality. The creation and use of our development index was a biologically minded means to include nestlings of different rank within a brood. Our goal was not to determine morphometric cutoffs for the best and oldest offspring, but a predictive model that incorporates some developmental variation and could predict the sex of younger brood mates. Future studies should consider that demographic mechanisms may shape the morphometrics of different age classes, in addition to a species' general development and dimorphism.

In comparison to nestlings, adult or fully developed Swainson's hawks exhibit greater dimorphism in wing chord (mean = -6.35%; mean = -6.92%; measurements provided match order of citations) and tail length (mean = -7.58%; not provided), while mass differences remain similar to nestlings (mean = -17.8%, mean = -23.9%) (Sarasola & Negro 2004; Kochert & Mckinley 2008). These differences in relative size dimorphism are double of nestlings (-3.58%) in the case of wing chord, and 7.5% greater dimorphism for tail length (Table 1-1). While these two studies don't provide tarsus width measurements, the similar differences in mass become apparent when visualizing our pseudo-growth trajectories for each sex (Ch. 1 Appendix C). We specify pseudo-growth as two visits limit us to linear trajectories yet avian growth rates are generally not linear (Ricklefs 1968). The fitted lines we included in our figures are based on polynomial/exponential curves, given this assumption (Ch.1 Appendix C.). While our two visits limit use to directly drawing a straight line, a crude evaluation of growth, we attempted to overcome this by obtaining a large sample size and creating an approximate growth curve for SWHA based on all individuals measured. Our ability to perform just two nest visits was enough to ascertain that certain morphological structures show little or no dimorphism during development and thus provide no insight into how growth varies between the sexes.

Unique to only studies involving developing nestlings, our data clearly show that soft (i.e., feathers) morphometric structures such as length of wing cord, 7th primary, or tail are not fully developed prior to fledging with no differences between the sexes (Ch.1 Appendix B). In studies involving adult birds, that have obtained full maturity and size, soft structures such as wing chord and tail length can be diagnostic and thus afford more points of discrimination. Hard structures that complete growth early in development (i.e., tarsus width) are vital to nestling classification. Thus the best metrics for predicting sex in adults may not be the same used for assigning sex to nestlings and certain features once fully developed might be more diagnostic and easier to measure. For example, measuring wing cord may be easier to reliably measure and take less experience than measuring length and width of the tarsus bone. It should also be noted that more than one correct method/model for assigning sex may exist for a single species. This is the case for determining sex in adult Swainson's hawks where a 93.3% overall accuracy was obtained using Forearm + Tail + Wing (Sarasola & Negro 2004) and a different study obtained 99.2% overall accuracy with Mass + Wing + Foot (Kochert & McKinley 2008). A useful review across different raptor families (i.e., Accipitridae, Cathartidae, Falconidae) would elucidate any trends in common morphometric structures that best identify sex across different age classes and levels of dimorphism, and could provide a useful first step to future work on species with no scientific documentation.

For many species of raptor the period from fledging to recruitment is often unobservable and can last for several years, particularly for migratory and long-lived species. Maximizing information collected during the nesting period is crucial. In the case of Swainson's hawks this juvenile phase can last up to at least five years (Vennum 2017). Thus, only about a three-week period, from the age that bands can be safely applied (21 days) to fledging (45 days of age on

average) is ideal for collecting information prior to the extended juvenile period. This juvenile phase represents a period with significant mortality, initial independence from parental care, the first migration, followed by potentially several years of nomadic existence (Watson 2021). It should not be surprising that a structure such as tarsus width, emerged with discriminatory power, given that we know it reaches almost full size by 21 days of age and allows for banding to occur. Given the complexities of nestling development, we tried to examine morphometric predictors across this entire crucial period of approximately three weeks. While our study preferentially aims to color band nestlings at or after 36 days of age (80% development; Steenhof 1987), we realize that other studies may not be able to control the timing of banding so specifically, and thus understanding what useful information can be collected at younger ages is important.

Unsurprisingly, sex assignment accuracy is highly and positively correlated with nestling age. We found that misclassification increased in our younger age group. Our statistical approaches also identified different morphometric predictors for the younger age class. Recursive partitioning identified a three-tier model with mass (706g), tarsus length (60mm), and culmen (17mm) while stepwise DFA selected only a singular predictor, tarsus width. They also varied in their accuracy, 86.8% for recursive partition (4.7% drop) and 76.3% for DFA (15.2% drop). There are many benefits to collecting data on older rather than younger nestlings, including increased confidence in fledging success and clearer understanding of brood dynamics. Thus banding nestlings at younger ages has a limited value compared to what can be gained closer to fledging ages when dimorphic differences have increased.

Very few studies describe how they chose which individuals to include in their analysis. Dykstra et al. (2012) uses average length of secondary feathers to classify individuals as young

or older nestlings. Future studies, regardless of species, would be improved by disclosing such information. The decision to include an individual nestling into the training data set is not trivial, when considering many factors can impact growth trajectories (e.g., too many siblings, inexperienced parents, poor natal territory quality, or climatic factors). For this study we examined growth differences between two visits and utilized a development index to determine which individuals to include. Ideally, more than two visits are necessary to adequately capture growth dynamics. Future studies should incorporate or at least discuss some metric for determining inclusion. While our original study plan attempted the use of a secondary dataset for validation purposes, a dataset from a different SWHA population would have been the best possible option. These approaches often divide datasets into smaller training and testing groups (i.e., splitting), and use resubstitution; techniques that can reduce sample size further or result in higher variance (Dechaume-Moncharmont et al. 2011).

Globally there are numerous species of raptor without published information on morphometrics to distinguish basic ecological components such as nestling sex. Collection of basic ecological data is still necessary. Such data represent the basics for studying population dynamics, life history decisions and trajectories, and can provide information on natal habitat and parental quality. We need more studies actively collecting and publishing basic morphometric data. There is already evidence that many avian species are getting smaller (Weeks et al. 2020), and that climatic factors could be causing this. If such processes are already taking place we need basic biological data as reference points so that it is possible to detect changes over time. Accurate sex assignment of offspring can inform on several key demographic processes (i.e., brood sex ratios, measures of fecundity, juvenile survival). It provides important information on pair quality and habitat characteristics, as greater production of females, the more

costly yet valuable offspring to produce, requires greater resources. Lastly, from a natural history standpoint the ability to accurately assign sex of offspring expands our knowledge.

Table 1-1. Morphometric data for Swainson's hawk nestlings hatched in Butte Valley, California and collected across multiple years (2014, 2017, and 2018). Measurement ranges (mean, standard deviation) and percentage dimorphism provided across sex and age classes. Young age class represents nestling between 21-30 days old, with the old age class comprised of 32-44 day old nestlings.

Measurement	Young Females Mean ± SD (n = 43)	Young Males Mean ± SD (n = 39)	Young Dimorphism %	Old Females Mean ± SD (n = 43)	Old Males Mean ± SD (n = 39)	Old Dimorphism %
Mass (g)	720 ± 127	624 ± 66	-13.27	877 ± 83	716 ± 67	-18.27
Tarsus Width (mm)	9.39 ± 0.68	8.57 ± 0.52	-8.77	9.65 ± 0.55	8.72 ± 0.47	-9.64
Tarsus Length (mm)	63.39 ± 5.96	62.74 ± 4.27	-1.04	70.47 ± 2.82	67.07 ± 2.33	-3.92
Hallux (mm)	19.14 ± 1.56	17.74 ± 2.02	-7.36	22.08 ± 0.88	20.28 ± 0.95	-8.14
Culmen (mm)	18.01 ± 1.22	16.72 ± 1.18	-7.13	20.26 ± 0.91	18.81 ± 0.81	-7.17
Footpad (mm)	77.06 ± 4.47	71.67 ± 3.69	-7.00	79.63 ± 2.85	73.92 ± 2.08	-7.17
Unflattened Wing Cord (mm)	162 ± 32	163 ± 24	0.55	261 ± 23	252 ± 27	-3.58
7th Primary (mm)	87 ± 24	88 ± 20	0.92	173 ± 19	172 ± 24	-0.89
Tail (mm)	49 ± 18	51 ± 15	3.20	115 ± 20	115 ± 19	-0.16

Table 1-2. Evaluation of linear discriminatory function models containing different combinations of morphometric predictors. Associated model accuracies are provided for an overall classification rate and sex-specific (CI; confidence interval). Young age class represented by nestling between 21-30 days old, with the old age class comprised of 32-44 day old nestlings.

Older Age Class		Percent Correctly Classified			
Variable	N	Females	Males	Overall	CI
(Global) Mass + Tarsus Width + Culmen + Hallux + Tarsus Length	82	93.0	94.8	93.9	0.86-0.98
(Stepwise) Mass + Tarsus Width	82	88.4	94.8	91.5	0.83-0.96
Tarsus Width	82	81.4	82.1	81.7	0.72-0.89
Culmen	82	74.4	74.4	74.4	0.64-0.83
Hallux	82	83.7	84.6	84.1	0.74-0.91
Tarsus Length	82	76.7	71.8	74.4	0.64-0.83
Mass	82	88.4	84.6	86.6	0.77-0.93
Footpad	57	79.3	92.9	85.9	0.74-0.94

Younger Age Class		Percent Correctly Classified			
Variable	N	Females	Males	Overall	CI
(Global) Mass + Tarsus Width + Culmen + Hallux + Tarsus Length	76	74.4	81.1	77.6	0.66-0.86
(Stepwise) Tarsus Width	76	79.5	72.9	76.3	0.65-0.85
Culmen	76	76.9	64.9	71.1	0.59-0.81
Hallux	76	79.5	51.4	65.8	0.54-0.76
Tarsus Length	76	64.1	32.4	48.7	0.37-0.60
Mass	76	64.1	78.4	71.0	0.59-0.81
Footpad	57	68.9	78.6	73.7	0.60-0.84

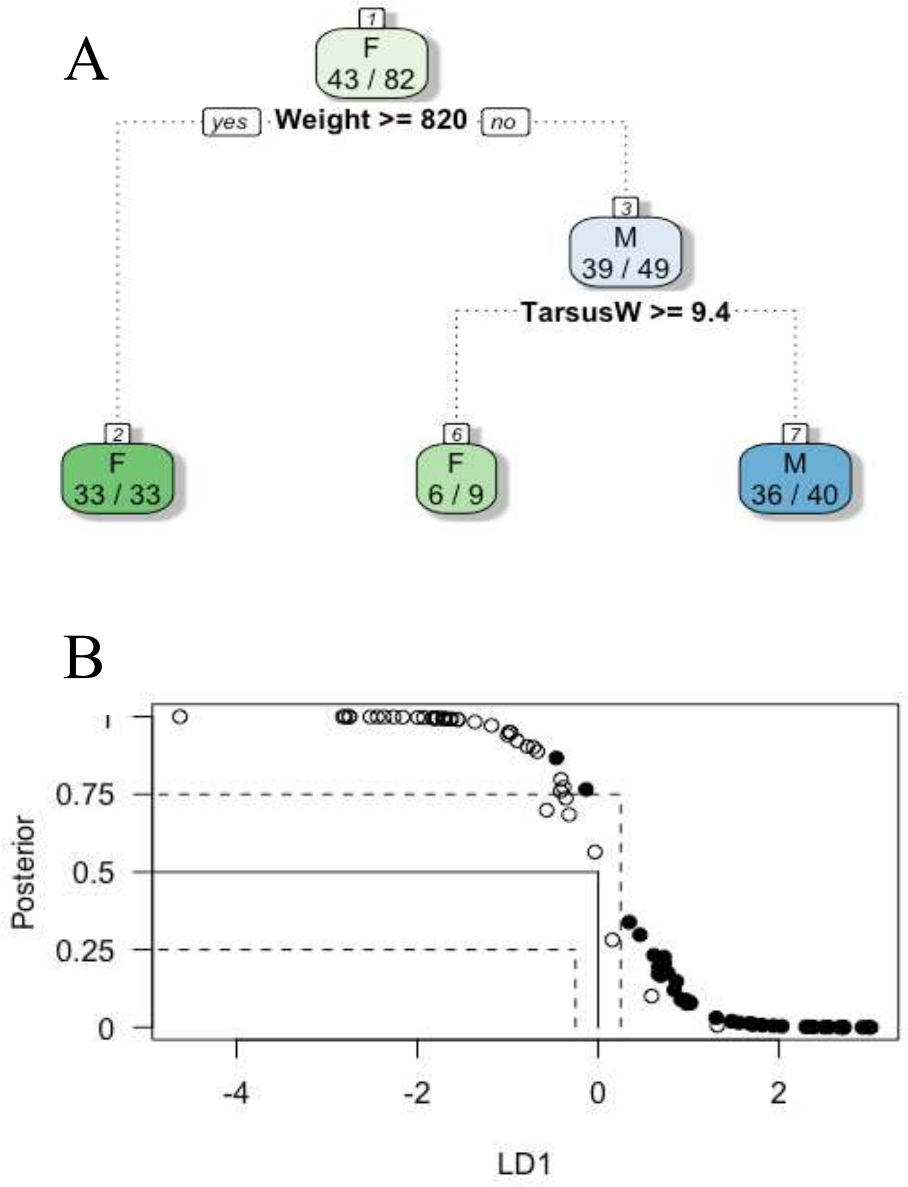

Figure 1-1. Morphometric discrimination of nestling Swainson's hawk from Butte Valley, California between the ages of 32-44 days old. (A) Recursive partition tree of older nestlings with the morphometric cutoffs applied. (B) Plot representing the probability of being classified as male (dark circle) or female (open circle) based on linear discriminatory function analysis of older nestlings. The solid line represents a discriminant score of zero and the probability of being male or female is 50%. Area with dashed lines (0.25-0.75) indicates the range of discriminant scores where the probability of correct assignment is < 75%.

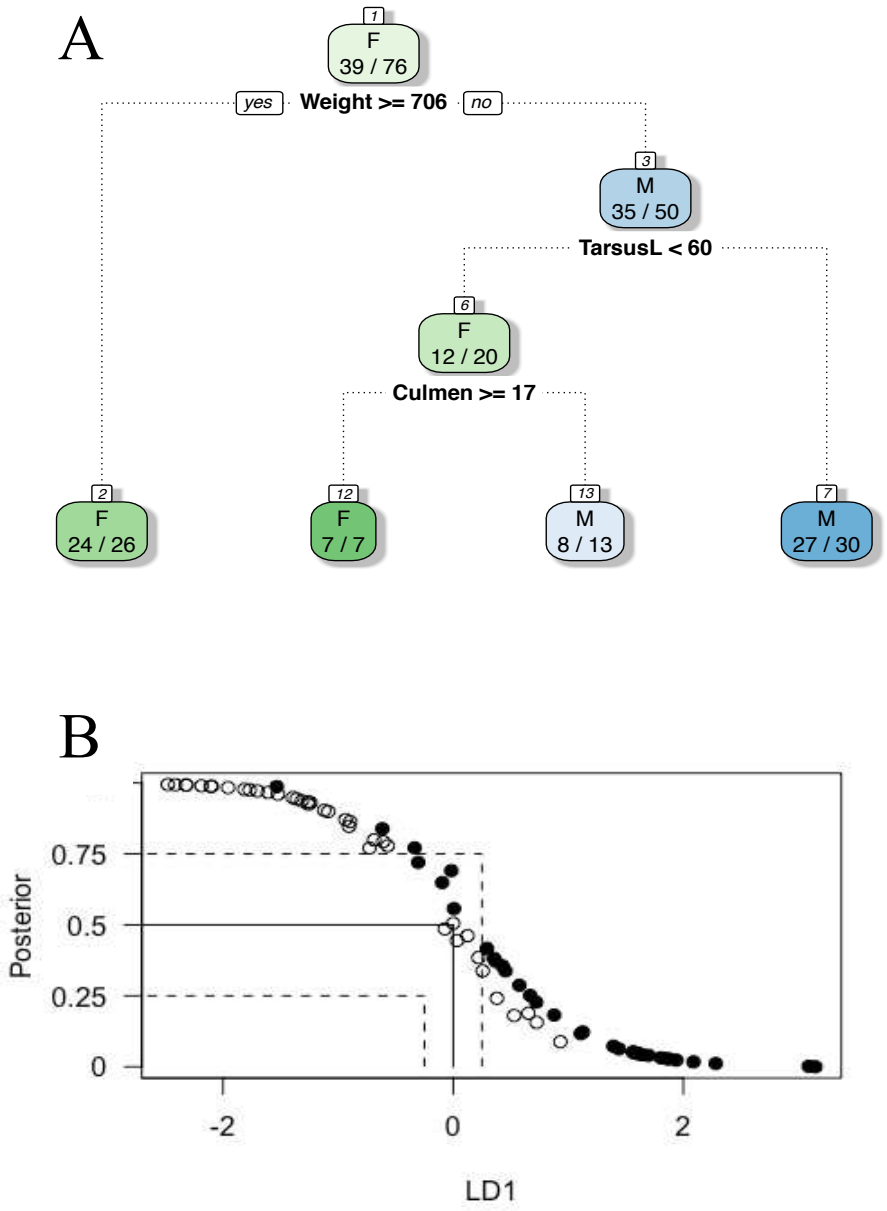

Figure 1-2. Morphometric discrimination of nestling Swainson's hawk from Butte Valley, California between the ages of 21-30 days old. (A) Recursive partition tree of "younger" nestlings with the morphometric cutoffs applied. (B) Plot representing the probability of being classified as male (dark circle) or female (open circle) based on linear discriminatory function analysis of older nestlings. The solid line represents a discriminant score of zero and the probability of being male or female is 50%. Area with dashed lines (0.25-0.75) indicates the range of discriminant scores where the probability of correct assignment is < 75%.

Chapter 2

DEVELOPING A SUPERVISED RANDOM FOREST CLASSIFICATION MODEL FOR MONITORING HISTORICAL CHANGES IN HUMAN AGRICULTURE AND ASSOCIATED HABITAT FOR NESTING BIRDS

Introduction

The history of agriculture has had multiple origins across the space and time of modern human existence, but has grown to such a state that it is now a defining feature of the current epoch – the Anthropocene (Lewis & Maslin 2015). Human-induced changes (e.g., land-conversion, changes in atmospheric chemistry) are now at a global scale with profound effects on ecosystem function and biodiversity of the planet. Agriculture, through direct (e.g., habitat conversion) and indirect (e.g., pesticides, fertilizers) factors is the largest contributor to biodiversity loss (Dudley & Alexander 2017), yet even more land will need to be appropriated for agricultural use in the future (Tilman et al. 2001). The cumulative effects of such landscape transitions and processes leading to species declines can be difficult to comprehend given the scale and complex nature of this problem, yet we can quantify the physical presence and intensity of agriculture on the landscape.

The availability of aerial imagery coupled with advances in technological platforms for analyzing "big data" with high computational speeds has made this quantification possible. Specific crops can be remotely identified, the dynamic nature and phenology of seasonal food production observed, and the physical space allocated to agricultural production can be measured. Through remote sensing technologies we can determine the scale and intensity of agricultural practices from the smallest fields to regions, and even countries. For some parts of the globe we can examine these exact dynamics across previous decades.

The dominance of agriculture across the terrestrial biome requires that we understand the impact of agriculture at a global scale to preserve room for nature and maintain the integrity of biological processes. The designation and protection of land solely for the preservation of nature is vital to conservation, but agricultural supply and the demand to feed a global population of 9 billion means that we must address conservation issues of working lands (Polasky et al. 2007). This need has sparked a recent debate in the scientific literature as to how we can balance the economics and production of food with nature present, a debate framed between "land sparing versus land sharing" (Fischer et al. 2014). Land sparing holds that through increasing agricultural intensity, less land will be required, allowing areas to be spared from conversion (Green et al. 2005). While land sharing would lower agricultural intensity and be designed to incorporate nature into the same space, a level where crop production can exist within the natural matrix of the environment and thus preserve biological processes and ecosystem services (Kremen & Merenlender 2018). However, it is becoming evident that neither of these two land use schemes can be applied universally. Differences in aridity and the way in which irrigation occurs varies greatly even at small spatial scales, requiring agricultural policies flexible enough to incorporate local dynamics.

While these land use frameworks are important for implementing policy, they still require an innate understanding of how native wildlife species interact and use agricultural crops. This interaction must be explored over time, due to the dynamic nature of agricultural practices and complex stochasticity often found in ecology processes. To understand species habitat interactions, we must first have accurate models of landcover classes. The USDA National Agricultural Statistics Service annually produces a cropland data layer that currently distinguishes 254 crop types across the contiguous United States. The CropScape database is

publicly available and provides spatial data down to individual agricultural fields, at 30m resolution, and enables a nationwide perspective on annual crop production and trends (USDA NASS 2022). However, we found significant inaccuracies within this database when examining agricultural fields within northern California and the area surrounding a long-term study of Swainson's hawks. Assuming many of these inaccuracies represent small areas, the effect on analyses of national production and trends is likely negligible, however for studies with small spatial scales seeking to understand local ecological processes, these inaccuracies may be too large and inject substantial biases into scientific inference.

Our objectives were therefore to create a remotely sensed image library dating back to 1985, construct a supervised classification model that incorporates local crop phenology and farming practices, and to produce metrics of landcover class abundance and proximity in relation territorial boundaries of a top avian predator. To achieve this, we used remote sensing technology housed within Google's Earth Engine platform to develop a supervised random forest classification model.

Methods

Study Area

Butte Valley is an agricultural valley (41˚ 49'N, 122˚ 0'W; 415 km^2) located in the northern most extent of California, U.S.A., and adjacent to the southern border of Oregon (Figure 2-1). State boundaries and the physical topology of this area influence long-standing water use practices and historic legal rights, that have shaped the history of agricultural production locally. Unlike major agricultural areas to the north (i.e., Klamath Basin), which often use flood irrigation, Butte Valley relies almost entirely on ground water-based irrigation. Located

at medium elevation (1,280 m to 1,340 m) the native landscape was comprised of sage-brush steppe, intermittent surface water, playas, with scattered juniper woodlands. The proliferation of ground-water wells and center pivot irrigation has led to a heterogenous landscape divided into irrigated agricultural, rainfed farming, and shrub-steppe mixed with exotic grasses.

Based on our local knowledge of landcover types from monitoring Swainson's hawk (SWHA; *Buteo swainsoni*) nests, we pre-determined the potential landcover types that were represented in our study system and that we desired our model to identify. Agricultural land could be grouped into several exclusive categories, including irrigated hay and grasses (i.e., alfalfa, timothy hay), dry land or rain feed cereal grains (i.e., wheat, rye), and row crops (i.e., strawberries, potatoes). One non-mutually exclusive category, bare dirt, while mostly associated with agriculture and crop rotation or periods of re-planting, could occur naturally. Two natural habitat types also occur, high-elevation sage-brush steppe and mixed grassland, and juniper woodlands. The majority of this more naturally occurring sage-brush steppe grassland occurs within the Butte Valley National Grassland and disjunct parcels of government owned land. The juniper woodlands, while mostly on private land, often outline agricultural field edges and offer abundant nesting structures for SWHA.

During the 2018 and 2019 field seasons, the entire study area was mapped at the spatial scale of individual agricultural fields. The crop type or status, in the case of fallow fields, was identified and recorded. This data was then digitized through hand-drawn polygons in Google's Earth Engine to create customized landcover layers for these years. With respect to the variety of row crops and dryland cereal grains grown within the study area, each were aggregated into respective landcover classes. Thus, our row crop layer included fields of strawberries, potatoes, garlic, and carrots. This aggregation was based on the biological assumption that all row crops

and all dryland cereal grains offer similar biological conditions to SWHA (e.g., habitat for small mammal prey). All areas of interest were classified into our six landcover types of interest, representing our ground-truth observations for building and testing the predictive accuracy of our model (see below).

Image Library

The historical range and consistent resolution of aerial imagery collected by the Landsat system allowed us to develop an image library that matched the longevity of our demographic study. This was achieved through the combined use of Tier-1 Landsat 5 (1985-2011), 7 (2012), and 8 (2013-2020) imagery. All satellites generate 30m resolution data. Although the quality of imagery and atmospheric corrections is not equal between Landsat 5 and Landsat 8, Landsat 5 images still provide enough accuracy to identify distinct landcover types. On an annual basis, images were temporally constrained between April-October, as weather during the boreal winter often creates high percentage cloud cover or snow coverage. Outside of this standard time constraint a few years required additional temporal censoring due to obstructions such as late snow melts, typically in the 1990s-early 2000s, and occasionally smoke from local forest fires. This was performed through visual inspection of individual images and allowed us to accurately represent the natural growing periods of vegetation on a local and annual scale. Images were inspected for small visual obstructions (i.e., clouds and shadows) and when necessary, we selectively removed single images from the composition or applied an image masking function for clouds and shadows using the QA_PIXEL Landsat band.

From this completed image library, we examined spectral image charts to determine the best time periods for defining distinct phenological seasons whereby different crops could be distinguished based on their individual growing patterns. Certain crop types present different

spectral signatures throughout the year, requiring an understanding of crop phenology and harvest practices to adequately classify through spectral signatures. For this region, irrigated alfalfa has the earliest start to the growing season (high near-infrared spectral values all year; Figure 2-2a) and routinely undergoes three harvests throughout the year. From an aerial perspective, a row crop field is mostly dirt in early spring, as plants are small, obtaining adequate biomass to be detected via remote sensing much later in the year (low near-infrared spectral values in spring; Figure 2-2b). While dryland cereal grains may present different spectral colors early in the year, all crops of this type have a distinctive fall period, where they must desiccate prior to harvest, presenting a distinct spectral signature. Areas of shrub-steppe and mixed grasses (e.g., Butte Valley National Grassland) show very homogenous spectral signals across the entire year, compared to crops (no spectral peaks; Figure 2-2c). Thus, we partitioned annual satellite imagery into three "seasons" to better match vegetative phenology and increase our predictive accuracy. The spring signature was based on images from April and May, summer from June-August, and the fall signature was defined with September and October images. As "season" images are composites of multiple aerial images we extracted the median pixel value for a season from the assigned image collection, resulting in three spectral values for annual classification.

Spectral Components

Landsat satellite sensors measure the intensity of several different wavelengths, known as the relative spectral response (RSR), where different wavelengths are represented by different channels or bands. Amongst the different wavelengths measured, six raw wavelengths (hereafter; bands) are relevant to modelling terrestrial vegetation. These raw spectral bands include BLUE (0.45-0.51), GREEN (0.53-0.59), RED (0.64-0.67), NEAR INFRARED (NIR; 0.85-0.88), SHORT-WAVE INFRARED 1 (1.57-1.65), and SHORT-WAVE INFRARED 2 (2.11-2.29). In

addition to using these raw spectral band values for predictive purposes we used two spectral index metrics, the normalized difference vegetation index (NDVI) and a soil-adjusted vegetation index (SAVI).

$$NDVI = (NIR-RED)/(NIR+RED)$$

$$SAVI = 1.5 * ((NIR - RED) / (NIR + RED + 0.5))$$

Values for these combined 8 spectral metrics (six raw bands, two indices) were extracted for each season (3). Thus, we initially started with 24 mean spectral values (hereafter "seasonal-bands") per year for classifying habitat types.

Spectral Qualities of Landcover Types

Our image library division into three seasons captured large scale phenological differences, however variation in farming practices produce finer scale differences that our seasonal division could not capture. Farming practices, such as the use of plastic to cover row crops (i.e., strawberry plants) early in the growing season create unique spectral signatures only in spring months. A signature that enabled us to classify row crops more accurately by modelling them separately (plastic vs non-plastic) and merging pixel types in Program R post classification. This same justification was used to model and classify two distinct vegetative types found primarily across the Butte Valley National Grassland. Two distinct "grassland classes" which were present across the study area (dark: big sagebrush (*Artemisia tridentata*) and rabbitbrush (Chrysothamnus spp.); light: open xeric and sparse exotic grasses) were modelled separately but combined in the final raster classification files. Overall, we identified six main landcover types that were most accurately modelled by defining eight unique spectral classes as it allowed us to incorporate our decades of local knowledge into the modelling process.

Variable Selection

To determine which seasonal-bands (24) were truly important for classifying landcover types and reduce the correlation between some spectral bands we performed a variable selection analysis in Program R. From our digitized "2018 ground truth" layer we extracted spectral values of representative points (84 average per landcover class; 672 total points) from each habitat type. Using the vsurf package (Genuer et al. 2019) we performed a three-step variable selection procedure. The initial [1]threshold step eliminates irrelevant variables, the [2]intrepretation step selects all variables relevant to our response, in this case landcover type, and finally a [3]refining step for those variables included in step two, which identifies our set of predictive seasonal-bands (Genuer et al. 2015). For our data the threshold step eliminated four seasonal bands, the interpretation step further reduced this by another four seasonal bands, and finally the refining step identified a list of fifteen seasonal bands useful for our prediction purposes (Figure 2-3a). We further reduced this list by eliminating band pairings that exceeded a correlation factor of 0.80 using the cor() function in the R Stats package (R Core Team 2021). We were left with seven seasonal bands (Figure 2-3b) that included at least one band from each of the three seasons, specifically spring (blue, ndvi, short-wave 2) summer (blue and ndvi), fall (short-wave 1 and savi) to use in our supervised random forest algorithm.

Classification & Accuracy

We constructed a training dataset using our 2018 ground-truthed pixel points and spectral values for our seven seasonal bands identified from our variable selection procedure. These points were fed into a random forest machine learning algorithm that identified unique spectral signatures for each of our eight landcover classes and classified each pixel within our defined study area boundary (Breiman 2001). We used hyperparameter tuning to determine the optimal

number of trees to use in our random forest model. Testing across a sequence between 10-150 trees, we found that the use of 110 trees provided the best validation accuracy. With a trained and tuned random forest model for 2018, we applied the model to the ground-truthed data in 2019. Due to the low number of non-plastic row crop fields in 2019 (e.g., potatoes, garlic), fields with these crops were over-sampled relative to their abundance on the landscape in our training model. The bare dirt feature class represents agricultural fields currently being fallowed, between plantings, or abandoned, presenting a challenge as given enough time and no disturbance, weeds will appear, which by the fall season can present a spectral signature different from bare soil. This model provided sufficient accuracy as a supervised classification model. We then applied this model across time to all years from 1985-2000. The result of this process producing a final classified raster for each year, representing our eight different landscape features.

Post-Classification

Annual raster files from each year were exported from the Earth Engine platform as GeoTIFF files under the coordinate reference system EPSG: 32610 (WGS 84, UTM zone 10N) and imported into program R (version 4.1.0; R Core Team 2021), where the two distinct grassland and row crop spectral classes were merged under single representative values. As no model scheme is perfect, our supervised classification model produced pixel noise, singular or small pixel clusters that are likely misclassified. For example, an alfalfa or row crop field will be larger than the area of a single pixel (30x30m). Such small-scale classification error does not overly impact measures of quantity but can introduce large errors in proximity measures (e.g., distance from a bird nest to a given category if land cover). Pixel noise was removed by creating separate rasters for each landcover type on an annual scale. To these single value rasters we applied the clump function (Raster Package; Hijmans 2021) to count the number of pixels within

each distinct pixel cluster. Clusters were identified as individual pixels connected through all 8-directions. Pixel groupings under the size of six were removed. Accurate proximity rasters (i.e., the value of each cell representing the distance to nearest pixel type of interest) were created using the distance function (Raster Package; Hijmans 2021). SWHA nest locations were then overlaid onto these proximity rasters to extract minimum distances between nest sites and landcover class.

Similar to calculating proximity values, we also obtained territorial habitat compositions by overlaying nesting locations with territorial buffers onto our annual raster files comprising all six landcover types. Swainson's hawks are a highly territorial species during the breeding season (e.g., April-August) and as such follow a central-forging strategy from nesting locations (Orians & Pearson 1979). We assigned each territory a 1000m radius buffer (3.14 km^2) based on the results and average of two previous radio-telemetry studies. Two years of radio-telemetry observations in the Dakotas found that the 95% minimum convex polygon (MCP) of home ranges = 1.91km^2, (n=10, 2013) and 95%MCP = 2.10km^2, (n=9, 2014; Inselman et al. 2016). While early telemetry work on this population found mean foraging distances for breeding males (0.917km; radius) and average home range size (4.05 km^2, n=12; Woodbridge 1991). Habitat composition within these defined boundaries was calculated through (extract function; Raster Package; Hijmans 2021) pixel counts of each landcover type, producing individual territory compositions as proportional landcover data.

Results

Using ground-truth data from 2018 as a training-dataset, the supervised landcover classification model achieved an 85% accuracy rate when tested against ground-truth landcover

classifications from a 2019 survey. Two landscape feature classes represented the majority of misclassification, the non-plastic row crop and bare dirt groups. Applying this model across Landsat imagery (5,7,8) spanning 1985-2020 produced annual landscape classifications with 30m pixel resolution (e.g., 2018; Figure 2-4), a level of detail capable of identifying and discerning long-term trends in crop abundance within the study area. It was clear that the amount of alfalfa had increased continuously in a linear fashion since 1985 (max 3145 km^2; Figure 2-6a). While the quantity of row crops had fluctuated more and showed no temporal trends, crops of this agricultural practice have always existed at a lower frequency than alfalfa (min alfalfa 1955 km^2; max row crop 1447 km^2; Figure 2-6b) in the Butte Valley landscape.

From this landscape classification model, we were able to characterize SWHA territories across time, and to identify trends in general proximity measures. The average distance from nest trees to the nearest alfalfa field was approximately half the distance (493m) observed between nest sites and nearest row crop field (822m). Irrigated alfalfa (21.8%), shrub-steppe grassland (22.9%), and cereal grains (25.2%) were proportionally the most common landcover types across territories (Table 2-1).

Discussion

It can be difficult for ecologist to gain inference on past environmental conditions with relevance to present biological status and observations, something that the advancement of remote sensing technologies and aggregation of (publicly available) historical imagery is quickly changing. The availability of training opportunities to utilize this data is also revolutionary, in that non-specialist (e.g., ecologists) can gain access and explore new ecological questions that are not necessarily inherent to the remote sensing field. The ability to combine ecological field

studies with a tool for examining temporal inference on potentially large spatial scales holds huge promise for scientific advancement.

To gain temporal perspectives on habitat changes in relation to our study system, we required accurate landcover data spanning decades. We were able to achieve this through modeling and machine learning practices that incorporated our local knowledge of farming practices in the Butte Valley region. While large scale modelling efforts (e.g., USDA NASS Cropland Data Layers) aimed at examining nationwide levels and trends in agricultural landcover are extremely useful for setting policy, they can only be obtained through coarse spectral analysis. Conversely, enhancing the understanding of wildlife habitat interactions requires habitat information at a much finer scale. Our modelling efforts allowed us to examine historical landcover uses all the way back to 1985, 22 years earlier than the NASS initiated modelling in the state of California. The NASS cropland data layer was initiated in 1997, but in its inaugural year only covered the state of North Dakota (USDA NASS 2022).

The value of our modeling effort goes beyond the measurement of long-term change in habitat for nesting and nestling SWHA in Butte Valley because it provides a general scheme for accessing, processing, and utilizing historical aerial imagery for classifying agricultural fields. It incorporates phenological and growing practices specific to individual crops and creates an image library that incorporates intra-annual seasons. This workflow provides instructions for modeling the presence of specific crop types through remote sensing, while simultaneously illustrating how to incorporate the multiple software platforms required to achieve this completed project (Figure 2-7). Many of the spectral and analytical steps in this modelling procedure have utility to other geographic areas and systems. This remote sensing procedure can also be used to examine landcover use for focal study areas across the entire world, a vast spatial improvement

compared to the NASS database, and a recognition of the potential value of Google's Earth Engine provides to the study of wildlife-habitat interactions in the Anthropocene.

Table 2-1. Summary statistics describing average habitat characteristics and population density metrics across 890 SWHA territories from 1985-2020. The compositional habitat metrics means (25% quantile, 75% quantile) represent the average proportion and proximity distance across all nests. The nearest neighbor distance is the straight line distance (meters) between nest trees of adjacent SWHA territories. The nearest neighbor count is the number of SWHA territories within 2,000m of the focal nest.

Territory Habitat Metrics	Mean	Q25	Q75
Alfalfa Proportion	0.218	0.04	0.316
Row Crop Proportion	0.039	0	0.05
Grassland Proportion	0.229	0.039	0.351
Dryland Hay Proportion	0.252	0.132	0.347
Dirt Proportion	0.076	0.007	0.098
Juniper Woodland Proportion	0.127	0.003	0.186
Distance to Nearest Alfalfa	493m	90m	676m
Distance to Nearest Row Crop	822m	270m	1106m

Territory Density Metrics	Mean	Q25	Q75
Nearest Neighbor Distance	1425	857	1705
Nearest Neighbor Count	2.4	1	4

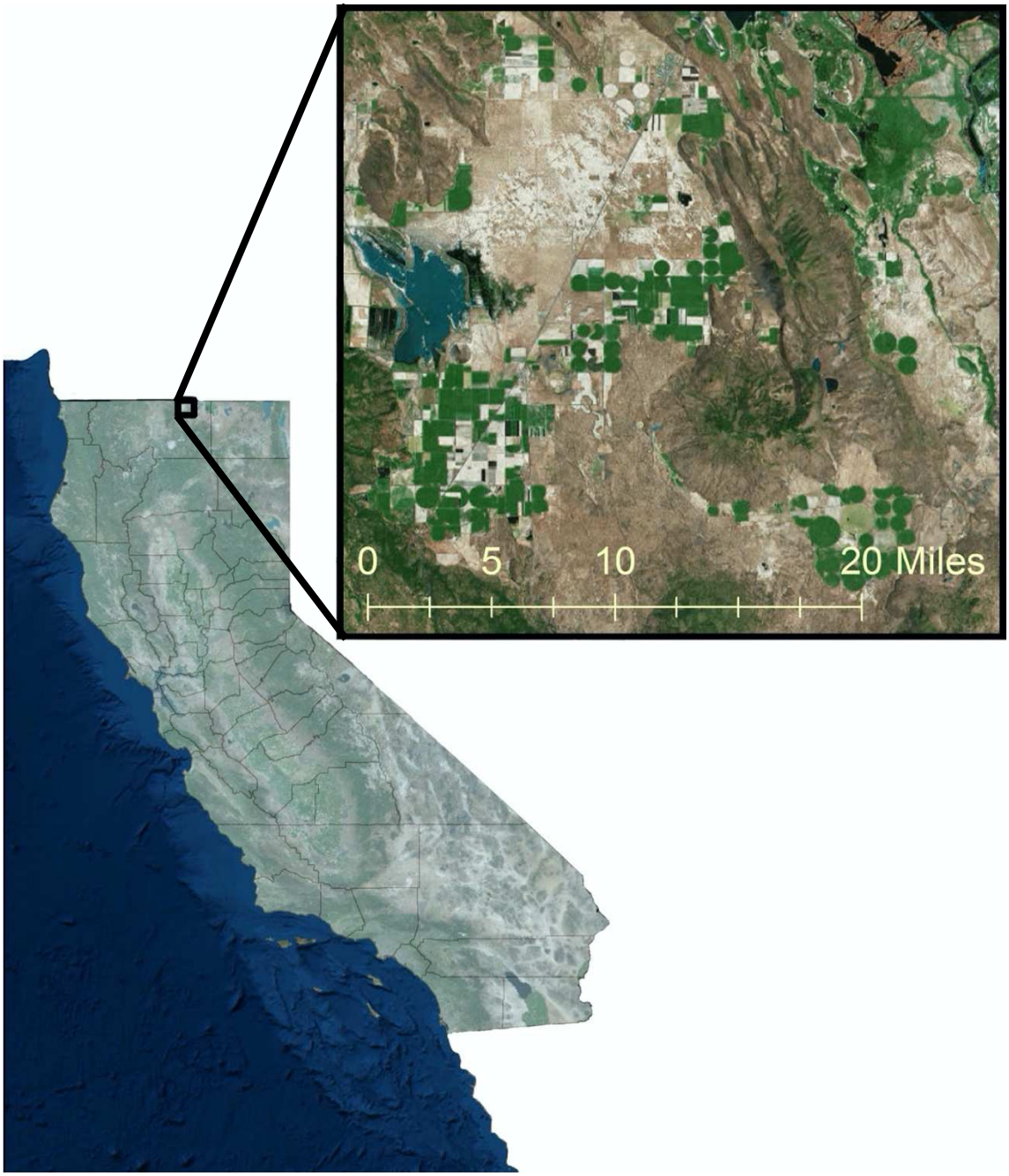

Figure 2-1. Geographic location of the Butte Valley study area in reference to the state of California, U.S.A. The inset image represents an aerial composite image of the study area boundaries.

A.

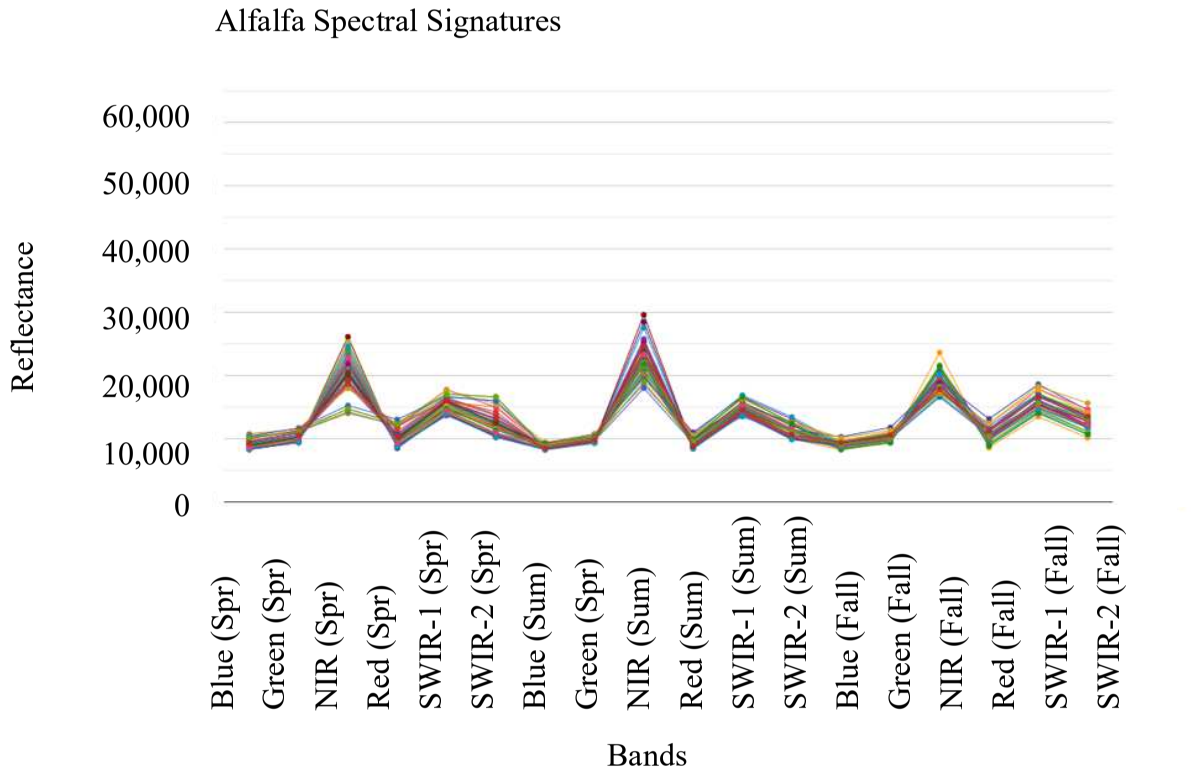
Alfalfa Spectral Signatures
Reflectance
60,000
50,000
40,000
30,000
20,000
10,000
0
Blue (Spr)
Green (Spr)
NIR (Spr)
Red (Spr)
SWIR-1 (Spr)
SWIR-2 (Spr)
Blue (Sum)
Green (Spr)
NIR (Sum)
Red (Sum)
SWIR-1 (Sum)
SWIR-2 (Sum)
Blue (Fall)
Green (Fall)
NIR (Fall)
Red (Fall)
SWIR-1 (Fall)
SWIR-2 (Fall)
Bands

B.

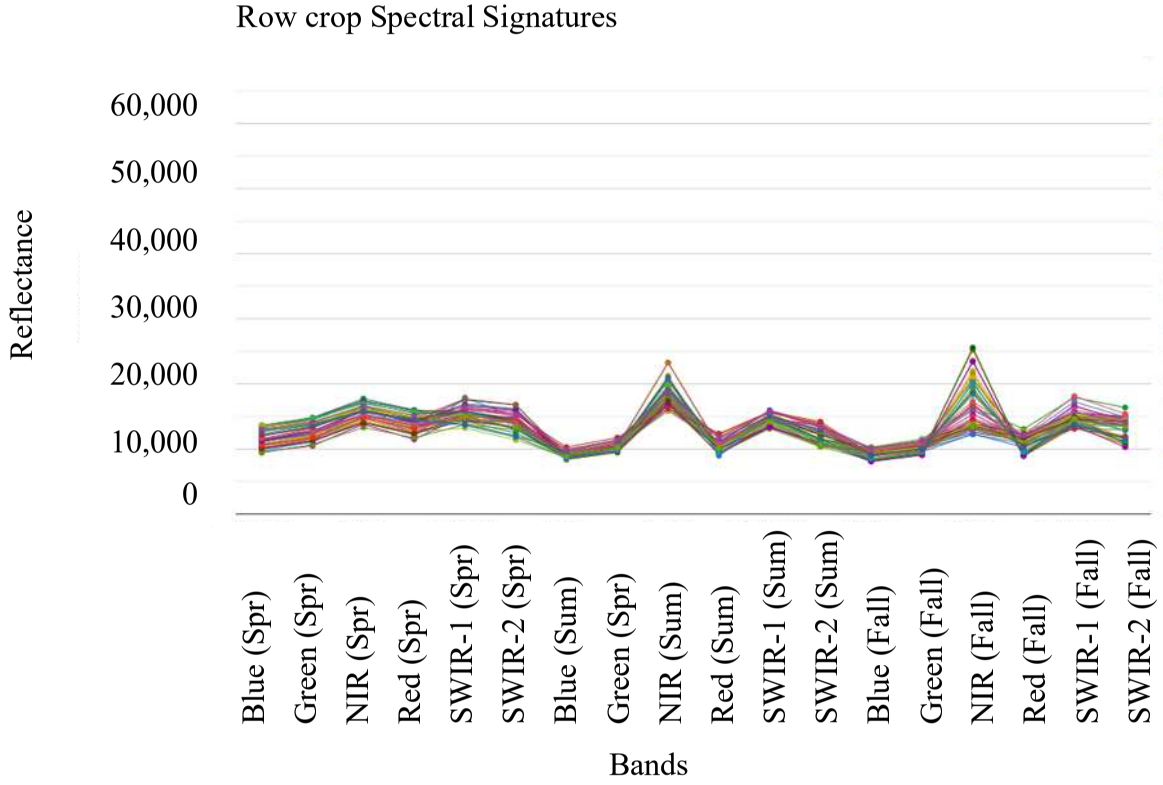
Row crop Spectral Signatures
Reflectance
60,000
50,000
40,000
30,000
20,000
10,000
0
Blue (Spr)
Green (Spr)
NIR (Spr)
Red (Spr)
SWIR-1 (Spr)
SWIR-2 (Spr)
Blue (Sum)
Green (Spr)
NIR (Sum)
Red (Sum)
SWIR-1 (Sum)
SWIR-2 (Sum)
Blue (Fall)
Green (Fall)
NIR (Fall)
Red (Fall)
SWIR-1 (Fall)
SWIR-2 (Fall)
Bands

C.

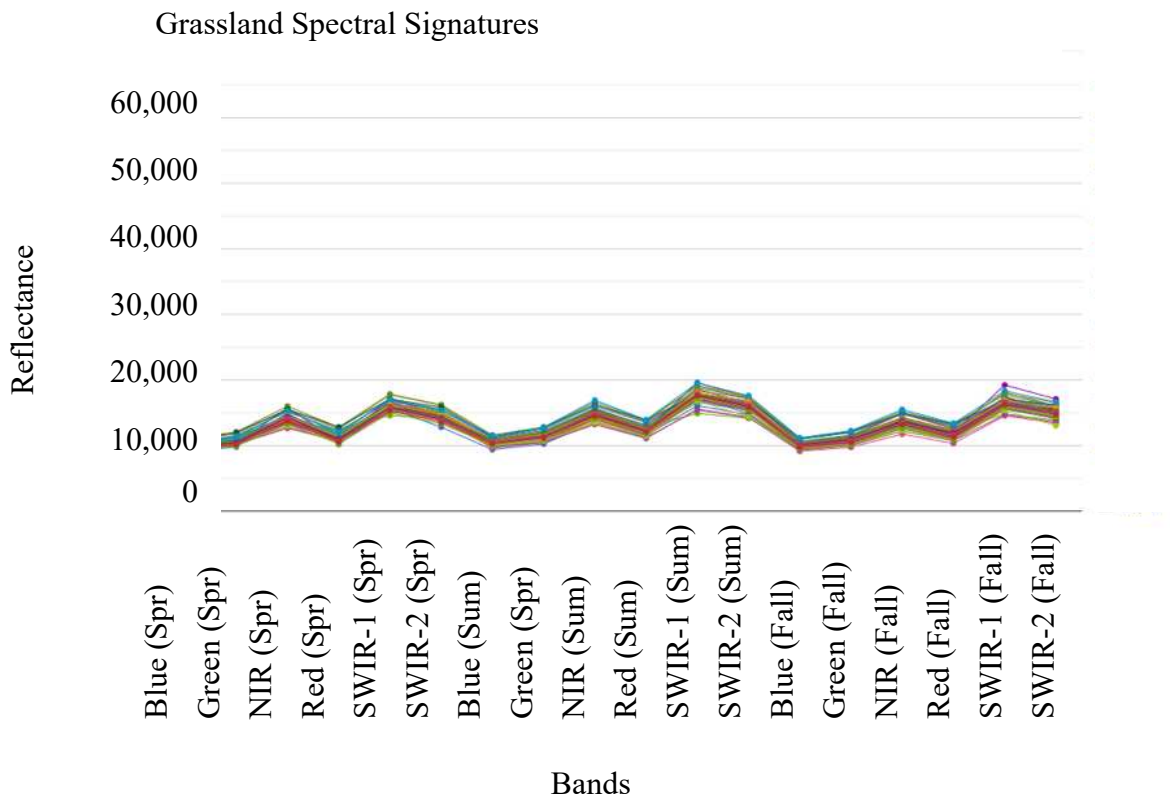

Figure 2-2. (A) Charts showing the spectral signatures from 2018 training points. Values represent raw reflectance data for six primary Landsat bands collected across all three seasons (1_spring; 2_summer; 3_fall). High near-infrared spectral values in all three seasons (three spectral peaks) is a diagnostic feature of classifying alfalfa fields. (B) High near-infrared spectral values in the summer and fall seasons (two spectral peaks), with homogenous reflectance values in the spring (1_bandname) is a diagnostic feature of classifying row crops. (C) Homogenous reflectance values across all three seasons is a diagnostic feature of classifying grassland habitats, which express lower primary productivity than irrigated agricultural fields.

A.

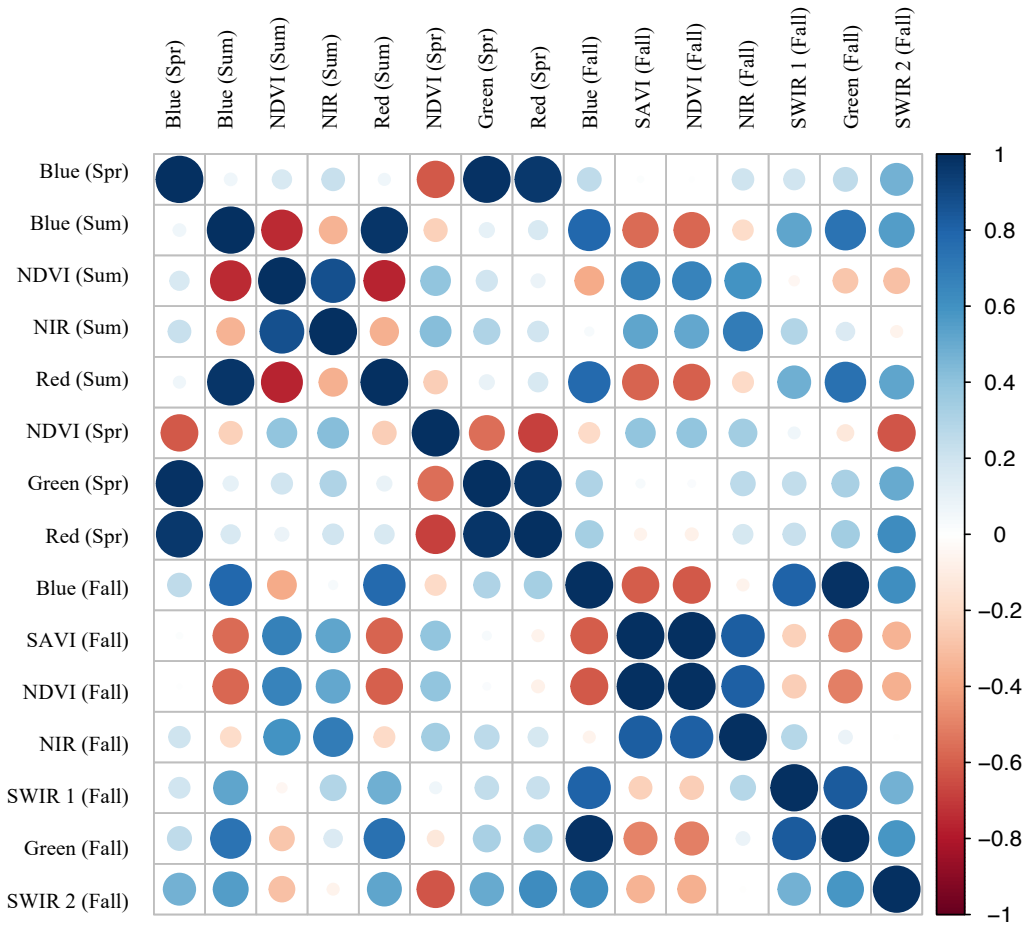
Blue (Spr)
Blue (Sum)
NDVI (Sum)
NIR (Sum)
Red (Sum)
NDVI (Spr)
Green (Spr)
Red (Spr)
Blue (Fall)
SAVI (Fall)
NDVI (Fall)
NIR (Fall)
SWIR 1 (Fall)
Green (Fall)
SWIR 2 (Fall)
1
0.8
0.6
0.4
0.2
0
−0.2
−0.4
−0.6
−0.8
−1

B.

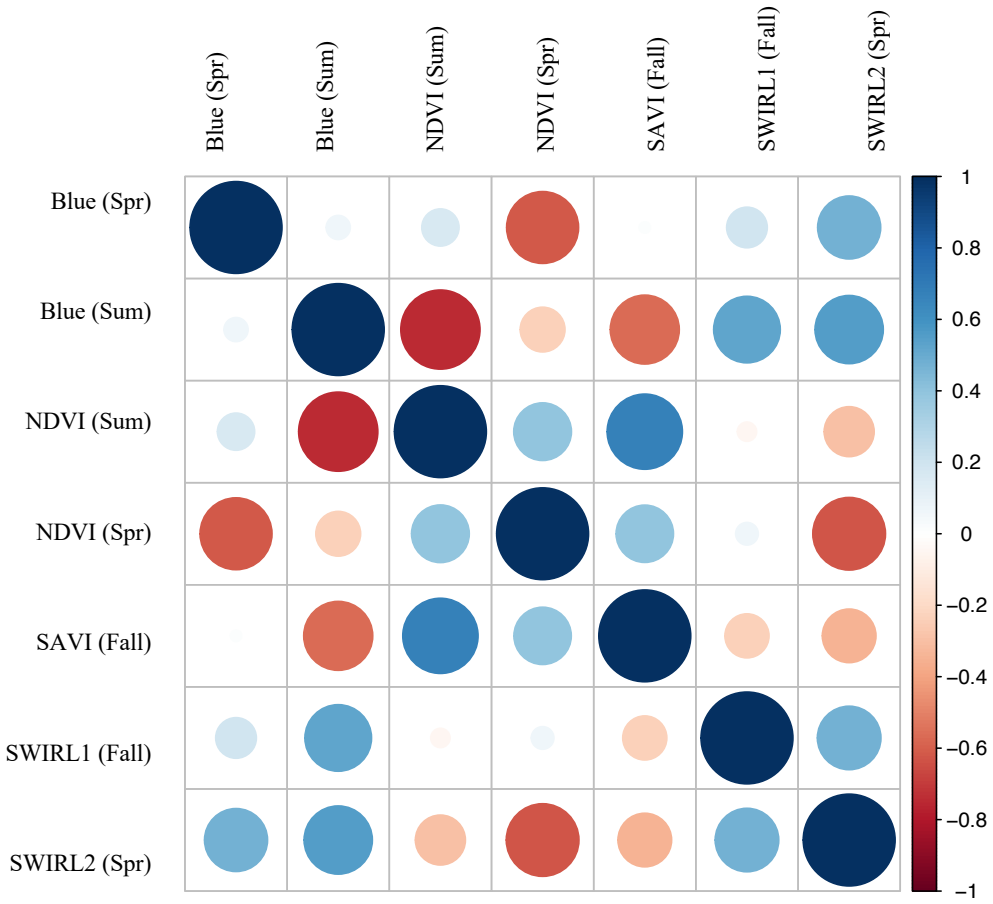

Figure 2-3. Correlograms of spectral reflectance data from the 2018 training data. (A) Shows the 15 seasonal-bands remaining after the threshold, interpretation, and refining steps of variable selection eliminated 8 seasonal bands for contributing no predictive power. Relationships between seasonal-bands with a correlation >0.8 (large dark blue or dark red dot) were removed. (B) Correlogram of the final seven seasonal-bands after correlation reduction.

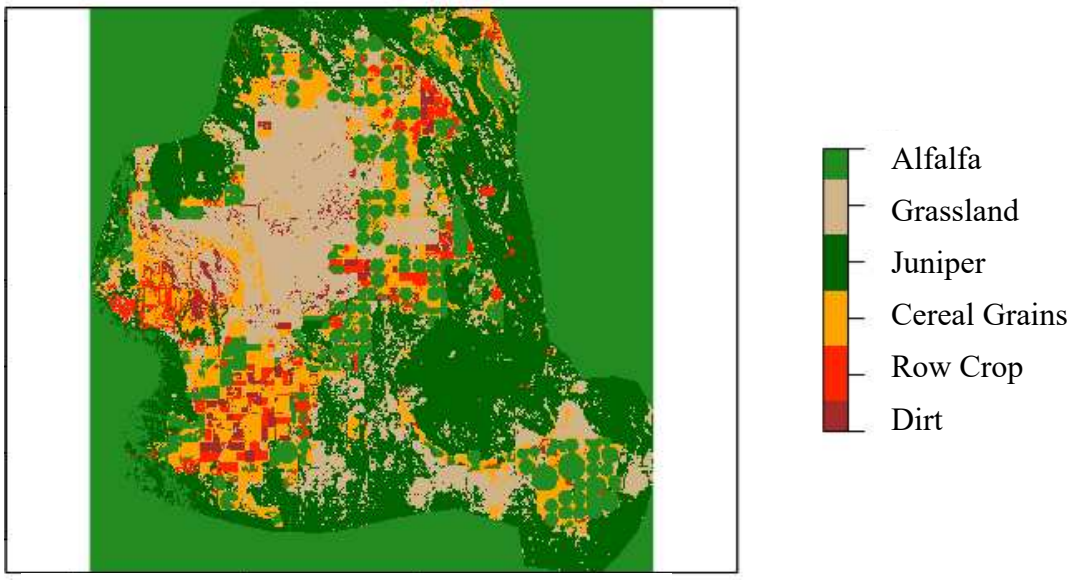

Figure 2-4. Raster output from supervised random forest classification model. Classified annual raster of Butte Valley, California from 2018 showing the general distribution of our six specified landcover types (alfalfa, row crops, cereal grains, grassland, juniper, dirt).

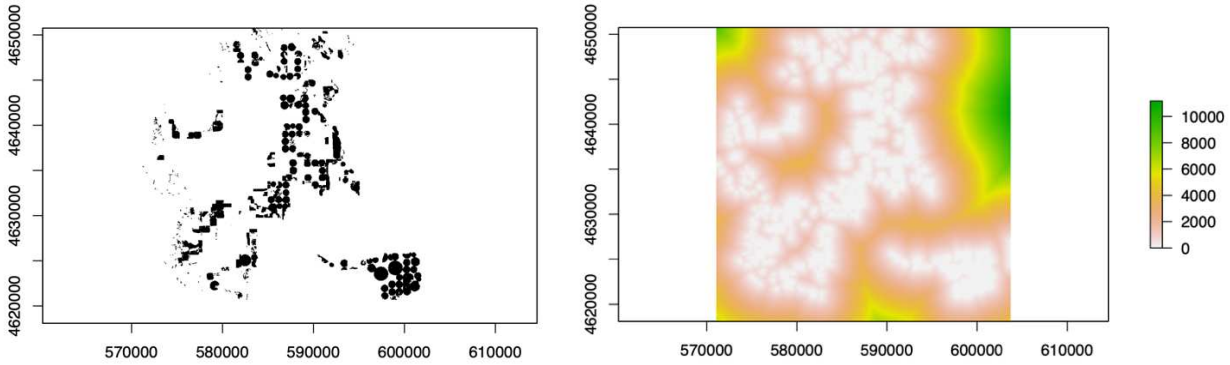

Figure 2-5. (A) Raster file illustrating the spatial layout of alfalfa fields in Butte Valley, California in 2018, post pixel noise cleanup. (B) Proximity raster of alfalfa (2018), produced from data in figure 5A. Each raster cell is assigned a value representing the distance (meters) to nearest alfalfa field.

A.

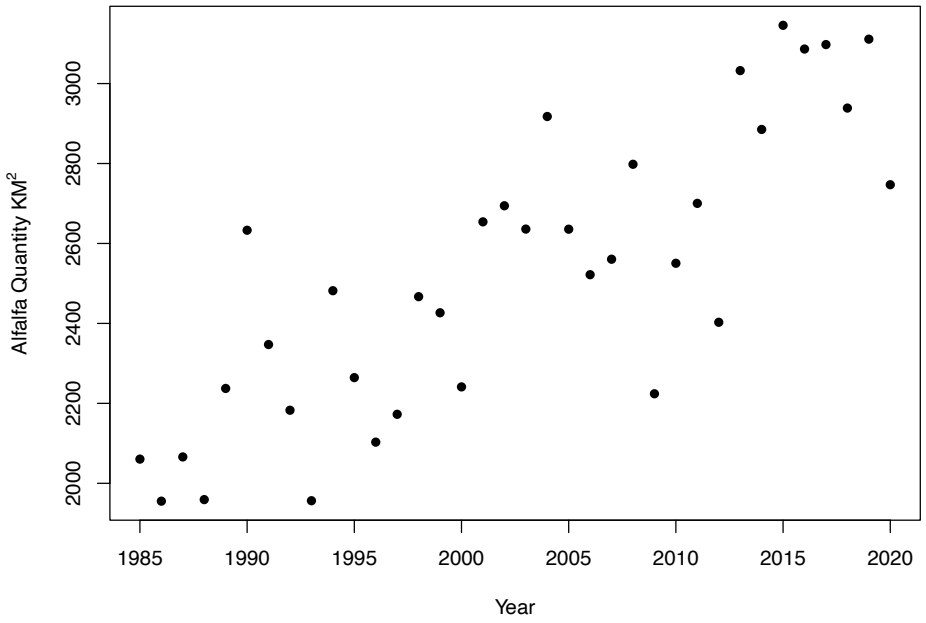

B.

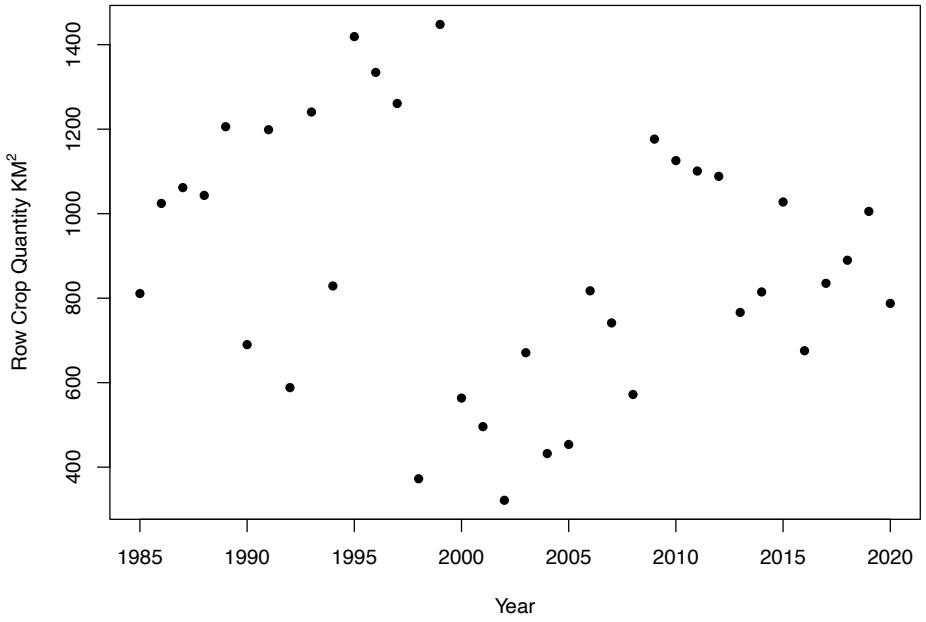

Figure 2-6. (A) Change in the quantity of alfalfa and (B) row crops (km^2) over the duration of the long-term study of Swainson's hawks breeding in Butte Valley, California between 1985-2020.

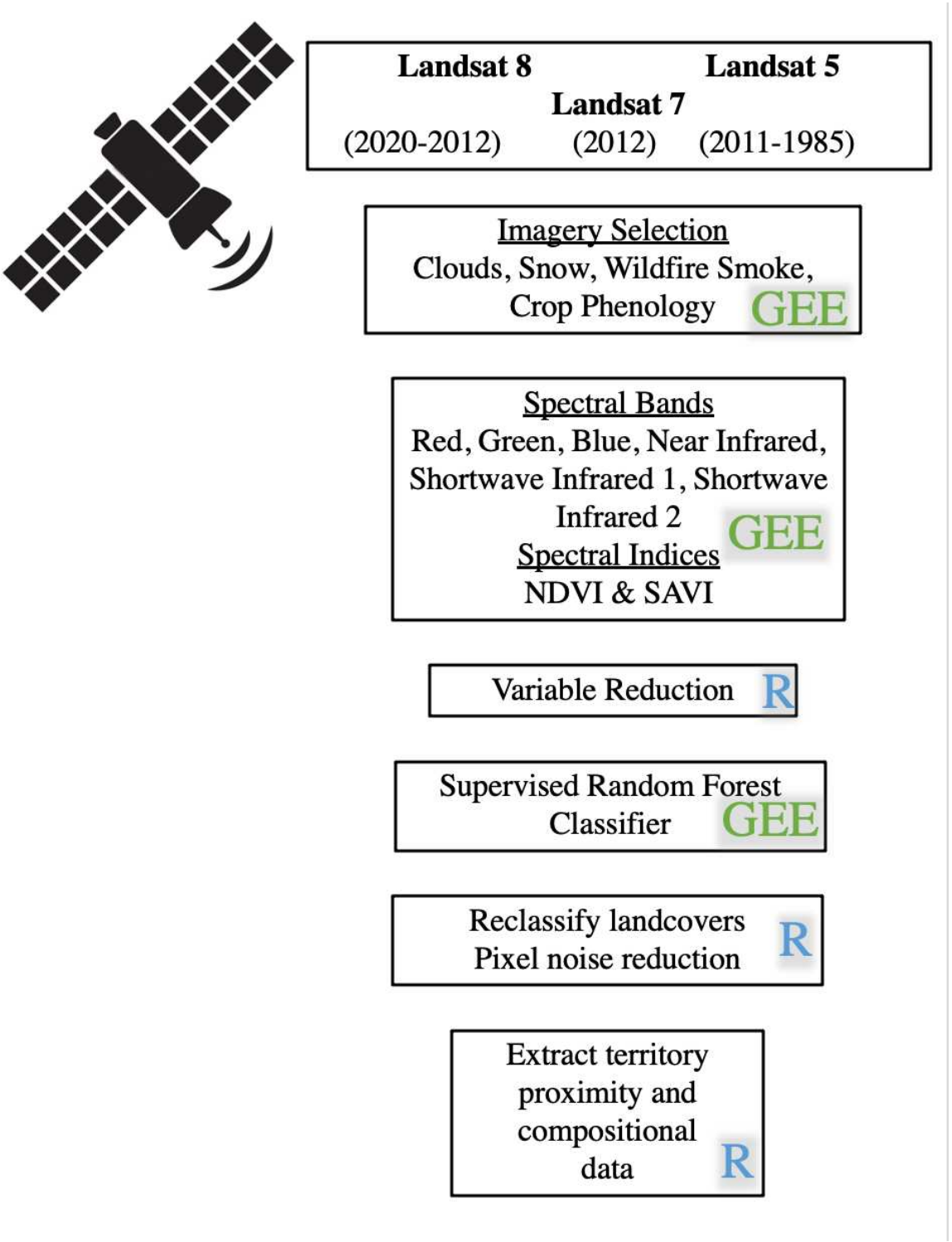

Figure 2-7. A workflow diagram illustrating the major steps required to produce annual classified raster files. Each step is labelled with the software platform used to complete the step.

Chapter 3

THE INFLUENCE OF AGE AND AGRICULTURAL HABITAT ON DELAYED RECRUITMENT IN A LONG-LIVED AVIAN PREDATOR

Introduction

For long-lived vertebrates the age of first reproduction is a particularly important demographic trait that may be under strong selection pressure (Fay et al. 2016), can vary substantially within a species, and is a crucial component in determining individual fitness and population dynamics (Cole 1954; Pradel & Lebreton 1999). Yet the early pre-breeding period of life leading up to this life-history milestone often receives far less attention than other parts of the life cycle because it can be difficult to separate permanent emigration (i.e., natal dispersal) from mortality (Lindberg et al. 1998; Bradley et al. 1999), and because non-breeding individuals are typically difficult to observe (Sedinger et al. 2008). However, the pre-breeding age classes can represent significant proportions of a population (Saether et al. 2013), commonly experience the highest rates of mortality, and are highly sensitive to environmental conditions given their inexperience. Under these condition, cohorts of young age classes are selectively thinned by the removal of frail individuals over time. Surviving to the age of recruitment is therefore a dynamic and complex process made increasingly difficult for many terrestrial species by the rapidly changing environment that defines the current epoch.

By definition, the Anthropocene has drastically altered environments from their natural trajectories due to anthropogenic sources (Hobbs et al. 2014), of which land conversion for agriculture use is a prominent force. Agricultural practices have influenced large areas of the planet, and future economic and food policies are expected to demand new and increased rates of agricultural conversion (Tilman et al. 2002). In the United States, land conversion has

dramatically decreased the extent of prairie and grassland ecosystems (Drum et al. 2015), with negative consequences for numerous avian species (Brennan & Kuvlesky Jr. 2005). Moving forward a better understanding of agricultural effects on species and their demography will be required as these landscapes modified for seasonal agricultural production are likely to be more dynamic than native landscapes. Depending on the global region and style of agricultural practice, landscapes may be altered annually or multiple times a year. And yet we know that the quality of natal environment can have dramatic consequences on ontogenetic development of offspring in wild species. Habitat quality is known to influence the fitness of territorial species (Newton 1989), and the quality thereof has been shown to directly influence the production of recruits into the breeding population (Sergio et al. 2009).

Understanding the reproductive consequences of farmland heterogeneity requires the combination of two primary modelling efforts, a spatio-temporal habitat component, and a model to generate robust demographic estimates. In the case of long-live species, delayed maturity and recruitment are quite common and require prolonged data collection to address observational uncertainties. Such uncertainties may arise from imperfect detection in the field, but they may also be biological in nature. For example, for most avian species it is challenging to determine sex during ontogeny, and failure to account for sex-specific demography may lead to flawed inference about the recruitment process (Becker & Bradley 2007). Current field methods for determining offspring sex for raptors are inadequate, impeding the understanding of sex differences in demography and especially recruitment. To overcome these shortcomings, we developed a hidden Markov multistate model, with state (i.e., sex) uncertainty built into the initial state of release (Nichols et al. 2004), which we informed using a separate logistic model

that predicts the probability of each individual being a given sex using morphological measurements of nestlings and verified with a genetic study (Ch. 1).

In agricultural environments, space use may vary annually, remain unchanged (i.e., perennial), or even change within a year depending on the type of crop and harvest practices. Agricultural fields therefore differ in their ecosystem properties in the value they provide to wildlife. Capturing this heterogeneity and understanding habitat dynamics required the development and use of remote sensing techniques (Ch. 2). Here we hypothesize that irrigated alfalfa benefits ontogeny, promoting higher survival during the pre-breeding phase of life and an earlier age of recruitment for our study species, Swainson's hawk (SWHA; *Buteo swainsoni*). The perceived benefit from alfalfa holds that this crop type supports several abundant prey species for raptors and nestlings developing in close association will be of higher quality. The opposite is assumed for row style crops, which often have high chemically use and are biologically sterile. Thus, increased row crop presence will have a negative impact on nestling development through resource restriction. In comparison, to these two main habitat types we expect the remaining landcover types providing marginal value to this species. In addition to providing a novel method for measuring sex-specific demography in species where sex is difficult to measure, our research provides needed insight into the ways in which long-lived wildlife are affected by, cope with, or benefit from specific types of crops in their surrounding landscape.

Methods

Study Area

Located on the western boundary of the Great Basin ecotype, Butte Valley, California (41˚ 49'N, 122˚ 0'W; 415 km^2) is a relatively high elevation (1,280 m to 1,340 m) sagebrush

steppe and juniper woodland environment. Through groundwater irrigation, agricultural fields have increased in abundance producing clear differences in primary productivity between arid natural sagebrush and irrigated agriculture, a common landscape feature in the western United States. Overall landcover can be defined by five categories: grassland shrub steppe, cereal grains, alfalfa, row crops, and juniper woodlots. An abundant crop and primary foraging habitat, irrigated alfalfa provides consistent and high prey densities for raptors. Belding's ground squirrels (*Urocitellus beldingi*) are the dominant prey species for the first half of the breeding season, a key food resource for hawks refueling after completing spring migration. Ground squirrel distribution is patchy, and densest in irrigated hay crops (i.e., alfalfa) until they locally estivate in late June, after which prey composition switches to include pocket gophers (*Thomomys* spp.), voles (*Microtus* spp.), reptiles, small bird species, and insects (Woodbridge 1991).

Study Species

Swainson's hawk territories are established primarily on the valley floor in shrub-steppe habitat or in the margins and field edges defining agriculture field boundaries, where juniper woodlots are abundant and provide nesting substrates. SWHA construct stick nests, almost exclusively in trees, with a shallow inner bowl depression and will readily reuse nests across years. For birds nesting in Butte Valley over 90% of nests are constructed in western junipers (*Juniperus occidentalis*; Woodbridge 1991). SWHA exhibit reverse sexual dimorphism (females larger than males) with some physical overlap (Kochert & Mckinley 2008) impeding accurate sex identification of nestlings, which can be further complicated by physical stunting and asynchronous effects of hatch order. Full adult plumage, the visual que of reproductive maturity, is not obtained until the age of three but recruitment is often delayed further. During the pre-

breeding (from fledging to recruitment) years individuals are generally unobservable. Juveniles are rarely observed within the study area during the breeding season and recent telemetry work has revealed that these early years are spent moving nomadically around the American southwest (Vennum unpublished). This age-dependent behavior makes the pre-breeder life stage unobservable without technology, leading to substantial uncertainty in the underlying process of recruitment and the factors that affect it (Clobert et al. 1994). Delayed recruitment also means that data on this demographic transition takes years to collect, and a large sample of marked offspring is needed to gain robust inference. As a territorial species, recruitment involves the probability of surviving to sexual maturity, obtaining a territory, a mate, and occurs across a range of ages. While the establishment of new territories continues to occur despite the population doubling in the last twenty years (Vennum 2017), annual turnover in established breeders is approximately 0.10-0.15 based on apparent adult survival of 0.85 to 0.90 (SE = 0.02; Briggs et al. 2011).

Demographic Data Collection

Annual surveys to locate and monitor reproductive pairs begins in late April and extends through early August when territorial boundaries break down. Observers enter nests starting in early July to individually mark offspring prior to achieving fledging age (45 days old; Bechard et al. 2020). The collection of high-quality recruitment data (i.e., accurate detection of first breeding attempt) started in 2008 when project banding protocols were improved. Prior to that, nestlings had only been marked with a United States Geologic Survey (USGS) aluminum band. Protocol changes added a secondary alphanumeric plastic color band and included the collection of morphometric data for nestling chicks (e.g., weight, tarsus width, etc.). Additionally, effort was made to mark nestlings after they reached a minimum of 36 days of age, which represents

the point in development at which they have reached 80% of peak structural size, and generally affords the assumption that a nestling will successfully fledge (Steenhof 1987). Color banding nestlings greatly improved detection probabilities, as newly recruited individuals could easily be identified through band re-sighting practices without the need for physical recapture.

Our field efforts to complete a yearly census confirm the annual status of each territory, generating a historical record that can be examined retrospectively. In cases where a breeding individual's alphanumeric color band wasn't read in a given year, band status and plumage color (i.e., red band on left leg; dark morph) are still recorded. SWHA are polymorphic and express morph invariance (Briggs et al. 2010). So when a recruitment event occurs at a territory we compare the band and plumage status of mated pairs in the previous year to the newly recruited individual or pair, adding confidence to our ability to accurately observe the age of first breeding attempt in a manner that is individual- as opposed to territory-specific. Such accurate distinctions allow us to model the age-specific probability of recruitment across multiple ages for each sex, despite imperfect detection.

Study protocols and procedures were approved by the Institutional Animal Care and Use Committee at the University of Nevada, Reno (IACUC approval no. 00115 and 00522) and Hamilton College (IACUC approval no. 18-R-3).

Habitat Evaluation

Swainson's hawks are a highly territorial species during the breeding season (e.g., April-August) and as such follow a central-forging strategy from nesting locations (Orians & Pearson 1979). To characterize territories, we defined a 1,000 m radius buffer (3.14 km^2) around a nest and used rasterized landcover layers on a yearly basis to evaluate habitat composition within this radius. This assumption was based on the results of two previous SWHA radio-telemetry studies.

Two years of radio-telemetry observations in the Dakotas found 95% MCP = 1.91km^2, (n=10, 2013) and 95% MCP = 2.10km^2, (n=9, 2014; Inselman et al. 2016). Early telemetry work on the Butte Valley study population estimated mean foraging distances for breeding males (0.917km; radius) and average home range size (4.05 km^2, n=12; Woodbridge 1991) that also corroborate evidence for our assumed territory size.

While national crop databases exist within the United States (e.g., USDS NASS Cropland Data Layers; USDA National Agricultural Statistics Service), we found this database to be inaccurate for our study site with respect to key crop types. We instead chose to develop our own classified landcover layers using remotely sensed imagery and ground-truth data, under a supervised classification scheme and random forest algorithm (Breiman 2001) within Google's Earth Engine platform. Aerial imagery was obtained using Landsat satellites 5 (2009-2011), 7 (2012), and 8 (2013-2020). The 30m pixel data generated by all three satellites provides sufficient resolution to accurately identify distinct crop types. Ground-truth data were collected in 2018 and 2019. The 2018 landscape cover data was used to train our random forest model, with the 2019 data used for validation purposes. Raw spectral band values (i.e., red, green, blue, shortwave infrared 1 & 2, and near infrared) were collected to be used as predictors and to calculate two spectral indices, the normalized difference vegetation index (NDVI), and the soil adjusted vegetation index (SAVI). With regard to spectral signatures of landcover types we had two concerns, first being spectral signature distinctness for individual classifications (i.e., cereal crops vs grasslands), and second the spectral variability within a unique landcover type (i.e., consistent signatures across space and time).

Prior to running our supervised classifier, we generated spectral response curves for each landcover type to visually inspect consistency of signal within a class and inspect differences

between landcover types. Examination of spectral signatures from our training data informed whether or not classes should be combined due to lack of spectral distinctiveness (e.g., irrigated grass and irrigated alfalfa have similar signatures). While we carefully inspected the spectral quality of each landcover type, most vegetative landscapes have a temporal component (i.e., seasonal green up) producing unique phenological characteristics. Certain agricultural crop types present different spectral signatures throughout the growing season, thus we defined three "seasons" across the year (Spring: April-May; Summer June – August; Fall: September-October). This phenology component allowed for accurate distinction between row crops and crops such as alfalfa, which may have similar spectral signatures at the height of the boreal summer but are completely different in the months defined as spring and fall. Prior to running the random forest classifier, we performed a variable selection process using the *VSURF* package (version 1.1.0; Genuer et al. 2015). This was necessary to reduce the number of spectral predictors applied to each season and eliminate collinearity (a cutoff of >0.8 was used).

Swainson's hawk territory habitat composition was then quantified as the percentage of each landcover class within the defined territory buffer. Given a high density of nesting birds and strong site fidelity observed in this species, the distribution of nesting territories likely form according to an ideal despotic process (Fretwell & Lucas Jr. 1970) where some territories will lack prime foraging habitat within the territorial buffer. These less desirable territories will require longer flights to obtain resources and which could be accounted for using proximity measures. In example, a shorter distance from a nest to the nearest alfalfa field (hypothesized negative beta coefficient; shorter distance better), might benefit nestling quality resulting in increased survival and recruitment probabilities. While increased distances to nearest row crop

(hypothesized positive beta coefficient) would be preferrable, as this habitat provides no foraging value to SWHA and high-quality territories will avoid such farms.

Statistical Approach

Subsection 1.1 Initial Bayesian Logistic Regression

Observational uncertainty manifests when SWHA individuals are marked and measured as nestlings, a period when ontogenetic development is still in progress and individual sex cannot be visually or morphometrically determined with 100% accuracy. This early life stage of rapid development can be heavily influenced by nest dynamics (i.e., brood size, provisioning rates, hatch order). Previous work on this population has delineated that mass and tarsus width are the most parsimonious predictors of nestling sex, with females achieving masses above 820grams and tarsus widths greater than 9.4mm (Ch. 1). These morphometric cutoffs were obtained using a molecular sexing technique (i.e., polymerase chain reaction; PCR) on a smaller subset of known-sex individuals included in this analysis (n= 88, see Ch.1 for details). Even at a young age SWHA display sexual dimorphism, however morphometric overlap exists, producing uncertainty in sex assignment. We accounted for this uncertainty in a probabilistic fashion by first constructing a Bayesian logistic regression (x_1 individual tarsus width data; x_2 individual mass data) using the same known sex individuals from chapter 1. The posterior distributions of each beta coefficient (β_0 intercept; β_1 tarsus width; and β_2 mass) produced from this initial model were then used as informative priors in a secondary logistic regression model to estimate probabilities of sex assignment (p) for all individual nestlings in the analysis (n=877, eq.1).

$$[\mathbf{p}, \boldsymbol{\beta}, | \, \mathbf{y}] \propto \prod_{i=1}^{877} \text{binomial}\,(y_i \mid n_i, p_i) \times \text{Bernoulli}(p_i \mid \text{invlogit}(\beta_0 + \beta_1 x_{1,i} + \beta_2 x_{2,i})) \times \text{normal}(\beta_o \mid 0.234, 9.239) \times \text{normal}(\beta_1 \mid 3.350, 1.491) \times \text{normal}(\beta_2 \mid 2.747, 1.555) \quad \{\text{eq. } 1\}$$

These probabilities (p) were then deterministically assigned (fixed to Π) in our larger hidden Markov multistate model (HMMM; McClintock et al. 2020), linking them to the initial state of each individual. This allowed us to parametrize the probability of being a female, Π, and the probability of being a male 1-Π.

This analysis was performed in Program R (Version 4.1.0) using the *R2jags* package (Version 0.7-1). Three independent Markov chains were run for 100,000 Monte Carlo iterations, with an initial burn-in of 20,000 samples, thinning rate of 4 (every 4th sample retained), thus each chain was represented by 20,000 runs, for a total of 60,000 saved samples for each posterior distribution. The sensitivity of the informed prior logistic regression was tested by calculating the area under the ROC (Receiver Operating Characteristic) curve (Hajian-Tilaki 2013, Beger 2016), and performed using the mcmcRocPrc function in the package *BayesPostEst* (v. 0.3.2; Karreth et al. 2021).

Subsection 1.2 Hidden Markov CMR

To incorporate the above-mentioned biological uncertainty into a demographic model we applied a hidden Markov modeling approach to examine longitudinal capture-mark-resight (CMR) data on sex-specific recruitment rates from 2009-2018 (Figure 3-1). State uncertainty models are advantageous as they allow more data to be incorporated (i.e., no censoring based on

missing sex identification), and have been shown to provide more precise and less biased estimates than traditional multistate models (Nichols et al. 2004; Pradel 2005). Under this framework, a separate likelihood statement, state matrix (M1), and observation matrix (M2) are required to model the initial state of release, and all individuals start as sex "unknown". For all subsequent time intervals, where sex becomes known (post recruitment), state and observation components are described in eq. 2 & 3 with associated matrices M3 & M4, following the nomenclature AF (alive and fledged) ANR (Alive Not Recruited), and AR (Alive Recruited). A clear distinction should be noted that ϕ (M1) represents a vector of initial states, while ϕ (M3) is a transition matrix from time t to t+1.

$$\phi_{i,t}^{init} = \begin{matrix} AF_{♀} \\ ANR_{♀} \\ AR_{♀} \\ AF_{♂} \\ ANR_{♂} \\ ANR_{♂\,2\mathrm{yr}} \\ AR_{♂} \\ Dead \end{matrix} \begin{bmatrix} \pi \\ 0 \\ 0 \\ 1-\pi \\ 0 \\ 0 \\ 0 \\ 0 \end{bmatrix} \quad \{\mathrm{M1}\}$$

$$\mathrm{P}_{i,t}^{init} = \begin{matrix} \\ AF_{♀} \\ ANR_{♀} \\ AR_{♀} \\ AF_{♂} \\ ANR_{♂} \\ ANR_{♂\,2\mathrm{yr}} \\ AR_{♂} \\ Dead \end{matrix} \begin{matrix} \begin{matrix} \text{Obs.} \\ \text{Rec}\,♀ \end{matrix} & \begin{matrix} \text{Obs.} \\ \text{Rec}\,♂ \end{matrix} & \begin{matrix} \text{Obs.} \\ \text{Sex}_{\mathrm{unk}} \end{matrix} & \begin{matrix} \text{Not Obs.} \\ \end{matrix} \\ \begin{bmatrix} 0 & 0 & 1 & 0 \\ 0 & 0 & 0 & 1 \\ 0 & 0 & 0 & 1 \\ 0 & 0 & 1 & 0 \\ 0 & 0 & 0 & 1 \\ 0 & 0 & 0 & 1 \\ 0 & 0 & 0 & 1 \\ 0 & 0 & 0 & 1 \end{bmatrix} \end{matrix} \quad \{\mathrm{M2}\}$$

Given the unobservable nature of the juvenile life stage and variation observed in recruitment ages, there are two different ways that this model could be parameterized following the initial state matrices and based on assumptions of survival probability (Lebreton et al. 2002). One assumption would be to treat first-year survival as a distinct parameter for each sex and assume that annual survival probabilities for all subsequent juvenile ages (years two to recruitment) are equivalent to adult survival for the relevant sex. Alternatively, one can assume a distinction in annual survival probabilities between the juvenile and adult periods of life, but constrain the survival probabilities to be equivalent for each pre-breeding age. Based solely on studies using telemetry technologies there is strong evidence across raptor species that first-year survival is quite low (0.07-0.48; Newton et al. 2016). However, studies that separate first-year, later juvenile years, and adult life are very limited. Based on long-term demographic research of Black Kites (*Milvus migrans*), a species very similar to SWHA in their ecology and body size, we parameterized our model to assume adult survival probabilities after the first year, because survival greatly increased in Black Kites after the first year (Sergio et al. 2011).

$$\mathrm{X_{i,t+1}}|\mathrm{X_{i,t}} \sim multinomial(1, \mathrm{X_{i,t}}, \Phi_{\mathrm{i},\mathrm{t}}) \quad \{\text{eq.2}\}$$

$$\boldsymbol{\phi_{i,t}} = \begin{array}{c} \\ AF_{♀} \\ ANR_{♀} \\ AR_{♀} \\ AF_{♂} \\ ANR_{♂} \\ ANR_{♂\,2\mathrm{yr}} \\ AR_{♂} \\ Dead \end{array} \begin{array}{c} \begin{array}{cccccccc} AF_{♀} & ANR_{♀} & AR_{♀} & AF_{♂} & ANR_{♂} & ANR_{♂\,2\mathrm{yr}} & AR_{♂} & Dead \end{array} \\ \begin{bmatrix} 0 & \phi_{juv} & 0 & 0 & 0 & 0 & 0 & 1-\phi_{juv} \\ 0 & \phi_{AD♀}*(1-R_{♀}) & \phi_{AD♀}*R_{♀} & 0 & 0 & 0 & 0 & 1-\phi_{AD♀} \\ 0 & 0 & \phi_{AD♀} & 0 & 0 & 0 & 0 & 1-\phi_{AD♀} \\ 0 & 0 & 0 & 0 & \phi_{juv} & 0 & 0 & 1-\phi_{juv} \\ 0 & 0 & 0 & 0 & 0 & \phi_{AD♂} & 0 & 1-\phi_{AD♂} \\ 0 & 0 & 0 & 0 & 0 & \phi_{AD♂}*(1-R_{♂}) & \phi_{AD♂}*R_{♂} & 1-\phi_{AD♂} \\ 0 & 0 & 0 & 0 & 0 & 0 & \phi_{AD♂} & 1-\phi_{AD♂} \\ 0 & 0 & 0 & 0 & 0 & 0 & 0 & 1 \end{bmatrix} \end{array} \quad \{\text{M3}\}$$

$$\mathrm{Y_{i,t+1}}|\mathrm{X_{i,t}} \sim multinomial(1, \mathrm{X_{i,t}}, \mathrm{P_{i,t}}) \quad \{\text{eq.3}\}$$

$$P_{i,t} = \begin{array}{c} \\ AF_{♀} \\ ANR_{♀} \\ AR_{♀} \\ AF_{♂} \\ ANR_{♂} \\ ANR_{♂\,2yr} \\ AR_{♂} \\ Dead \end{array} \begin{array}{c} \begin{array}{cccc} \text{Obs.} & \text{Obs.} & \text{Obs.} & \text{Not Obs.} \end{array} \\ \begin{bmatrix} \text{Rec}♀ & \text{Rec}♂ & \text{Sex}_{\text{unk}} & \\ 0 & 0 & 0 & 1 \\ 0 & 0 & 0 & 1 \\ p & 0 & 0 & 1-p \\ 0 & 0 & 0 & 1 \\ 0 & 0 & 0 & 1 \\ 0 & 0 & 0 & 1 \\ 0 & p & 0 & 1-p \\ 0 & 0 & 0 & 1 \end{bmatrix} \end{array} \quad \{M4\}$$

Subsection 1.3 Parametrization and Priors

Differences in the range of recruitment ages exists between the sexes, a biological feature that is incorporated in the design of the state matrix (M3). Female SWHA need only survive a minimum of two years prior to entering the breeding population, while males must survive a minimum of three years before recruiting. Baseline recruitment probabilities were modeled with logistic priors on both the intercept and an age-effect coefficient. A multinomial logit link function ensured that upon back-transformation these transition parameters (recruitment) jointly summed to one (Kery & Schaub 2012). Apparent first year survival probabilities of both sexes were each modeled with separate truncated logistic priors dlogis(0,1)T(,0.4) on the intercepts, which helped with estimation convergence, and a temporal random effect. All explanatory variables were given logistic priors dlogis(0,1) as parameters modeled with a logit link function and traditionally vague normally distributed priors (e.g., dnorm(0,100) can produce an unintentional influence on the probability scale (Northrup & Gerber 2018). Adult survival was estimated for each sex, similarly, using a logistic prior on the intercept and temporal random effect, but no explanatory variables were included because our focus here is on early-life demography. Detection probabilities were estimated with full annual time-variation and a uniform(0,1) prior on the probability scale for each year.

Subsection 1.4 Model and Variable Selection

To identify inferential explanatory variables, we employed a multi-step variable selection process that considered both the precision of within-model posterior densities of linear coefficients (Arnold 2010) and model WAIC scores (Watanabe 2013) using a plural approach to inference. The initial model set consisted of only intrinsic morphological and brood-related variables (tarsus width, mass, hatch date, and brood size) with each variable fitted to both survival and recruitment parameters of each sex. At this preliminary stage we did not consider contrasting model parameterizations for survival and recruitment, nor for different sexes, to avoid data dredging and because we had no *a priori* reasons to do so. Beyond single explanatory variable models, we considered two-variable additive effects (tarsus width + mass; hatch date + brood size). In the case of SWHA, large brood sizes (i.e., 3-4 offspring) generally appear earlier in the season, with later fledging nests often producing only a single chick; hence we also considered a model specifying an interaction between brood size and hatch date.

When WAIC model scores were similar, variables were retained in step 2 using liberal inference if their posterior densities were more than 85% negative or positive (Arnold 2010). For example, if the coefficient for male mass on recruitment had > 85% of its posterior density above zero, but the female coefficient for mass was evenly distributed across zero, we retained the mass variable within the male linear equation for recruitment but excluded it from the female linear equation. This process of variable retention identified the morphological and brood variables pertinent to predicting sex-specific variation in survival and recruitment probabilities, given the observed data. The result of this initial and secondary selection step is referred to as the '85% group'. We recognize that more formal approaches to variable selection exist, but they are challenging to implement in HMMMs (Hooten and Hobbs 2015).

In our third step of model and variable selection, we considered density-dependent explanatory variables in addition to variables retained from the previous steps. Two different metrics of population density were considered, the distance from a focal nest to the nearest conspecific neighbors' nest (NND; nearest neighbor distance), and the number of SWHA nests within 2000m meters (NNC; nearest neighbor count) that were each fit to the data in separate models. The consideration of population density indices seemed necessary because the local population has approximately doubled over the past two decades (Vennum 2017). To construct a final model that considered the best morphological, brood, population-density, and habitat variables without dredging the data by fitting all possible combinations of variables, we fit a "slack" model (Lawson 2014) comprising proportional habitat data, plus the variables identified in the previous three selection steps. Analytically, the composition of a SWHA territory (or any space within a defined boundary) is a mixture of landcover types that proportionally sum to one and are thus correlated. To deal with this correlation one of the primary habitat types, in this case proportion of juniper habitat, is simply dropped from the equation, ensuring that the mixture of variables examined no longer sums to one (Lawson 2014).

The HMMM analyses were performed in Program R (Version 4.1.0) using the *jagsUI* package (Version 1.5.1) to construct models and the *MCMCvis* package (Version 0.15.2) to visualize results and confirm parameter convergence. Posterior distributions for annual survival and recruitment estimates were estimated using Markov chain Monte Carlo (MCMC) simulations (King et al. 2012). Five independent Markov chains were set to run for 100,000 iterations each, after an adaption phase of 2,500 iterations, followed by an initial burn-in of 45,500 iterations, and a total of 20,960 posterior samples were retained. Convergence was confirmed using visual inspection and $\hat{R}$ values < 1.2 as recommended in Gelman et al. (2004).

Results

From 2009-2018 a total of 877 individual SWHA nestlings were banded and morphometrically measured in Butte Valley, California. These individuals obtained the minimum nestling age and appropriate development score required by our species-specific tool for predicting sex (32 days of age; ≦ -6 development index, see chapter 1). Within this population we found a slight bias favoring the production of female offspring (53% female; 467 predicted females, 410 predicted males). The sensitivity of our initial logistic regression, used to estimate sex assignment probabilities, was quite high based on area under the ROC curve (AUC = 0.96, credible interval 0.95-0.97; Figure 3-2), where an AUC=1 represents a perfect diagnostic test. In total 475 unique nesting attempts spanning 10 years were included in the analysis. Across these nests the average distance to nearest alfalfa field (529m) was approximately half of that observed between nest trees and agricultural fields containing row crops (911m; Table 3-1). This increased separation from row style crops is also reflected in the low compositional proportion of them within an average territory (4.2%), while territories contained higher percentages of irrigated alfalfa (19.7%), shrub-steppe grassland (32.3%), and cereal grains (20.3%; Table 3-1) on average.

Extensive annual field surveys resulted in 111 resightings of SWHA previously marked as nestlings and observed attempting to breed within the Butte Valley study area (12.7%; 55 females, 56 males). Upon recruiting adult female survival ranged from 0.76-0.80 and adult male survival ranged from 0.79-0.83 (Ch. 3 Appendix A). Mean annual detection was 0.73 (0.52-0.95; Bayesian credible interval) and ranged from 0.58-0.94 (Ch. 3 Appendix B). Age variation in the latent first reproductive attempt differed slightly between the sexes (females 2-6yr; males 3-7yr). Based on yearly band and plumage status observations of mated pairs, we're confident that all

female recruitment events for 2, 3, and 4 year-old individuals were observed accurately. This same degree of confidence can be stated for male recruitment at ages 3, 4, and 5. While the model allows for older recruitment ages for both sexes, our confidence in the observed recruitment age decreases because it is possible (even likely) that they recruited at an earlier age but went undetected. However, the majority of all recruits entered the breeding population within the age ranges of high observational certainty (49/55; 89%) females and (51/56; 91%) males. The most common age for females to recruit was age 3 (48.94%) and age 4 for males (47.82%; Table 3-2). Overall, age-specific recruitment probabilities (mean, BCI: 95% Bayesian credible interval) for females were $R^{2yr} = 0.17$ (0.11-0.25); $R^{3yr} = 0.51$ (0.32-0.69); $R^{4yr} = 0.81$ (0.55-0.96); $R^{5yr} = 0.93$, (0.75-0.99); $R^{6yr} = 0.97$, (0.88-0.99); (Figure 3-3a), and for males $R^{3yr} = 0.23$ (0.16-0.33); $R^{4yr} = 0.38$ (0.26-0.51); $R^{5yr} = 0.55$, (0.32-0.75); $R^{6yr} = 0.69$ (0.38-0.90) ; $R^{7yr} = 0.79$ (0.43-0.96); Figure 3-3b). Across the range in age at recruitment, we observed an array of age-specific reproductive outcomes upon the first breeding attempt. The youngest recruitment ages for both males (3yr) and females (2yr) generally failed to produce fledglings on their first attempts, while individuals that recruited at older ages (females 3-4yr; males 4-5yr) had improved reproductive success on their first attempts (Table 3-2).

None of the intrinsic body size or brood related variables were related to female recruitment probabilities, only distance to nearest neighboring nest explained variation in female recruitment probabilities ($\beta_{nnD} = 0.58$, BCI -0.09,1.24; Figure 3-4). As a density-dependent measure of the population, smaller distances (i.e., negative relationships) indicate a higher density of nesting pairs but also suggests congregation in higher quality habitat. We found this exact relationship with male recruitment ($\beta_{nnD} = -0.51$, BCI -1.05,0.00; Figure 3-4) as distance to

nearest neighbor decreased male recruitment probability increased, but the opposite was true in females.

The intrinsic nest dynamics of hatch date and number of siblings were moderately correlated (cor = -0.39; t=-12.41, df = 879, p = 0.0^-16) with earlier nests fledging more offspring, yet there was no support for an interaction term (posterior densities centered on zero), despite our expectations. Hatch date was the only variable that exhibited explanatory power for both the survival (females) and recruitment (males) parameter. Male recruitment showed a strong relationship with earlier hatch dates ($\beta_{hatch♂}$ = -0.22, BCI -0.67,0.22; Figure 3-4), however hatch date did not explain female recruitment (posterior density broadly overlapped zero) and had a positive relationship (later hatch dates better) with female survival ($\beta_{hatch♀}$ = 0.48 BCI 0.02,1.09; Figure 3-4), the sex that requires a longer development time. We observed a strong positive relationship between apparent first year survival with the brood size ($\beta_{brood♂}$ = 0.36, BCI -0.26,1.25; Figure 3-4) and tarsus width ($\beta_{tarsus♂}$ = 1.09, BCI 0.31,1.95; Figure 3-4). Male survival improved with increased structural size and when hatching from a natal nest with more siblings. Estimates of apparent first year survival showed higher rates of male survival, compared to females (Figure 3-5).

Our attempts to model the association between landcover types within natal territories (e.g., composition and proximity variables) yielded no relationships with apparent first year survival nor recruitment probabilities. Model separation, based on WAIC, for distinct single-variable habitat models did not occur and posterior densities were uninformative under the 85% criteria applied (Ch.3 Appendix C). Within the restrictions imposed by our global slack model, there was again no support for relationships between habitat and early life demographic parameters (i.e., posterior densities of habitat variables were uninformative). Because of this and

a similar WAIC score (2 unit separation; Table 3-3) we assert that the "85% group + Nearest Neighbor Distance" (bolded; Table 3-3) is the best explanatory model and use it to provide demographic estimates.

Discussion

By combining a genetically verified morphometric tool for determining ontogenetic sex, hierarchically with a hidden Markov model, we were able to make inference about the early life demography a hemispheric migrant predatory bird. Without the aid of technology, the pre-recruitment years of SWHA are generally unobservable, and nomadic movements of non-breeding juvenile SWHA occurring within the American southwest have only recently been documented (Vennum unpublished). The ability to generate sex-specific demographic rates is crucial for understanding the ecology of a dimorphic species that exhibits sex-linked variation in recruitment age (Becker & Bradley 2007). The age at first reproduction is a demographically important trait (Cole 1954; Stearns 1976), sensitive to a multitude of intrinsic and extrinsic factors, directly influencing individual life history trajectories, fitness, and ultimately population growth rates (Pradel & Lebreton 1999, Oli & Dobson 2003, Stahl & Oli 2006). It is also an individual trait that differs between SWHA sexes, as we illustrated with females proportionally recruiting at younger ages. Given the dynamic range of ages between fledging and recruitment in our study (females 2-6; males 3-7), we expected the environmental covariates to explain variation in estimates of apparent first year survival and recruitment probabilities. The migratory nature and delayed maturity observed in SWHA expose young birds to unmeasurable factors across fourteen different countries, two hemispheres, and demanding an individual survive several complete migrations prior to breeding (Bechard et al. 2020). Yet our modelling efforts

accounting for sex classification uncertainty and long-term field monitoring allowed us to explore the demographics of this relatively unobservable period in their life cycle. Dealing with these challenges is vital to identifying early life conditions or natal habitat types that impart survival advantages (silver spoon effect; Grafen 1988).

An unexpected result of this analysis was the lack of association between any natal habitat variable, proportion or proximity, and our estimated vital rates. Previous work has found that adult survival was negatively correlated with distance from nest sites to nearest agriculture field of any type (Briggs et al. 2011). Yet we found no such relationships for early life demographic performance. However, given the low WAIC score for the nearest neighbor distance model and that three associated parameters (β_{hatch} ♀ ϕ, β_{tarsus} ♂ ϕ , β_{brood} ♂ ϕ) had posterior densities > 85% higher or lower than zero, this suggests that density-dependent processes may be directly important, but could also be masking direct relationships between habitat and early life demographics. Typically, under ideal despotic theory, increases in population density would result in new territories being pushed to lower quality habitats. Given our historic understanding of this population, areas that once held a single breeding pair now contain multiple territories. Increased nesting density and associated reduction in distance between conspecific neighbors could cause the habitat composition of territories to become relatively similar, reducing the inter-territory variation to a point where distinctive habitat effects are not apparent. During the boreal winter this species is quite gregarious on its wintering ground, forming large social flocks into the thousands (Sarasola 2008), a behavior that might explain some measure of tolerance for conspecifics on the breeding grounds. Assuming having closer neighbors is a sign of higher quality habitat (i.e., nearest neighbor distance coefficient with strong negative value) as we find with male recruitment, then we might infer that increased

structural size and brood number, that explained male survival, is related to habitat quality, but masked by density-dependent processes.

Ecological studies have previously found that increased structural size and mass in offspring leads to earlier recruitment later in life (Weimerskirch 1992). Yet recent evidence suggests that climate change is causing many avian species to become structurally smaller (Weeks et al. 2020). Gaining related insights into a dimorphic guild, such as birds of prey, requires accurate sex classification to reveal any similar responses. We did find sex-based differences in how structural size relates to demographic responses, with structurally larger males (compared to smaller males) experiencing higher probabilities of apparent first year survival. However no size-related metrics were identified as good predictors of female demographic parameters. Of the other intrinsic variables in our final model, we also observed a recruitment advantage for males hatched earlier in the season, yet later hatch dates were indicated to be better for female apparent first-year survival. This is an unexpected result given females are the larger sex, requiring more time to fully develop (Chapter 1), and we had originally assumed that hatch date would be a more important trait for females. Moreover, we found that larger natal brood size conferred a positive juvenile survival advantage for only males, not females.

Several studies on long-lived birds with delayed and dynamic ages of first reproduction have explored questions related to the optimal age of recruitment. An individual decision where young birds must weigh the risks of early-life breeding and potential reduction in survival or obtaining poor territory quality, with the potential benefits gaining increased breeding experience and potential fitness gains (Becker & Bradley 2007), trade-offs that could be the result of different individual strategies or intrinsic quality (Fay et al. 2016). For example, female

goshawks (*Accipiter gentilis*) recruiting earlier than the optimal age were observed achieving lower lifetime reproductive success despite no reduction in lifespan (Krüger 2005). While examining fitness related metrics is beyond the scope of this paper, the youngest age classes of recruits, for both females (2yrs) and males (3yrs), generally failed to successfully reproduce the year they recruited, but birds that recruited at older ages often did fledge young on their first attempts (Table 1).

While this study focused on the front end of the recruitment process (i.e., fledging to recruitment), future work should examine the consequences of recruitment age (i.e., younger ages 2-3yrs vs older ages 4-5yrs) on lifetime fitness metrics and disparities between early and delayed recruitment ages. This work should examine the reproductive success of early breeding attempts with specific consideration of mate quality and of the territory obtained upon recruitment. While difficult to directly observe, the number of years spent in a pre-recruitment non-breeding state (floater; Hunt 1998) likely influences the amount of time spent prospecting for territories and influences decisions about mate choice. There are two likely scenarios for birds delaying recruitment age, either there is an advantage to waiting longer (i.e., more time prospecting) that might ensure a higher quality mate or territory, or individuals requiring a longer time to recruit are of lower quality and thus take longer to achieve reproductive status. Our results, while only examining the first reproductive attempt, suggest there may be an advantage to delaying recruitment. Individuals who recruit at early ages have less experience, which could explain their poor breeding success upon the first breeding attempt (Aubry et al. 2009).

While recruitment strategies might vary, the importance of breeding habitat should not be ignored despite our results, as fragmented agricultural landscapes are becoming more common and are likely to increase in global scale (Tilman 2001). Studies able to connect demographic

outcomes to specific crop types could provide mechanistic descriptions on how anthropogenic decisions can enhance or degrade species coexistence and ultimately biodiversity. As the demand to increase agricultural production expands globally, what crops are planted and their ability to simultaneously provide resources for other species will heavily impact species abundance and biodiversity. Where and how we plant crops will also matter as evidenced by the growing scientific debate between land sharing and land sparing (Green 2005). It is easy to appreciate taxa such as raptors, that from a human perspective, provide easily identifiable ecosystem services in the form of pest management control (Kross et al. 2012, Shave et al. 2018), but not all species provide such clear benefits. As conservation practices and laws advance into the future, they will need to consider the implications of human food production and sustainability of ecosystems.

Table 3-1. Summary statistics describing average habitat characteristics and population density metrics across 475 SWHA territories from 2009-2018. The compositional habitat metrics mean (25% quantile, 75% quantile) represent the average proportion and proximity distance across all nests. The nearest neighbor distance is the straight line distance (meters) between nest trees of adjacent SWHA territories. The nearest neighbor count is the number of SWHA territories within 2,000m of the focal nest.

Territory Habitat Metrics	Mean	Q25	Q75
Alfalfa Proportion	0.197	0.032	0.294
Row Crop Proportion	0.042	0.001	0.054
Grassland Proportion	0.323	0.125	0.496
Cereal Grain Proportion	0.203	0.089	0.293
Distance to Nearest Alfalfa	529m	120m	702m
Distance to Nearest Row Crop	911m	355m	1232m

Territory Density Metrics	Mean	Q25	Q75
Nearest Neighbor Distance	1177m	734m	1524m
Nearest Neighbor Count	3	1	4

Table 3-2. Sex specific recruitment rates, delineated by age of first reproductive attempt. Column three (Number %) specifies the proportion of individuals that recruit at each age while column four (success %) is the proportion of individuals who successfully reproduced on their first observed attempt.

	Age (yrs)	Recruit Probability Mean (95% BCI)	Number (%)	Success (%)	Total Fledged
Females	2	0.17 (0.11-0.25)	24.48 (12/49)	16.66 (2/12)	2
	3	0.51 (0.32-0.69)	46.94 (23/49)	47.82 (11/23)	23
	4	0.81 (0.55-0.96)	28.57 (14/49)	50.00 (7/14)	12
Males	3	0.23 (0.16-0.33)	35.29 (18/51)	22.22 (4/18)	7
	4	0.38 (0.26-0.51)	45.10 (23/51)	34.78 (8/23)	14
	5	0.55 (0.32-0.75)	19.61 (10/51)	30.00 (3/10)	3

*SD: standard deviation
*BCI: Bayesian Credible Interval

Table 3-3. WAIC model selection table separated into the three respective steps taken by our statistical approach. The defined "85 group" for each group lists the variables and associated relational direction (+ or -) for those with posterior densities >85% in the same direction as the mean. The habitat variables used to create the global slack model provided no added explanatory power (posterior densities overlap zero), thus biological inference was made from the 85% Group + Nearest Neighbor Distance model.

Intrinsic Models	**Δ W_{aic}**	**W_{aic}**	**W_{aic} (SE)**	**K n.eff**	**K n.eff (SE)**	**ELPD**	**ELPD (SE)**
Tarsus Width	0.0	407.3	38.2	74.6	5.5	-203.6	19.1
Tarsus Width + Mass	1.3	408.6	38.3	75.2	5.6	-204.3	19.1
Hatch Date + Brood Size	2.4	409.7	37.7	75.6	5.1	-204.9	18.8
Hatch Date	2.6	409.9	38.0	75.0	5.4	-204.9	19.0
Brood Size	2.6	409.9	38.0	75.2	5.3	-205.0	19.0
Mass	2.7	410.0	38.2	74.9	5.4	-205.0	19.1
Hatch Date + Brood Size + Hatch*Brood	2.9	410.2	37.5	76.1	5.1	-205.1	18.8
Null	3.0	410.3	38.1	75.1	5.4	-205.1	19.1

Female 85% group = **Survival**(Hatch Date(+)) **Recruit**()
Male 85% group = **Survival**(Tarsus(+) + Brood Size(+)) **Recruit**(Hatch Date(-))

Density Models	**Δ W_{aic}**	**W_{aic}**	**W_{aic} (SE)**	**K n.eff**	**K n.eff (SE)**	**ELPD**	**ELPD (SE)**
85% Group + Nearest Neighbor Distance	**0.0**	**404.1**	**37.7**	**74.8**	**5.2**	**-202.1**	**18.9**
85% Group + Nearest Neighbor Count	6.0	410.1	37.7	75.6	5.2	-205.0	18.8

Global "Slack" Model	**Δ W_{aic}**	**W_{aic}**	**W_{aic} (SE)**	**K n.eff**	**K n.eff (SE)**	**ELPD**	**ELPD (SE)**
85% + Alf + Row + Grassland + Hay + nnD		402.1	37.5	74.8	5.1	-201.0	18.7

*K n.eff is the effective number of parameters in a model
*ELPD is the expected log pointwise predictive density
*nnD = nearest neighbor distance

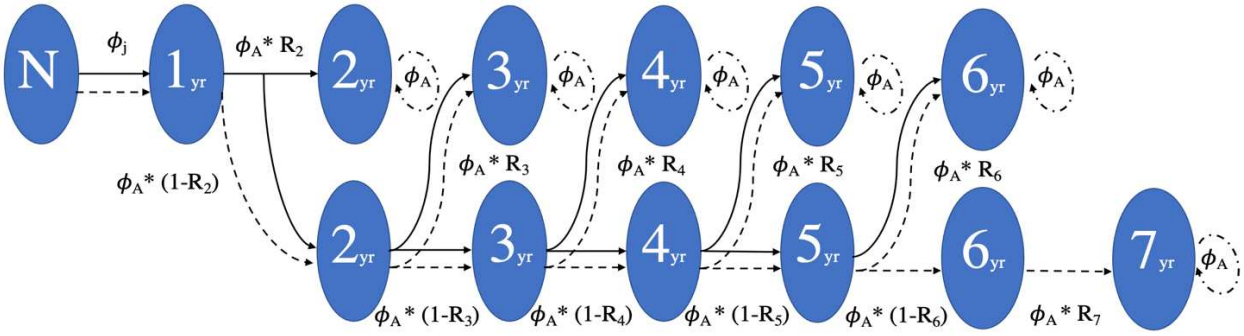

Figure 3-1. Demographic model diagram, where sex is delineated by line type (solid line - females; dashed line – males). Females can recruit at the age of two, but males cannot recruit until three years of age. Female recruitment ages range from 2-6 years old, while the male age range is 3-7 years old.

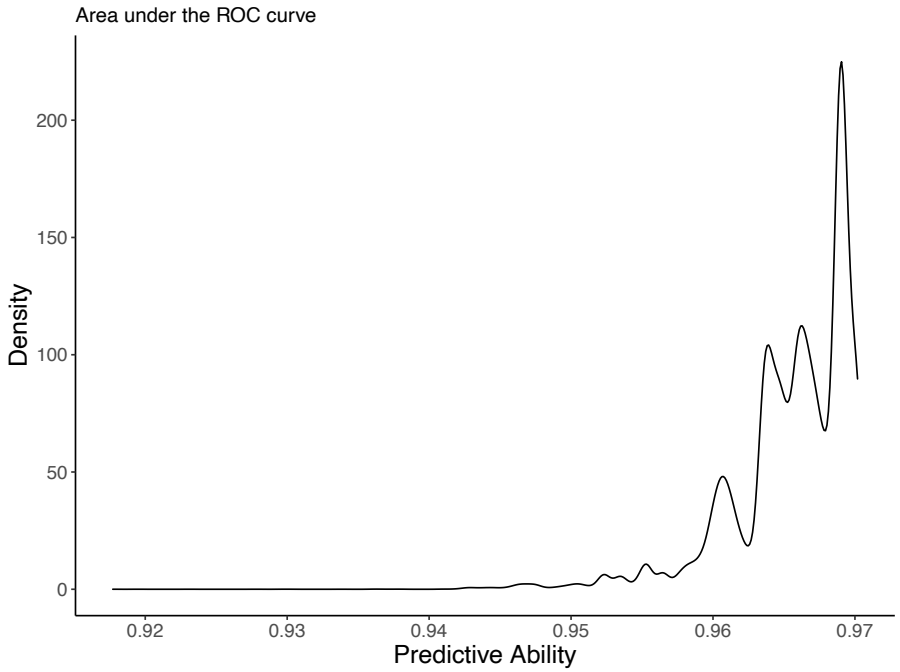

Figure 3-2. ROC curve plot showing the predictive ability of our logistic regression to accurately classify sex.

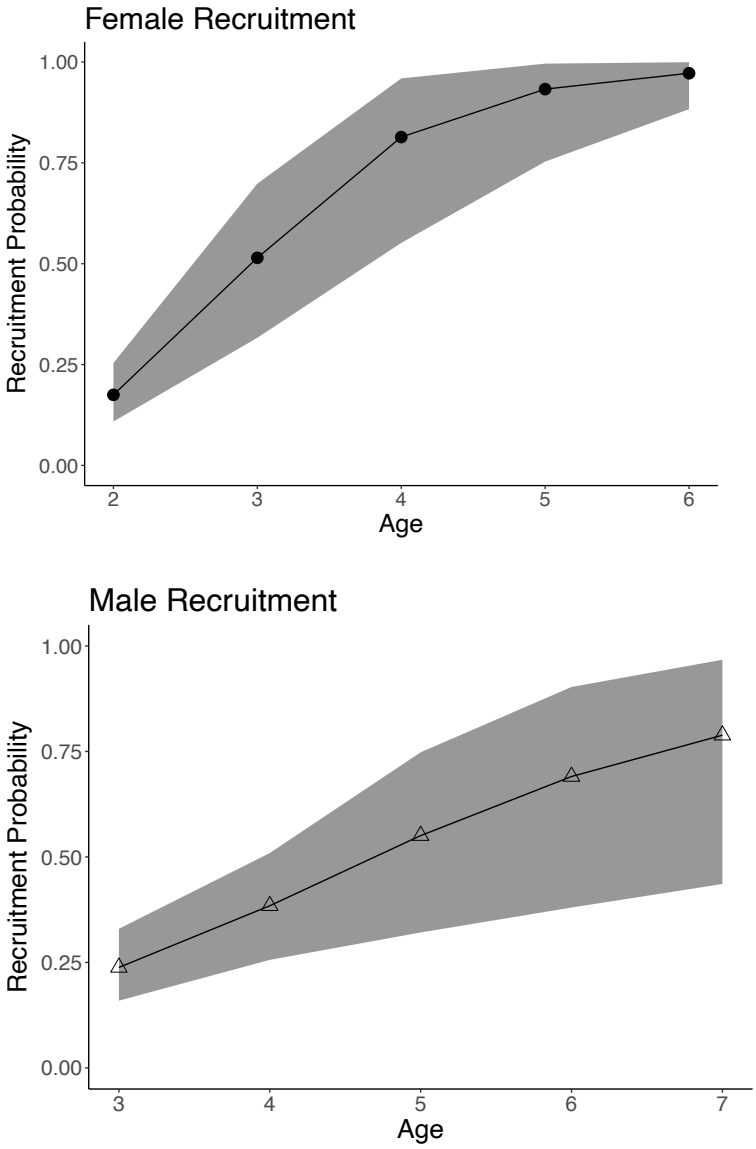

Figure 3-3. Conditional sex- and age-specific recruitment probabilities with 95% Bayesian credible interval. Female (solid circle) recruitment ages range from 2-6 years old, while the male (hollow triangle) age range is 3-7 years old.

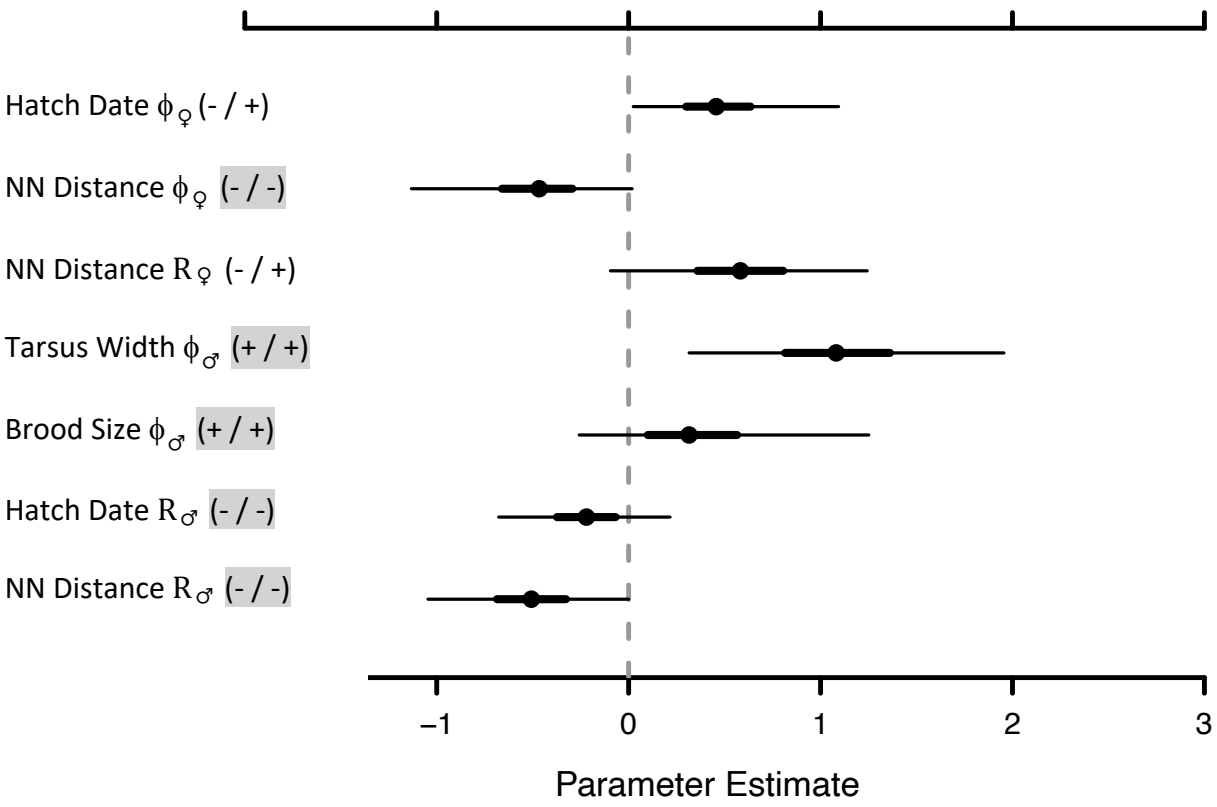

Figure 3-4. Coefficient estimates of the linear predictors from the top inferential model (85% Group + NND). Only variables with posterior densities with > 85% on the same side of the mean are shown. Variables on the y-axis are labelled with a ϕ (apparent first year survival), R (recruitment). Each variable is labelled with the hypothesized relationship direction and the actual result (e.g., - / - ; negative relationship expected / negative relationship found). The y-axis labels highlighted in grey indicate variables where our prediction and actual result match. Error bars on parameter estimates denote 95% Bayesian credible intervals.

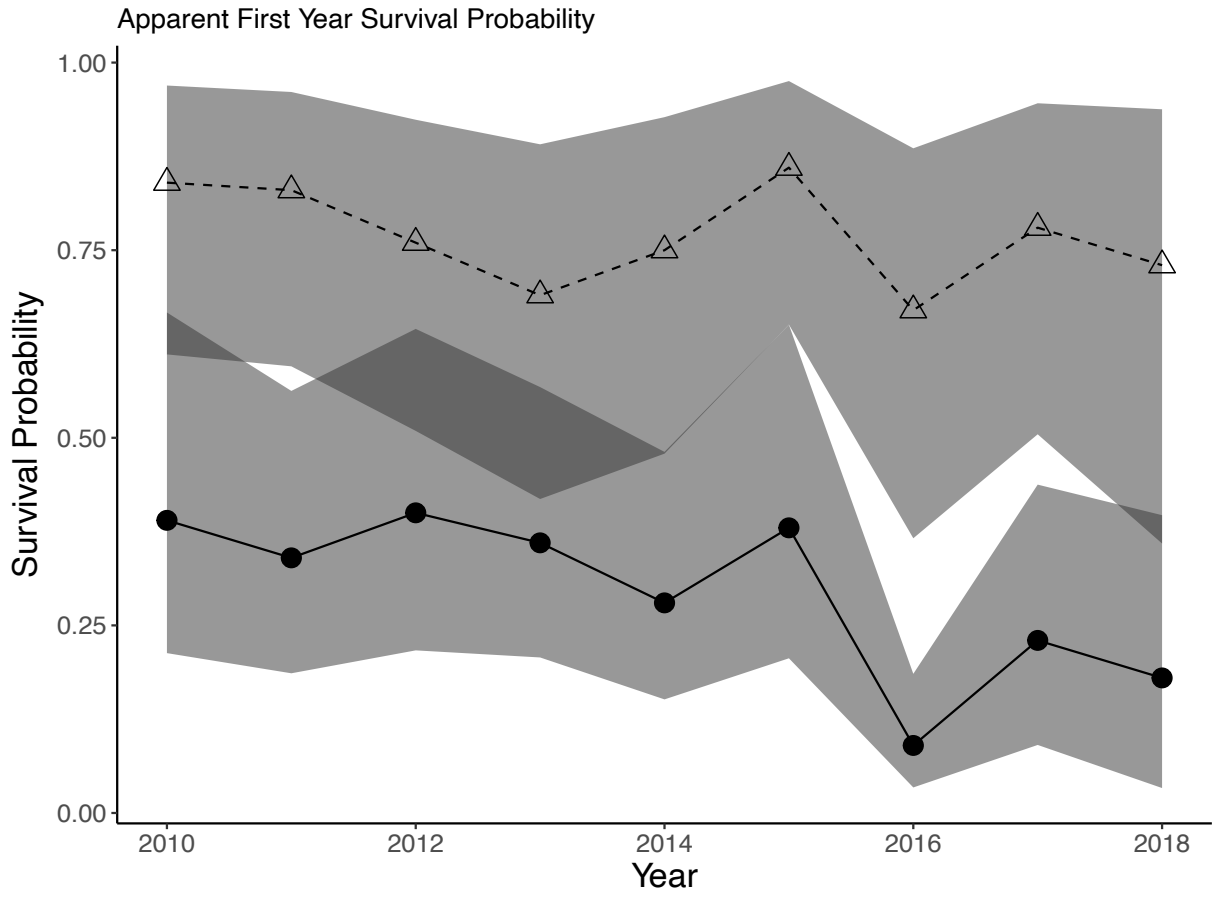

Figure 3-5. Sex-specific apparent survival probabilities during the first year after fledging (conflated with permanent emigration). Males are denoted by triangles with darker grey 95% Bayesian credible intervals, females are denoted by circles with lighter grey 95% credible intervals.

Chapter 4

AGE AND AGRICULTURAL HABITAT EFFECTS ON LIFETIME FITNESS OF A LONG-LIVED AVIAN PREDATOR

Introduction

For a large portion of terrestrial landcover, land has become or is increasing likely to be converted for agricultural or pastural purposes (Foley et al. 2011). Globally, agricultural land already represents a significant proportion of total possible arable land (Tilman et al. 2002), and in the United States has already claimed and converted the most productive areas (Scott et al. 2001). A growing human population will require more land converted to agriculture and more intense growing methods, which will be exacerbated by conversion of lower-quality and less productive lands (Tilman et al. 2001; Haberl et al. 2007). With the increase in agricultural landscapes each year, there are significant concerns associated with declines in biodiversity (Benton et al. 2003; Brennan & Kuvlesky Jr. 2005), especially in a future where the boundaries between nature and anthropogenic land use continue to dissipate.

Whether agricultural lands can provide adequate foraging and other resources needed for wildlife to sustainably reproduce and survive is of paramount concern. For many species to persist amidst global landcover change, they will need to adapt or move into alternative habitats that are becoming increasingly crowded during the Anthropocene (Kremen & Merenlender 2018). However, agricultural activities vary in type and intensity across space and time (Ramankutty et al. 2008). In some regions, crops are well adapted to local conditions and can be incorporated into the natural habitat matrix (e.g., land sharing; Phalan et al. 2011), while other areas require distinct dichotomies between native landcovers (e.g., land sparing in semi-arid landscapes; Fischer et al. 2011). In addition to how agriculture is integrated into the local

environment, individual crop types vary in foraging value to wildlife (Paini et al. 2016). Crops such as irrigated hay and grasses, particularly alfalfa *(Medicago sativa)* are perennial, representing a stable landcover with consistent phenology that can support a diverse food web (Putnam et al. 2001). Foods grown through row-crop styles of practice (e.g., potatoes or strawberries) are generally annual crops, require large and intense soil disruption, are effectively sterile environments for wildlife, and are constantly changing (though some, such as cereal grains, can provide substantial amounts of food to wildlife at particular times of the year).

This concept of stable vs dynamic landcover types is particularly important for migratory species that are biologically under strong phenological constraints to successfully reproduce each year. Extended migrations restrict the time available for prospecting new areas, emphasizing the importance of habitat quality and consistency across space and time. Habitats that provide environmental constancy may be important yet limited in a future where global food production requires rapid rates of land conversion to agriculture, a scheme that changes frequently due to local or global demand and economics. Identifying crops that can fulfill human needs, support wildlife, and can provide constancy of habitat on the landscape will be important to conservation. While many different metrics could be used to examine the effects of crop types on wildlife (e.g., occupancy, utilization time, reproductive attempts), none are better than evolutionary fitness.

Yet obtaining fitness data, especially for long-lived species, can require decades of intense effort, and observational uncertainty is a *sine qua non* in studies of wild populations that presents additional challenges (Gimenez & Gaillard 2018). Longitudinal studies commonly observe heterogeneity in survival and reproductive success among individuals and groups (Jenouvrier et al. 2018), particularly in avian and mammalian species where a few individuals produce a disproportionate number of recruits into the breeding population (Clutton-Brock 1988;

Newton 1989). Such variation in fecundity often produces a zero-inflated and highly skewed distribution of reproductive success (Tuljapurkar et al. 2020). A variety of factors have been noted to explain this variation, such as environmental conditions (Jenouvrier et al. 2015), individual heterogeneity (Cam et al. 2002), and age (Fay et al. 2016). A growing body of evidence suggests much of this variation in fitness across individuals might be explained by stochasticity (Caswell 2009; Caswell & Vindenes 2018), and that random "luck" can impede inference about mechanistic relationships between fitness and individual traits (Snyder & Ellner 2018).

We examined relationships between the environment and individual reproductive success of Swainson's hawks (*Buteo swainsoni;* hereafter SWHA), a hemispheric migrant and top avian predator that has adapted well to agricultural environments (Bechard et al. 2020). Specifically, we matched an individual-based demographic dataset (1985-2020) with remote sensing techniques to understand the dynamic interaction between agricultural practices at the territory level and individual fitness across nearly four decades. To account for imperfect detection and potential biases in estimating fitness metrics, we used hierarchical Bayesian multi-event models (Gimenez & Gaillard 2018). We examine lifetime reproductive success (LRS) across several themes representing the spatial and temporal extent of agriculture practices across the landscape, while considering potential effects of density dependence, given the recent increase in population abundance and decreasing inter-territory distances. Overall, we examine important demographic parameters under the assumption of non-stationary environmental processes, key to advancing our understanding of vertebrate populations (Hoy et al. 2020) and hopefully useful for informing future land use policies and agricultural development.

Methods

Study Area

Butte Valley, California (41˚ 49'N, 122˚ 0'W; 415 km^2) was natively a high elevation (1,280 m to 1,340 m) sagebrush steppe environment, but now contains a heavily grazed national grassland and abundant agriculture fields (Woodbridge 1991). Located on the western boundary of the Great Basin ecotype, there are clear differences in primary productivity between arid natural grassland/sagebrush and groundwater irrigated agriculture, a common landscape feature in the western United States. An abundant local crop and primary foraging habitat, irrigated alfalfa provides consistent and high prey densities (Whisson et al. 1999). Belding's ground squirrels (*Urocitellus beldingi*) are the dominant prey species for the first half of the breeding season, a key resource for hawks refueling after completing spring migration. Ground squirrel distribution is patchy, and is densest in irrigated hay crops, which is why increased alfalfa availability is thought to have a positive effect on SWHA reproduction (Battistone et al. 2019). Additionally, alfalfa is a perennial crop, often with a stand life in the Intermountain West of 6-8 years (Orloff 1997), so not only does it support food web communities, it is a relatively constant habitat feature on the local landscape. Belding's ground squirrels locally estivate in late June after which time SWHA prey composition broadens in diversity to include pocket gophers (*Thomomys* spp.), voles (*Microtus* spp.), reptiles, small bird species, and insects (Woodbridge 1991).

Demographic Data Collection

From 1985 – 2020 the study area was annually surveyed for breeding SWHA. Surveys typically began in late April, corresponding with the arrival of hawks from a northerly spring migration and terminated in mid-August after all young have fledged and territorial boundaries diffuse. Nests were routinely monitored to determine the presence and status of offspring so they

could be marked upon reaching a suitable age for banding (see below). Unmarked adults were trapped using a Great Horned Owl (*Bubo virginianus*) lure with a dho-gaza net (Bloom et al. 1992) or opportunistically with a bal-chatri (Berger & Mueller 1959) and subsequently marked with both a U.S. Geological Survey (USGS) aluminum band and a unique alphanumeric color band. Extensive time and effort were spent each year resighting color-banded individuals within their territories. From 1985 to 2007, nestlings were only banded with a USGS aluminum band after they reached ≥3 weeks of age. After 2007 all offspring were individually marked with a USGS aluminum band and a unique alphanumeric plastic color band. Color banding nestlings improved detection probabilities, as newly recruited individuals could easily and accurately be identified through band re-sighting without the need for physical capture. We assumed any nestling that reached 36 days of age fledged successfully (i.e., 85% of fledging age; Steenhof 1987) and was thus included in the dataset for fitness estimation. Because our main goal here is to examine drivers of individual fitness, we focus specifically on the sample of color-marked breeding adults and their annual reproductive success. For those breeders that were marked as nestlings and then later settled in the study area (i.e., recruits), we could assign an exact known age. For previously unmarked adults displaying full adult plumage at the time of initial marking, we assigned an age of 3 years for their first observed breeding attempt (Briggs 2011), thus assignment of individual age for some breeders is conservative.

Study protocols and procedures were approved by the Institutional Animal Care and Use Committee at the University of Nevada, Reno (IACUC approval no. 00115 and 00522) and Hamilton College (IACUC approval no. 18-R-3).

Habitat Evaluation

While rasterized crop databases exist for the United States (i.e., USDS NASS Cropland Data Layers; USDA National Agricultural Statistics Service) we found that these databases were inaccurate for our study site with respect to key crop types. We opted instead to implement a supervised classification scheme using a random forest algorithm (Breiman 2001) and Google's Earth Engine platform (Gorelick et al. 2017). Landcover classification rasters were created using Landsat 5 (1985-2011), 7 (2012), and 8 (2013-2020) satellite imagery to match the longevity of our demographic dataset. All satellites generate 30m resolution data, accurate enough to identify distinct crop types. Ground-truthed data were collected in 2018 and 2019. Raw spectral band values for six bands (red, green, blue, near infrared, short-wave infrared 1, and short-wave infrared 2), in addition to calculating a normalized difference vegetation index (NDVI) and a soil-adjusted vegetation index (SAVI) were used to define the spectral signatures of each landcover feature class. We identified eight distinct landcover types within our study area that could be represented by distinct spectral signatures across a calendar year. These included [1]alfalfa, [2]dryland hay, [3]juniper, [4]bare dirt, [5]grassland dark, [6]grassland light, [7]row crop type #1, and [8]row crop #2.

As certain crop types present different spectral signatures throughout the growing season, we partitioned annual satellite imagery into three "seasons" to better match vegetative phenology and increase our predictive accuracy. The spring signature was based on images from April and May, summer from June-August, and the fall signature was defined with September and October images. Of the 36 years modelled, most followed these exact phenological time definitions, while a few years required temporal adjustments due to obstructions such as late spring snows and fall smoke haze from forest fires. When necessary, we selectively removed images from the

composition or applied an image masking function for clouds and shadows (i.e., QA_PIXEL Landsat band). As "season" images are composites of multiple aerial images we extracted the median pixel value for a season from the assigned image collection, resulting in three spectral values for annual classification.

Representative pixels of each of eight landcover types from all three seasons were extracted from our 2018 ground-truth data, exported out of GEE, and imported in program R (Version 4.1.0). Using the package *VSURF* (version 1.1.0; Genuer et al. 2015) we performed a three-step variable selection procedure to reduce the number of spectral bands inputted into our supervised random forest algorithm and collinearity, thus band pairings exceeding correlation factors of 0.80 were eliminated. This reduced band set was then used to train our classification model based on ground-truth data from 2018. The accuracy of which was then tested by its ability to predict a sample of points from 2019 imagery, also ground-truth data.

Post creation of annual classified habitat rasters, the number of landcover classes was reduced from the original eight to six types. Farming practices, such as the use of plastic to cover row crops (i.e., strawberry plants) early in the growing season create unique spectral signatures, a feature that enabled us to classify row crops more accurately by modelling them separately (plastic vs non-plastic) and merging pixel types in Program R post classification. We applied this same process (separate classification, post analysis recombine) with two distinct vegetative types (darker sage and lighter grasses) found primarily across the Butte Valley National Grassland to better account for the vegetative complexity of this habitat type. Our finalized raster images, comprised of six landcover types, were overlaid with nest locations and territorial buffers to extract habitat data. Our supervised raster classifications produced pixel noise, which can introduce error into the nearest-distance measures of a nests' proximity to particular categories of

habitat. Pixel grouping size of identical landcover types were measured using the clump function in the Raster package (v3.6-3; Hijmans 2021) with cells connected through 8-directions and all pixel groupings under six pixels in size were removed.

Swainson's hawks are a highly territorial species during the breeding season (e.g., April-August) and as such follow a central-forging strategy from nesting locations (Orians & Pearson 1979). We assigned each territory a 1 km radius buffer (3.14 km^2). An assumption that we formed based on averaging the results of two previous radio-telemetry studies for this species. Two years of radio-telemetry observations in the Dakotas found a 95% MCP = 1.91km^2, (n=10, 2013) and 95% MCP = 2.10km^2, (n=9, 2014; Inselman et al. 2016). In addition, early telemetry work on this population found mean foraging distances for breeding males (0.917km; radius) and average home range size (4.05 km^2, n=12; Woodbridge 1991). Thus the habitat composition of each individual territory was defined by the extracted pixel counts of each landcover type within this defined boundary and conveyed as proportional data. Given the high density of nesting birds and strong site fidelity observed in this species, the distribution of nesting territories likely forms according to an ideal despotic process (Fretwell & Lucas 1970) where some territories will lack prime foraging habitat within the territorial buffer, and thus will be forced to travel farther to obtain resources, which may influence adult survival (Briggs et al. 2011a) and reproductive success, the latter of which has not yet been investigated. Thus, we measured the distance from each nest to the nearest alfalfa and row crop field and included them as explanatory variables as they may affect demographic performance in ways not explained by habitat composition within the 1 km radius territory.

Statistical Approach -Transitions in Reproductive Success over the Lifespan

We applied a multi-event modelling approach (Pradel 2005) with longitudinal capture – mark – resight (CMR) data collected at the individual level to understand how fine scale territorial habitat features influence survival and transition probabilities between reproductive states (Kendall et al 2003; Kendall et al 2004; Figure 4-1). By using these models in a state-space framework, we were able to accommodate 'reproductive state uncertainty' for some observations collected during the breeding season, such as cases where we saw an individual and knew it was alive but we did not see the individual at a nest. The multi-event framework allows the observations to be associated probabilistically with latent state dynamics of actual breeding success, amidst state-assignment uncertainty for certain types of observations (Pradel 2008, Gimenez & Gaillard 2018). In turn, this allows for the incorporation of more data (i.e., no censoring) so that more individuals can be included in the analysis, and such models have been shown to provide more precise and more representative estimates than traditional multistate models (Conn & Cooch 2009), while ignoring such instances of imperfect state assignment could lead to flawed estimation of focal parameters if censoring is not random (Gimenez et al. 2008). In most cases the annual breeding success of individual SWHA was observed without ambiguity (e.g., failed breeder, 1 nestling fledged, etc.). The maximum brood size for SWHA is four nestlings, which occurs uncommonly, thus nests that produced 3 or 4 fledglings were combined into a single state of breeding success (3+). State assignment uncertainty manifests when individuals are resighted but their reproductive status could not be ascertained, creating a fifth observational category. Past annual detection probabilities for this study population (i.e., the chance a live bird on the study area is detected at all), while high most years (i.e., above 70%), is also not perfect (Briggs 2011) and requires attention when modeling observation probabilities.

Multinomial likelihoods were constructed under a Bayesian framework (eq. 1 & 2), with an associated generalized logit link function, which upon back-transformation ensures that the joint probability sums of the state transitions do not exceed 1.0 (Williams et al. 2002). The apparent survival and transition probabilities (state matrix, M1) between reproductive states were used to estimate individual trajectories of latent breeding success ($X_{i,t+1}$). These statistical transitions represent the biological effect of the previous breeding attempt on the current reproductive success. For example, if an individual produces one fledgling in year ($X_{i,t}$) then we estimate the probability in $X_{i,t+1}$, of being in four possible states (fail, 1, 2, or 3+ offspring). With four possible annual reproductive states, this produces sixteen total transition probabilities (ψ). Probabilities that are conditional on previous breeding success ($X_{i,t}$), apparent survival probability ($\phi_{i,t}$), and hierarchically, the state-assignment (δ) and detection probabilities (p) corresponding to the observed encounter histories ($Y_{i,t}$):

$$X_{i,t+1}|X_{i,t} \sim multinomial(1, X_{i,t}, \boldsymbol{\phi}_{i,t}) \quad \{eq.1\}$$

$$Y_{i,t}|X_{i,t} \sim multinomial(1, X_{i,t}, \boldsymbol{P}_{i,t}) \quad \{eq.2\}$$

where bold font denotes matrix notation.

While detection probabilities (p) are based on annual resights of breeding individuals and modelled using an auto-regressive time random effect (Funatogawa & Funatogawa 2018), we applied a multi-event framework to account for the occasional inability to determine the reproductive outcome of a given breeding attempt with certainty. This was achieved by adding probabilities of 'state assignment uncertainty' to the probabilistic map between observations and latent states (eqn. M2; Pradel 2005; Kendall 2009).

This observation uncertainty is specifically associated with annual reproductive status (observation matrix, eqn. M2) and represented by two separate δ parameters that accounted for observations where individuals were observed alive in the study area during the breeding season, but their nest was not located. One parameter (δ_1) was assigned to the failed reproductive state, while (δ_2) represented all three successful reproductive states. This assumes that our ability to find nests is similar if there are any number of offspring in the nest, which will prolong adult presence and localization of daily activities around the nest.

$$\boldsymbol{\phi}_{i,t} = \begin{array}{c} \\ Fail \\ Fledge\ 1 \\ Fledge\ 2 \\ Fledge\ 3^{+} \\ Dead \end{array} \begin{array}{c} \begin{array}{ccccc} Fail & Fledge\ 1 & \text{Fledge 2} & \text{Fledge } 3^{+} & Dead \end{array} \\ \begin{bmatrix} \phi^{s1}\psi^{s1\to s1} & \phi^{s1}\psi^{s1\to s2} & \phi^{s1}\psi^{s1\to s3} & \phi^{s1}\psi^{s1\to s4} & 1-\phi^{s1} \\ \phi^{s2}\psi^{s2\to s1} & \phi^{s2}\psi^{s2\to s2} & \phi^{s2}\psi^{s2\to s3} & \phi^{s2}\psi^{s2\to s4} & 1-\phi^{s2} \\ \phi^{s3}\psi^{s3\to s1} & \phi^{s3}\psi^{s3\to s2} & \phi^{s3}\psi^{s3\to s3} & \phi^{s3}\psi^{s3\to s4} & 1-\phi^{s3} \\ \phi^{s4}\psi^{s4\to s1} & \phi^{s4}\psi^{s4\to s2} & \phi^{s4}\psi^{s4\to s3} & \phi^{s4}\psi^{s4\to s4} & 1-\phi^{s4} \\ 0 & 0 & 0 & 0 & 1 \end{bmatrix} \end{array}$$

{M1}

$$\mathbf{P}_{i,t} = \begin{array}{c} \\ Fail \\ Fledge\ 1 \\ Fledge\ 2 \\ Fledge\ 3^{+} \\ Dead \end{array} \begin{array}{c} \begin{array}{ccccccc} \text{Obs. Fail} & \text{Obs. F1} & \text{Obs. F2} & \text{Obs. F3}^{+} & \text{Obs. Alive Rep.} & \text{Unk} & \text{Not Obs.} \end{array} \\ \begin{bmatrix} \delta_1 * \mathcal{P} & 0 & 0 & 0 & (1-\delta_1) * \mathcal{P} & & 1-\mathcal{P} \\ 0 & \delta_2 * \mathcal{P} & 0 & 0 & (1-\delta_2) * \mathcal{P} & & 1-\mathcal{P} \\ 0 & 0 & \delta_2 * \mathcal{P} & 0 & (1-\delta_2) * \mathcal{P} & & 1-\mathcal{P} \\ 0 & 0 & 1 & \delta_2 * \mathcal{P} & (1-\delta_2) * \mathcal{P} & & 1-\mathcal{P} \\ 0 & 0 & 0 & 0 & 0 & & 1-\mathcal{P} \end{bmatrix} \end{array}$$

{M2}

Statistical Approach - Age

For many long-lived species aging is a dynamic process (gained experience, senescence) known to affect reproductive performance (Hamilton 1966) and survival probabilities (Weimerskirch 1992). Earlier work on this population found that the average age of breeding adults is nine years old (Kane et al. 2020). Using a model selection approach with the WAIC scoring statistic, we built models that classified individuals into two age groups (prime-age vs. old). We searched for the break in age between the two groups, from a range of 7-13 years of age for the break, and used WAIC to evaluate which break in age was most supported by the data. Once defined, an individual's age ($Age_{i,t}$) was applied in a linear fashion to explain variation in the apparent survival parameters by reproductive state (denoted subscript "s" eq.3 & eq.4).

$$logit\left(\phi_{s,t}^{PrimeAge}\right) = \beta\emptyset_s + \varepsilon_t \quad \{eq.3\}$$

$$logit(\phi_{s,t}^{OldAge}) = \beta\emptyset_s + \beta_s^{Age} + \varepsilon_t \quad \{eq.4\}$$

This was done in a deterministic fashion, producing eight different apparent survival parameters, four for prime ages and four for old-age categories matching the four possible reproductive states. Each survival parameter included a unique intercept and shared time random effect (i.e., an additive random effect of year), with the old age classes distinguished by an additional coefficient for age. A logit link was applied to ensure all estimated survival probabilities were constrained between 0-1.

Statistical Approach - Covariates

To explain spatial and temporal variation in the probabilities of transitioning ($\psi_{state,time}$) from one reproductive state at time *t* to any other at *t* + 1, we applied a mixed link-linear model function of environmental covariates and random effects. This was accomplished statistically by

specifying a series of linear models (12; last four transitions calculated complementary) for the starting state of possible transitions, where each model has a random intercept ($\beta 0_{1\rightarrow 12}$) and random slope coefficient parameter ($\beta habitat_{1\rightarrow 12}$). The explanatory covariates were allowed to be unique among origin transitions (i.e., covariate effects were allowed to interact with the starting state). A random time effect was also added across transitions for each state block (e.g., the four transitions involving origination in "failed" state all received the same random time effect; see eq.5 below for an example of a link-linear prediction equation).

$$\psi_{s,t}^{Fail\rightarrow 1} = \beta 0_x + \beta habitat_x + \varepsilon_t^{Fail} \qquad \{\text{eq.5}\}$$

To ensure the use of vague priors on these habitat covariates we applied a dlogis(0,1) distribution to each estimated β coefficient as the typically applied normal priors can unintentionally influence posterior estimates on the probability scale (Northrup & Gerber 2018).

We built separate models for each landcover explanatory variable using the respective proportional amounts of each category within the defined territory buffers. To evaluate the effect of proximity of a nest from our perceived best habitat (alfalfa, which supports ample small mammal food resources required for SWHA rearing of chicks) and worst habitat (row crops, provides zero food resources), we specified similar blocks of mixed link-linear model structures with covariates specifying the distance between a nest location and the nearest patch of these 'best' or 'worst' habitats. Distance metrics to agriculture have previously been shown to influence apparent survival in this population (Briggs et al. 2011a), but agriculture was defined as an aggregate term where crop types were not separated, and possible effects on reproductive success have never been evaluated. Additionally, we considered two indices of population density because the SWHA study population roughly doubled over the past two decades

(Vennum 2017). These were represented by the distance (meters) to nearest neighboring conspecific nest and the number of SWHA nests within 2000m meters of a given nest.

Statistical Approach – Bayesian Estimation

Within Program R (Version 4.1.0) we utilized the jagsUI package (Version 1.5.1) to construct models and the MCMCvis package (Version 0.15.2) to visualize results and confirm parameter convergence. Posterior distributions were obtained for annual survival and state transitions using Markov chain Monte Carlo (MCMC) simulations across three independent Markov chains (King et al. 2010). Each chain was run for 100,000 iterations, with a 1,500 adaption phase, followed by an initial burn-in of 8,500 samples, and a thinning rate of 5. Each chain was represented by 18,300 runs generating a total of 54,900 saved samples. Convergence was confirmed using visual inspection and $\hat{R}$ values <1.2, which measures the within and between variability of chains initiated at different starting values, as recommended in Gelman et al. (2004).

Statistical Approach – Derived Parameters & Lifetime Fitness

In studies of wildlife where imperfect detection is the norm, not the exception, it is impossible to estimate lifetime reproductive success (LRS) and other measures of lifetime individual fitness directly (Clutton-Brock 1988). But recent advances in Bayesian CMR methods have revealed how latent states of per-time-step fitness performance, $X_{i,t}$, can be estimated and summarized over an estimated lifetime to derive measures of lifetime fitness in a probabilistic manner (Gimenez and Gaillard 2018). The advantages of the Bayesian approach are that a) when reproductive outcomes are not observed (i.e., unobserved reproductive state or not observed at all) the latent state of being alive and reproducing at a given level can be estimated, and b) full posterior distributions of each $X_{i,t}$ can be estimated, allowing for exact propagation of

uncertainty up to derived measures of lifetime fitness, such as LRS. This in turn allows one to examine fitness-related study objectives comprehensively, as opposed to studying components of fitness one at a time.

$$LRS_i = \sum X_{i,t} \quad (for\ all\ X \neq Dead\ State; eq.M1)$$

Results

From 1985-2020 a total of 211 individually marked adult female Swainson's hawks were monitored to determine annual survival and reproductive outcomes across their lifespan, representing 890 observed reproductive events. Of these observed attempts 27.53% (245) were failed nesting occasions, followed by 20.67% (184) fledging a single chick, 30.22% (269) two chicks, 20.57% (192) three or more chicks fledged, with an additional 65 observations classified as reproductive status unknown. While the age of breeding females ranged from 2 years to a maximum age of 28 years, we identified a biological age distinction in apparent survival between prime-aged and older individuals. By estimating survival probabilities, conditioned on current reproductive state (in year *t*), we found that classifying individuals < 10 years old as prime-aged, and individuals ≥ 10 as older, fit our data best and provided a metric for distinguishing age effects on SWHA demographic performance (Ch. 4 Appendix).

The transitions among reproductive states also indicated relatively consistent reproductive output at the individual level. For each reproductive state, except the most successful breeding state (3^+), the highest probabilities were associated with remaining in the same state from one year to the next (Figure 4-2). A high probability of remaining in the same reproductive state represents a high degree of reproductive constancy for individuals. Regardless of age, individuals that failed to reproduce in a given year experienced lower survival

probabilities (mean 0.81 BCI 0.76,0.85 prime aged; mean 0.75 BCI 0.54,0.92 old aged) compared to conspecifics that were reproductively successful. The lower survival probability for failed breeders is exacerbated by a strong probability that once an individual failed to successfully reproduce, they were likely to consecutively fail again ($\Psi^{0\rightarrow0}$), with a probability of 0.41 (BCI 0.29,0.51) (Table 4-1). For reproductively successful individuals, annual survival probabilities remained high for individuals in all successful reproductive states (e.g., 1, 2, 3+ chicks fledged), the exception being "old" breeders that produced two offspring in a given year, which had a markedly lower survival probability (mean 0.63 BCI 0.45,0.80). Annual apparent survival probabilities, distinguished by age class and reproductive state are shown in Figure 4-3.

Lifetime reproductive success values produced a left-skewed distribution (Figure 4-4). Illustrated by many individuals (12.3%; n=26) failing to fledge any offspring over their entire life, and a large percentage (40.3%, n=85) fledged four or less over their lifespan, a quantity that can potentially be achieved in a single reproductive attempt for this species. In fact, 31.8% (n=67) of females fledged 10 or more offspring, and only 9.0% (n=19) fledged 20 or more offspring, with the maximum for any female being 36 fledged offspring. While our results show substantial variation in LRS, we failed to find a relationship between any of the environmental or population density explanatory variables and the (ψ) transitions among reproductive states, and therefore a lack of any relationship with LRS. In fact, only the proportion of juniper woodlands, a habitat representing nesting substrate, received more support than our null model for explaining spatial and temporal variation in the (ψ) reproductive transitions (ΔWAIC 12.1, Table 4-2). All remaining models of habitat proportions within the breeding territory were outcompeted by the null model. Similarly, both habitat proximity measures (alfalfa and row crops), had the worst fit to our data, as indicated by the highest ΔWAIC values (ΔWAIC 17.3 alfalfa; ΔWAIC 17.4 row

crop; Table 4-2). While model selection provided no distinction between the proximity models (ΔWAIC 0.1), alfalfa fields were consistently closer to nesting sites. The average distance to the nearest alfalfa field was 493m, while the average distance to the nearest row crop field was nearly double (822m, Table 4-1).

Over the course of this study, the population of nesting SWHA consistently grew in abundance and doubled since 2000, a population feature that is evident in the decreasing average distance to nearest conspecific neighbors' nest from 1985-2020 (Figure 4-5c). Yet, our two measures of population density, nearest neighbor distance and number of neighbors within 2,000m (Table 4-1), both received less support than the null model for explaining annual reproductive outcomes (Table 4-2). However, the increase in nesting density does correlate with the abundance of alfalfa over time (-0.48; t = -3.25, df = 34, $P = 0.002$), which through our remote sensing modelling revealed an overall increase in the amount of alfalfa, the primary foraging habitat over the study duration (Figure 4-5a). The overall field space allocated to row crop production has remained below that of alfalfa, despite some annual fluctuations in quantity and lack of trend over the same time (Figure 4-5b.).

The probability of correct assignment for successful breeders ($\hat{\delta}_2$) was 0.98 (BCI 0.95,1.00), while the assignment for failed breeders ($\hat{\delta}_1$) was lower 0.77 (BCI 0.702,0.855; Table 4-3). Overall, detection probabilities ranged from 0.39-0.94 across 1986-2019, with a mean of 0.71 (BCI 0.68,0.73) and a few years of lower resight probability in the early 2000's due to decreased field crew size (Figure 4-6).

Discussion

The lifetime reproductive success values estimated here reveal the cumulative efforts and variation in fitness among individuals existing within a dynamic landscape that is heavily modified by the anthropogenic sources of modern agriculture (Reynolds et al. 2019; Tuljapurkar et al. 2021). However, our analysis failed to find direct associations between the spatial and temporal components of agricultural crops, native shrub-steppe habitat, or conspecific nesting densities and the annual components of reproductive success that comprise this metric of lifetime fitness. Although the juniper woodlands model did outcompete the null model, biologically we interpret this landcover type more so as the availability of nesting substrate (Woodbridge 1991). Juniper woodlots commonly exist on the edges between agricultural fields providing limited foraging opportunities. The weak explanatory power of our remaining landcover types, consequently, implies that we could not draw inference on how the availability of other habitats within the breeding territory (ranging from 0-100%) might influence annual SWHA reproductive success and net fitness (LRS). Our CMR statistical methods accounted for both imperfect detection and observed breeding state uncertainty, producing quality measures of individual fitness that are not confounded with nuisance parameters (as in many historical studies of LRS). Yet, our hypotheses that proportions (or distance to) of irrigated alfalfa and intensive row crop agriculture within an assumed territory radius would strongly explain spatio-temporal variation in reproductive success were not supported by the data. This lack of association between habitat and annual reproductive success, nor LRS, suggests at least three potential avenues of explanation. First, despite our monitoring efforts of nearly 900 nesting attempts across more than three decades, it may be that we still do not have enough data to model the annual reproductive transitions across the range of brood sizes for this species at an individual level (annual sample sizes ranged from 12-53). This raises concern as to how scientific monitoring can inform the

impact of management and land-used practices on fitness, when this quantity of data may be insufficient for nearly all birds of prey. Second, the roles of individual heterogeneity and stochasticity across the 211 studied individuals may be strong in long-lived vertebrates, and overriding more subtle effects of occupied nesting habitat (Steiner & Tuljapurkar 2012; Hamel et al. 2018). For example, if there are individual traits that have a stronger influence on fitness than nesting habitat, the sample size of 211 individuals may make it difficult to detect subtle but potentially important effects of breeding territory habitat. Thirdly, wildlife-habitat relationships depend on how an individual uses information about the landscape to make decisions, and individuals are likely using information at multiple spatial scales (Stuber et al. 2017). Accurately incorporating habitat characteristics into any modeling framework can be difficult when a relevant spatial scale is unknown and when different ecological processes interact across multiple scales. Our decision to use a fixed single scale 1km radius buffer, while informed by previous studies, could create a mismatch between the spatial scale of our analysis and actual biological processes, hindering biological inference (Keitt et al. 2002). Continued effort into this study system will consider alternative scales in forthcoming work.

For wildlife managers and those creating conservation strategies, ideally a large portion of variation in fitness could be explained through direct habitat associations, but it is important to note that individual fitness values are the cumulative sum of random events (e.g., longevity, reproduction) across a lifetime (Tuljapukar et. al. 2020) and subject to both individual heterogeneity and stochasticity (Jenouvrier et al. 2022). Heterogeneity refers to individual trait differences (Cam et al. 2016), which in this study of a territorial species includes variability in territory habitat composition. Stochasticity, on the other hand represents demographic outcomes due to random chance (e.g., coin flip outcomes; Snyder & Ellner 2016; Tuljapurkar et al. 2020).

The contributions of these two forces to life-history outcomes varies across studies (e.g., Caswell & Vindenes 2018; Jenouvrier et al. 2018), but recent work suggests that these two factors can contribute differently under certain types of environmental conditions. For another long-lived avian species, the southern fulmar (*Fulmarus glacialoides*), favorable (less limiting) conditions decreased the contributions of individual heterogeneity, while increasing that of individual stochasticity, and vice versa, consistent with expectations that natural selection would be strongest in limiting environments (Jenouvrier et al. 2022).

Within the Butte Valley study system and the generally arid Intermountain West region, annual precipitation is a major driver of primary productivity. Yet the constant irrigation of alfalfa decouples this habitat type from fluctuations in rainfall. Our habitat modeling has shown a constant increase in alfalfa abundance over time (Figure 4-5), and its consistency on the landscape could reduce the importance of annual precipitation to drive primary and secondary productivity, shielding individual SWHAs from unfavorable environmental conditions. Yet, the environmental decoupling and constancy of irrigated alfalfa on the landscape may still be an important driver behind local SWHA population growth. Despite strong breeding site fidelity, our simplified post-hoc examination of the "territory constancy" (variance) of habitat proportions across time also failed to reveal any notable correlations with LRS (Table 4-2). Our lack of hypothesized findings may lend more credibility to the role of stochasticity in shaping individual dynamics and life history outcomes than actual individual heterogeneity in traits and habitat use per se.

A large portion of the literature on avian life history variation focuses on colonial systems (e.g. Sedinger et al. 1995, Hadley et al. 2006, Aubry et al. 2009, Fay et al. 2018). Even outside avian taxa, the long-term mammalian studies examining individual heterogeneity such as Soay

sheep (*Ovis aries*; Coulson et al. 2006), Red deer (*Cervus elaphus*; Moyes et al. 2006), and Weddell seals (*Leptonychotes weddellii*; Chambert et al. 2013) are colonial, exhibit gregarious herd behavior, or occur on isolated islands. Studies involving territorial species are discussed less commonly, possibly due to the difficulty of obtaining adequate sample sizes compared to high density colonial or herding species. Yet understanding these dynamics is no less important, especially in agricultural environments where habitat types have clear distinctions and are easily quantified. However, gaining biological inference about these systems requires working on and around private land boundaries.

Despite occasional issues of private land access, our ability to annually resight individual marked females was quite high across our 36-year study duration (mean 0.71 BCI 0.68,0.73; Figure 4-6.) and the additional incorporation of state uncertainty parameters (δ) for occasions when nests were not located provided a robust statistical methodology (Pradel 2005). In most cases the likely reason for not observing the reproductive state was that an individual had a nest failure very early in the breeding season and field crews simply hadn't located the nest yet. Despite this problem our estimates of δ_1 (failed reproduction group) were still quite high (77%). For those occasions classified into the successful reproductive group (δ_2), our estimates of 98% provide strong support that our field surveys routinely find almost all successful nests, leading to accurate estimation of fitness components. Properly accounting for imperfect detection is vital to fitness estimation and questions of evolutionary inference (Gimenez et al. 2008). Working on private land creates unique challenges for long-term studies, however the importance of private land cannot be understated, given the predominance of private holdings, agricultural practices on these lands, and the large number of threatened species existing upon them (Knight 1999).

Within the United States, private lands tend to be at lower elevations where more productive soils exist and have already been converted from their native state, often for agriculture (Scott et al. 2001). Given the effects agricultural and grazing practices can have on biodiversity (Brennan & Kuvlesky 2005), informed policies are needed to maintain and possibly reverse biodiversity declines within agricultural environments (Fahrig et al. 2011). Agricultural systems vary in their effects and have been shown to maintain the abundance of some avian species, despite the declines in species richness (Wilson et al. 2017). While this analysis did not establish a strong relationship between agricultural habitat types and fitness components, nor lifetime fitness, understanding the fitness consequences or benefits for species utilizing these spaces is vital across the world.

Table 4-1. Summary statistics describing average habitat characteristics and population density metrics across 890 SWHA territories from 1985-2020. The compositional habitat metrics means (25% quantile, 75% quantile) represent the average proportion and proximity distance across all nests. The nearest neighbor distance is the straight line distance (meters) between nest trees of adjacent SWHA territories. The nearest neighbor count is the number of SWHA territories within 2,000m of the focal nest.

Territory Habitat Metrics	Mean	Q25	Q75
Alfalfa Proportion	0.218	0.04	0.316
Row Crop Proportion	0.039	0	0.05
Grassland Proportion	0.229	0.039	0.351
Dryland Hay Proportion	0.252	0.132	0.347
Dirt Proportion	0.076	0.007	0.098
Juniper Woodland Proportion	0.127	0.003	0.186
Distance to Nearest Alfalfa	493m	90m	676m
Distance to Nearest Row Crop	822m	270m	1106m

Territory Density Metrics	Mean	Q25	Q75
Nearest Neighbor Distance	1425	857	1705
Nearest Neighbor Count	2.4	1	4

Table 4-2. WAIC selection table comparing models of territory habitat components and population density metrics on annual changes in reproductive success of breeding female SWHA from (1985-2020). Habitat variables are represented by territory composition data (proportions of habitat type) and two proximity measures. Metrics of population density include distance to nearest conspecific neighbor and number of conspecifics within 2,000m). The last two columns show the correlation values and summary statistics between territory habitat variances and individual derived LRS values.

Model	Δ W_{aic}	W_{aic}	W_{aic} (SE)	K n.eff	K n.eff (SE)	ELPD	ELPD (SE)	LRS Corr	t, df, pvalue
Juniper	0	1668.6	104.4	180.9	8.4	-834.3	52.2	-0.053	-0.681,167,0.497
Null	12.1	1680.7	105.3	184.5	8.7	-840.4	52.7	-	-
Grassland	12.6	1681.2	105.4	184.6	8.8	-840.6	52.7	-0.046	-0.591,167,0.555
Row Crop Proportion	14.3	1682.9	105.6	185.0	8.9	-841.5	52.8	0.140	1.82,167,0.070
Alfalfa Proportion	15.8	1684.4	105.7	185.7	8.9	-842.2	52.8	0.002	0.021, 167, 0.983
Dryland Hay	16.7	1685.3	105.7	185.8	8.9	-842.7	52.9	0.118	1.54,167,0.126
Distance to Nearest Row Crop Field	17.3	1685.9	105.7	186.1	8.9	-842.9	52.8	0.140	1.82,167,0.070
Distance to Nearest Alfalfa Field	17.4	1686.0	105.8	185.9	8.9	-843.0	52.9	0.002	0.021,167,0.983

Model	Δ W_{aic}	W_{aic}	W_{aic} (SE)	K n.eff	K n.eff (SE)	ELPD	ELPD (SE)	LRS Corr	t, df, pvalue
Null	0	1680.7	105.3	184.5	8.7	-840.4	52.7	-	-
Nearest Neighbor Count	3.1	1683.8	105.6	185.3	8.9	-841.9	52.8	0.081	1.05,167,0.296
Nearest Neighbor Distance	3.4	1684.1	105.6	185.5	8.9	-842.0	52.8	0.003	0.037,167,0.97

Table 4-3. Parameter estimates and 95% credible intervals. All survival, transition, and detection parameter values provided in the Table were averaged across female SWHA breeding in Butte Valley, CA between 1985-2020.

Parameter	Posterior Mean Estimate (CI)
Survival of prime aged failed breeders Φ^{0}_{pa}	0.81 (0.76-0.85)
Survival of old aged failed breeders Φ^{0}_{old}	0.75 (0.54-0.92)
Survival of prime aged fledged 1 breeders Φ^{1}_{pa}	0.91 (0.86-0.95)
Survival of old aged fledged 1 breeders Φ^{1}_{old}	0.95 (0.80-1.00)
Survival of prime aged fledged 2 breeders Φ^{2}_{pa}	0.91 (0.87-0.94)
Survival of old aged fledged 2 breeders Φ^{2}_{old}	0.63 (0.45-0.80)
Survival of prime aged fledged 3^{+} breeders Φ^{3+}_{pa}	0.87 (0.82-0.91)
Survival of old aged fledged 3^{+} breeders Φ^{3+}_{old}	0.99 (0.94-1.00)
Transition failed breeder to failed breeder $\Psi^{0\rightarrow0}$	0.41 (0.29-0.51)
Transition failed breeder to fledged 1 chick $\Psi^{0\rightarrow1}$	0.18 (0.12-0.24)
Transition failed breeder to fledged 2 chicks $\Psi^{0\rightarrow2}$	0.24 (0.16-0.31)
Transition failed breeder to fledged 3^{+} chicks $\Psi^{0\rightarrow3+}$	0.17 (0.04-0.40)
Transition fledged 1 chick to failed breeder $\Psi^{1\rightarrow0}$	0.32 (0.18-0.42)
Transition fledged 1 chick to fledged 1 chick $\Psi^{1\rightarrow1}$	0.28 (0.16-0.37)
Transition fledged 1 chick to fledged 2 chicks $\Psi^{1\rightarrow2}$	0.22 (0.13-0.31)
Transition fledged 1 chick to fledged 3^{+} chicks $\Psi^{1\rightarrow3+}$	0.18 (0.02-0.50)
Transition fledged 2 chicks to failed breeder $\Psi^{2\rightarrow0}$	0.30 (0.19-0.38)
Transition fledged 2 chicks to fledged 1 chick $\Psi^{2\rightarrow1}$	0.18 (0.12-0.25)
Transition fledged 2 chicks to fledged 2 chicks $\Psi^{2\rightarrow2}$	0.33 (0.22-0.42)
Transition fledged 2 chicks to fledged 3^{+} chicks $\Psi^{2\rightarrow3+}$	0.17 (0.03-0.43)
Transition fledged 3^{+} chicks to failed breeder $\Psi^{3+\rightarrow0}$	0.28 (0.16-0.40)
Transition fledged 3^{+} chicks to fledged 1 chick $\Psi^{3+\rightarrow1}$	0.16 (0.09-0.23)
Transition fledged 3^{+} chicks to fledged 2 chicks $\Psi^{3+\rightarrow2}$	0.29 (0.17-0.40)
Transition fledged 3^{+} chicks to fledged 3+ chicks $\Psi^{3+\rightarrow3+}$	0.26 (0.06-0.56)
Detection of breeders p	0.71 (0.68-0.73)
Assignment failed breeder δ^{1}	0.77 (0.71-0.83)
Assignment succesful breeder δ^{2}	0.98 (0.95-1.00)

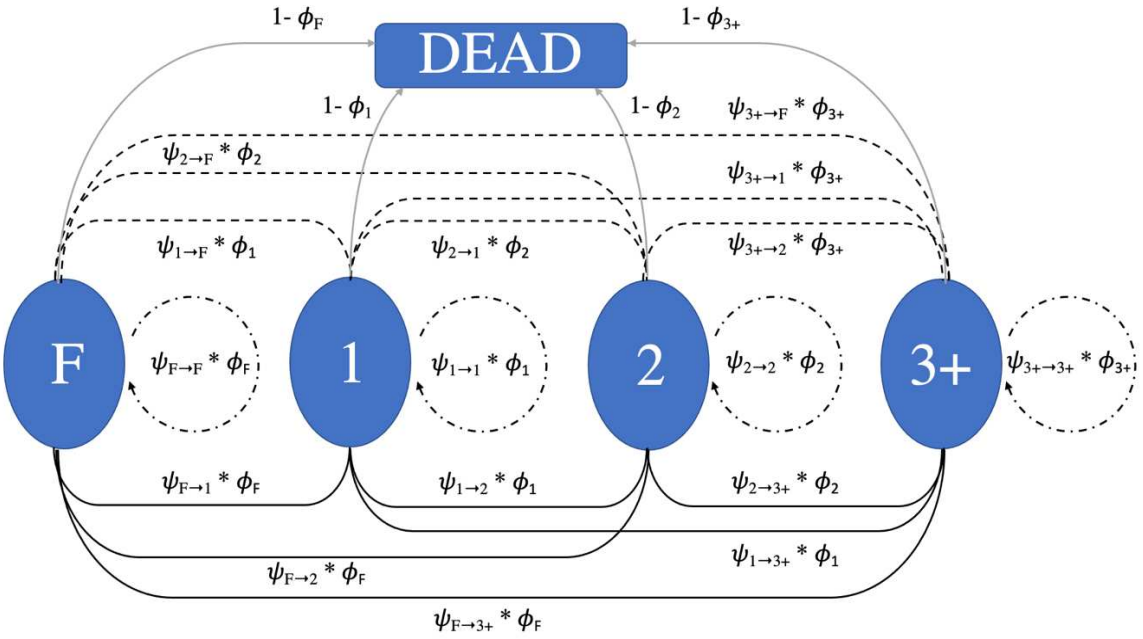

Figure 4-1. Demographic model diagram showing the four reproductive states and how individuals transition between them in a probabilistic manner. Reproductive states (large circles) and subscripts are as follows: F (failed attempt), 1 (fledged single chick), 2 (fledged two chicks), 3+ (fledged 3 or 4 chicks). Symbols for demographic parameters are as follows: ϕ (apparent survival for adult females, subscript represents current state) ψ (transition between reproductive states, subscript denotes state in time t → state t+1). Dash lines represent a transition to a lower reproductive state, while solid lines are transitions to higher states.

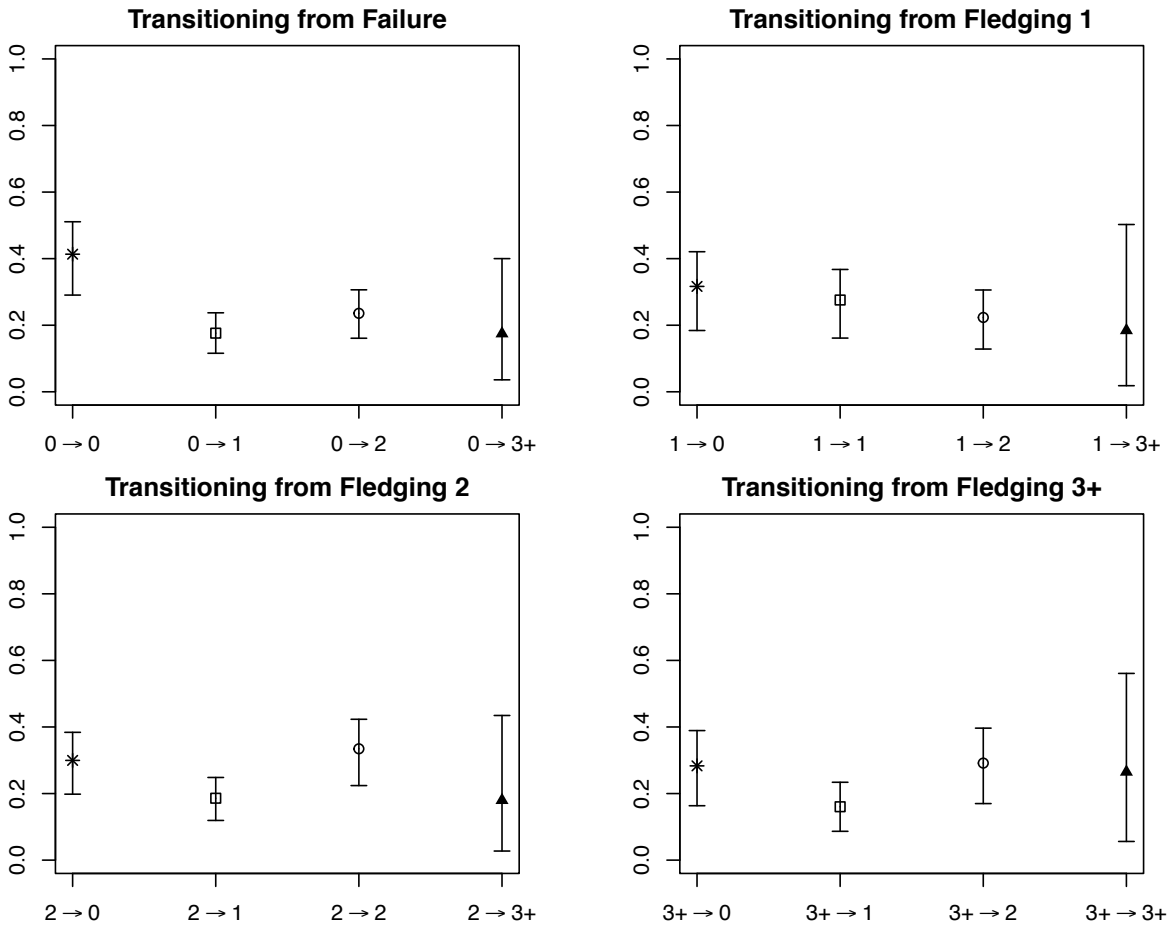

Figure 4-2. Annual probabilities of moving from one reproductive state (*t*) to another reproductive state the following year (*t*+1). Shared characters (asterisk, square, circle, triangle) represent parameter groups that were modelled with similar linear model parameterizations.

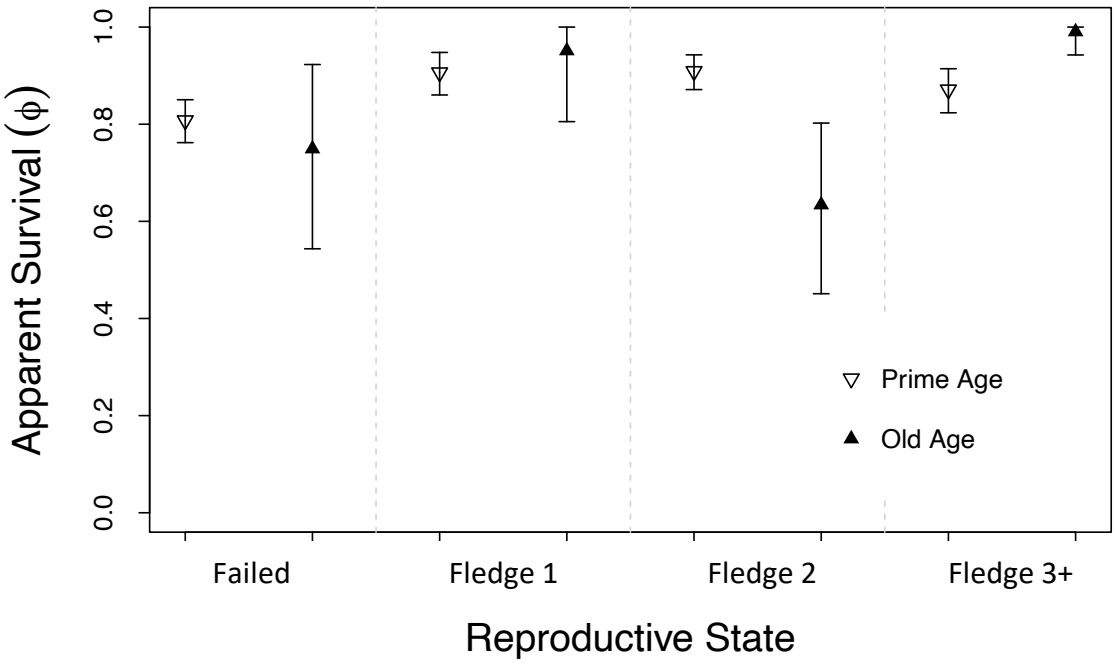

Figure 4-3. Annual apparent survival probabilities for adult female Swainson's hawks breeding in Butte Valley, California from 1985-2020 according to reproductive state (dashed grey line) and age class (∇ prime age; Δ old age).

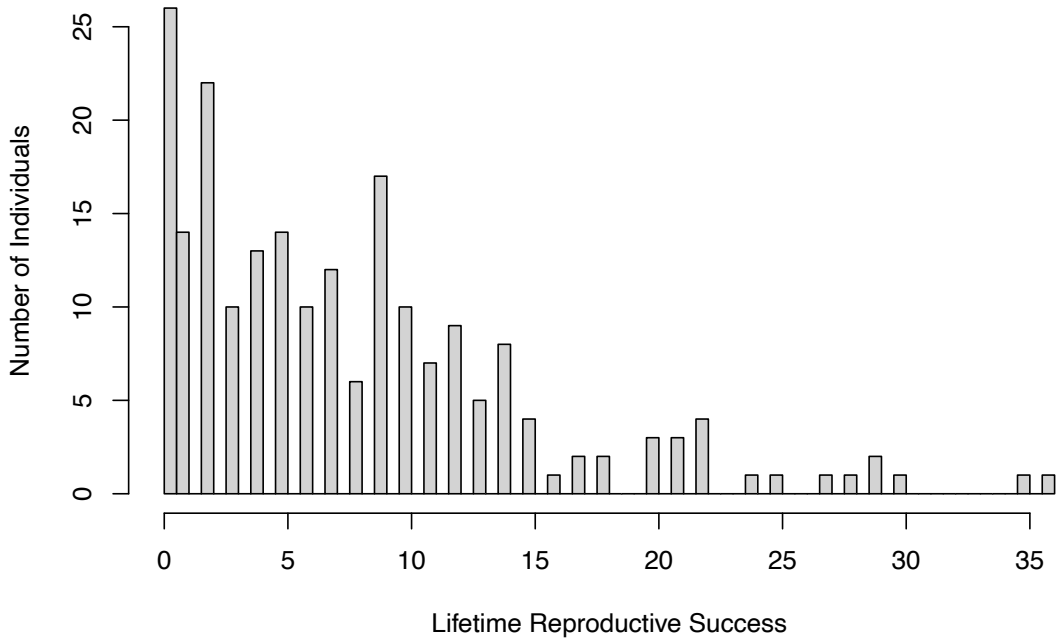

Figure 4-4. Histogram of lifetime reproductive success for female Swainson's hawks breeding in Butte Valley, California between 1985 and 2020.

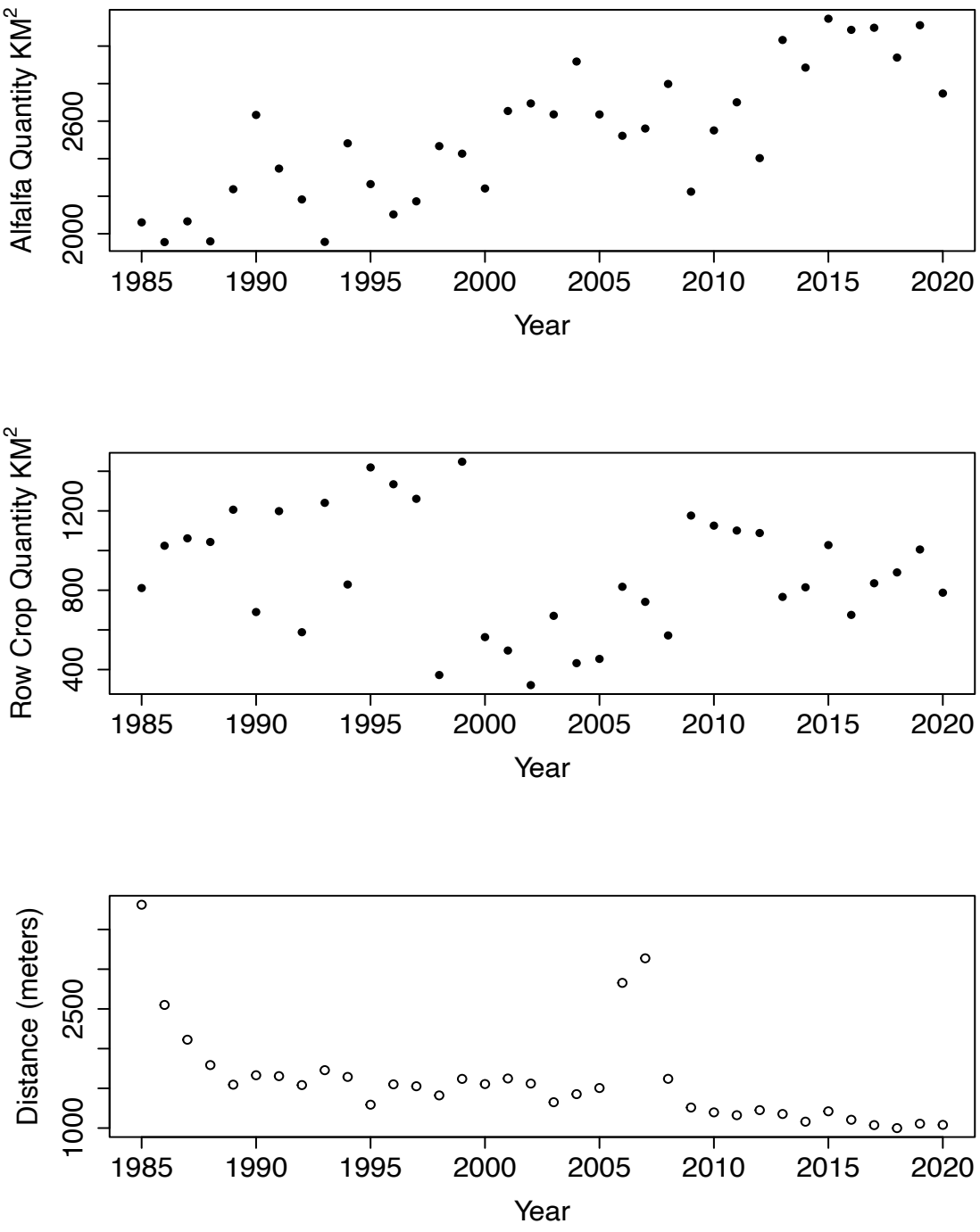

Figure 4-5. (A) Change in the quantity of alfalfa and (B) row crops (km^2) over the duration of the long-term study of Swainson's hawks breeding in Butte Valley, California between 1985 and 2020. (C) Average nearest neighbor distance between Swainson's hawk nests from 1985-2020.

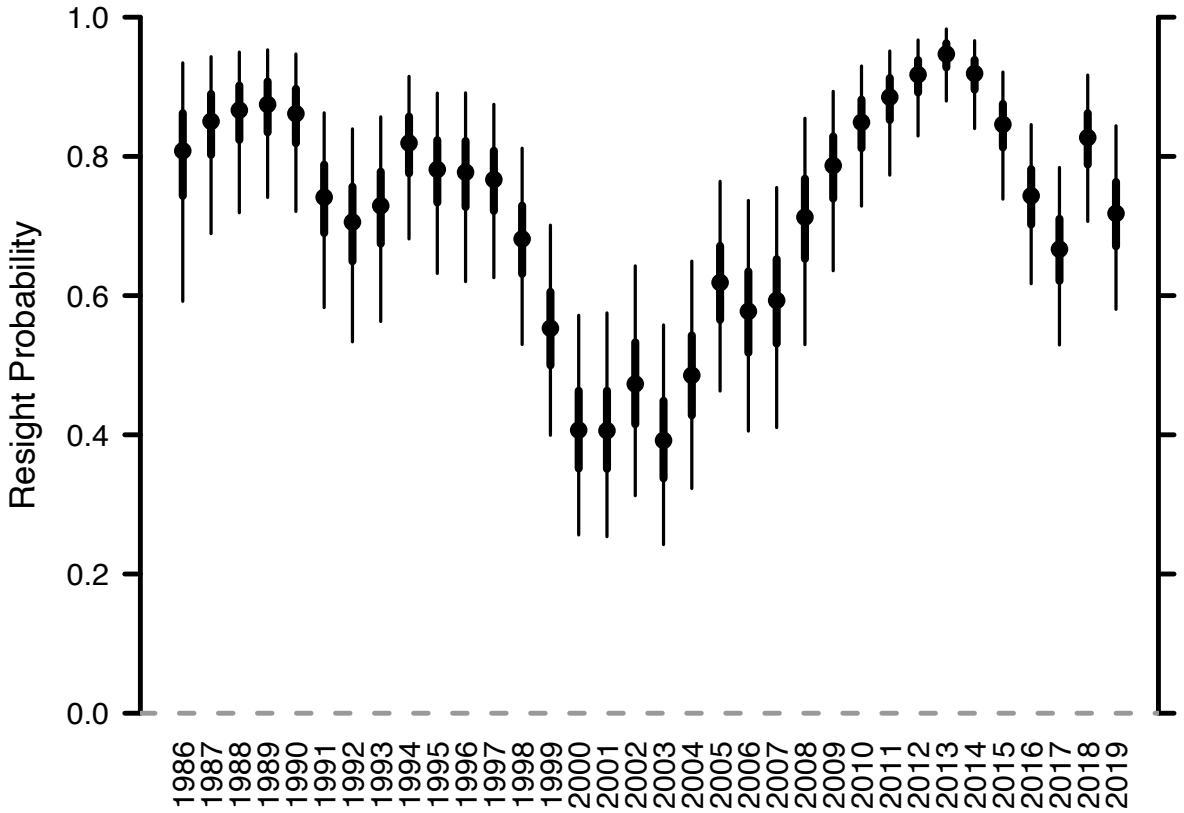

Figure 4-6. Resight probabilities for female Swainson's hawks breeding in Butte Valley, California between 1985 and 2020.

LITERATURE CITED

Airola D., Estep J., Krolick D., Anderson R., Peters J. 2019. Wintering Areas and Migration Characteristics of Swainson's Hawks That Breed in the Central Valley of California. Journal of Raptor Research 53:237–252.

Arnold, T. 2010. Uninformative Parameters and Model Selection Using Akaike's Information Criterion. The Journal of Wildlife Management 74(6):1175-1178.

Aubry, L., Koons D., Monnat, J., Emmanuelle, C. 2009. Consequences of Recruitment Decisions and Heterogeneity on Age-Specific Breeding Success in a Long-Lived Seabird. Ecology 90:2491–2502.

Batbayar N., Sukhchuluun S., Fuller M., Watson R. 2014. Morphometrics of Nestling Cinereous Vultures (*Aegypius monachus*) In Mongolia. Тоодог 1:21–25.

Battistone, C., Furnas, B., Anderson, R., Dinsdale, J., Cripe, K., Estep, J., Chun, C., Torres, S. 2019. Population and Distribution of Swainson's Hawks (*Buteo swainsoni*) in California's Great Valley: A Framework for Long-Term Monitoring. Journal of Raptor Research 53(3):253-265.

Bechard M., Houston C., Sarasola J., England S. 2020. Swainson's Hawk (*Buteo swainsoni*), version 1.0. Birds of the World (A.F. Poole, Editor). Cornell Lab of Ornithology.

Becker, P., Bradley, J. 2007. The Role of Intrinsic Factors for the Recruitment Process in Long-Lived Birds. Journal of Ornithology 148:377–384.

Beger, A. 2016. Precision-Recall Curves. http://dx.doi.org/10.2139/ssrn.2765419

Benton, T., Vickery, J., Wilson, J. 2003. Farmland Biodiversity: is Habitat Heterogeneity the Key? Trends in Ecology & Evolution 18:182–188.

Berger, D., Mueller, H. 1959. The Bal-Chatri: A Trap for the Birds of Prey. Bird-Banding 30:18–26.

Bloom, P., Henckel, J., Henckel, E., Schmutz, J., Woodbridge, B., Bryan, J., Anderson, R., Detrich, P., Maechtle, T., McKinley, J., McCrary, M., Titus, K., Schempf, P.1992. The Dho-Gaza with Great Horned Owl Lure: an Analysis of its Effectiveness in Capturing Raptors. Journal Of Raptor Research 26:167–178.

Bortolotti G. 1984. Criteria For Determining Age And Sex Of Nestling Bald Eagles. Journal of Field Ornithology 55:467–481.

Bradley, J., Gunn, B., Skira, I., Meathrel, C., Wooller, R. 1999. Age-Dependent Prospecting and Recruitment to a Breeding Population of Short-Tailed Shearwaters (*Puffinus tenuirostris*). Ibis 141:277–285.

Breiman, L. 2001. Random Forests. Machine Learning 45(1): 5-32.

Brennan, L., Kuvlesky Jr, W. 2005. North American Grassland Birds: An Unfolding Conservation Crisis? Journal of Wildlife Management 69:1–13.

Briggs, C., Woodbridge, B., Collopy, M. 2010. Temporal Morph Invariance of Swainson's Hawks. Journal of Raptor Research 44:70–73.

Briggs, C. 2011. Carry-Over Effects and Plumage Polymorphism in Swainson's Hawks. Dissertation. University of Nevada, Reno.

Briggs, C., Woodbridge, B., Collopy, M. 2011. Correlates of Survival in Swainson's Hawks Breeding in Northern California. The Journal of Wildlife Management 75:1307–1314.

Buechley E., Santangeli A., Girardello M., Neate-Clegg M., Oleyar D., McClure C., Şekercioğlu Ç. 2019. Global Raptor Research and Conservation Priorities: Tropical Raptors Fall Prey to Knowledge Gaps. Diversity and Distributions 25:856–869.

Cam, E., Aubry, L., Authier, M. 2016. The Conundrum of Heterogeneities in Life History Studies. Trends in Ecology & Evolution 31(11):872-886.

Cam, E., Link, W., Cooch, E., Monnat, J., Danchin, E. 2002. Individual Covariation in Life-History Traits: Seeing the Trees Despite the Forest. The American Naturalist 159:96–105.

Caswell, H. 2009. Stage, Age and Individual Stochasticity in Demography. Oikos 118:1763–1782.

Caswell, H., Vindenes, Y. 2018. Demographic Variance in Heterogeneous Populations: Matrix Models and Sensitivity Analysis. Oikos 127(5):648-663.

Chambert, T., Rotella, J., Higgs, M., Garrott, R. 2013. Individual Heterogeneity in Reproductive Rates and Cost of Reproduction in a Long-Lived Vertebrate. Ecology and Evolution 3:2047–2060.

Clobert, J., Lebreton, J., Allaine, D., Gaillard, J. 1994. The Estimation of Age-Specific Breeding Probabilities From Recaptures or Resightings in Vertebrate Populations: II. Longitudinal Models. Biometrics 50(2):375-387.

Clutton-Brock, T. 1988. Reproductive Success: Studies of Individual Variation in Contrasting Breeding Systems. University of Chicago Press.

Cole L. 1954. The Population Consequences of Life History Phenomena. The Quarterly Review of Biology 29:103–137.

Conn, P., Cooch, E. 2009. Multistate Capture-Recapture Analysis Under Imperfect State Observation: An application to Disease Models. Journal of Applied Ecology 46:486–492.

Coulson, T., Benton, T., Lundberg, P., Dall, S., Kendall, B., Gaillard, J. 2006. Estimating Individual Contributions to Population Growth: Evolutionary Fitness in Ecological Time. Proceedings of the Royal Society B: Biological Sciences 273:547–555.

Dechaume-Moncharmont, F., Monceau, K., & Cezilly, F. 2011. Sexing Birds Using Discriminant Function Analysis: A Critical Appraisal. The Auk 128(1):78-86.

Drum, R., Ribic, C., Koch, K., Lonsdorf, E., Grant, E., Ahlering, M., Barnhill, L., Dailey, T., Lor, S., Mueller, C., Pavlacky Jr, D. 2015. Strategic Grassland Bird Conservation Throughout

the Annual Cycle: Linking Policy Alternatives, Landowner Decisions, and Biological Population Outcomes. PloS one 10(11):e0142525.

Dudley, N., Alexander S. 2017. Agriculture and biodiversity: a review. Biodiversity 18(2-3): 45-49.

Dykstra C., Mays Jr H., Hays J., Simon M., Wegman A. 2012. Sexing Adult and Nestling Red-Shouldered Hawks Using Morphometrics and Molecular Techniques. Journal of Raptor Research 46:357–364.

Fahrig, L., Baudry, J., Brotons, L., Burel, F., Crist, T., Fuller, R., Sirami, C., Siriwardena, G., Martin, J. 2011. Functional Landscape Heterogeneity and Animal Biodiversity in Agricultural Landscapes. Ecology letters 14(2):101-12.

Fay R., Barbraud C., Delord K., Weimerskirch H. 2016. Variation in the Age of First Reproduction: Different Strategies or Individual Quality? Ecology 97:1842–1851.

Fay, R., Barbraud, C., Delord, K., Weimerskirch, H. 2018. From Early Life to Senescence: Individual Heterogeneity in a Long-Lived Seabird. Ecological Monographs 88:60–73.

Fischer, J., Abson, D., Butsic, V., Chappell, M., Ekroos, J., Hanspach, J., Kuemmerle, T., Smith, H., von Wehrden, H. 2014. Land Sparing Versus Land Sharing: Moving Forward. Conservation Letters 7(3):149-157.

Fischer, J., Batáry, P., Bawa, K., Brussaard, L., Chappell, M., Clough, Y., Daily, G., Dorrough, J., Hartel, T., Jackson, L., Klein, A. 2011. Conservation: Limits of Land Sparing. Science *334*(6056):593-593.

Fitzner R. 1980. Behavioral Ecology of the Swainson's Hawk (*Buteo Swainsoni*) in Washington. Richland, WA.

Foley, J., Ramankutty, N., Brauman, K., Cassidy, E., Gerber, J., Johnston, M., Mueller, N., O'Connell, C., Ray, D., West, P., Balzer, C. 2011. Solutions for a Cultivated Planet. Nature 478(7369):337-342.

Fretwell, S., Lucas Jr., H. 1970. On Territorial Behavior and Other Factors Influencing Habitat Distribuion in Birds. Acta Biotheoretica 14:16–36.

Fridolfsson A-K., Ellegren H. 1999. A Simple and Universal Method for Molecular Sexing of Non-Ratite Birds. Journal of Avian Biology 30:116–121.

Funatogawa, I., Funatogawa, T. 2018. Autoregressive Linear Mixed Effects Models. In: Longitudinal Data Analysis. Springer Briefs in Statistics. Springer, Singapore.

Gelman, A., Carlin, J., Stern, H., Rubin, D. 2004. Bayesian Data Analysis. Chapman & Hall. CRC Texts in Statistical Science.

Genuer, R., Poggi, J-M., Tuleau-Malot, C. 2015. VSURF: an R Package for Variable Selection Using Random Forests. The R Journal 7.2: 19-33.

Gimenez, O., Gaillard, J. 2018. Estimating Individual Fitness in the Wild Using Capture–Recapture Data. Population Ecology, 60(1):101-109.

Gimenez, O., Viallefont, A., Charmantier, A., Pradel, R., Cam, E., Brown, C., Anderson, M., Brown, M., Covas, R., Gaillard, J. 2008. The Risk of Flawed Inference in Evolutionary Studies When Detectability Is Less than One. The American Naturalist 172:441–448.

Gorelick, N., Hancher, M., Dixon, M., Ilyushchenko, S., Thau, D., Moore, R. 2017. Google Earth Engine: Planetary-Scale Geospatial Analysis for Everyone. Remote Sensing of Environment.

Gossett D., Makela P. 2005. Photographic Guide for Aging Nestling Swainson's Hawks.

Grafen, A. 1988. On the Uses of Data on Lifetime Reproductive Success. Reproductive Success pp.454-485.

Green, R., Cornell, S., Scharlemann, J., Balmford, A. 2005. Farming and the Fate of Wild Nature. Science 307(5709):550-555.

Haberl, H., Erb, K., Krausmann, F., Gaube, V., Bondeau, A., Plutzar, C., Gingrich, S., Lucht, W., Fischer-Kowalski, M. 2007. Quantifying and Mapping the Human Appropriation of Net Primary Production in Earth's Terrestrial Ecosystems. Proceedings of the National Academy of Sciences 104:12942–12947.

Hadley, G., Rotella, J., Garrott, R., Nichols, J. 2006. Variation in Probability of First Reproduction of Weddell seals. Journal of Animal Ecology 75:1058–1070.

Hajian-Tilaki, K. 2013. Receiver Operating Characteristic (ROC) Curve Analysis for Medical Diagnostic Test Evaluation. Caspian Journal of Internal Medicine 4(2):627.

Hamel, S., Gaillard, J., Yoccoz, N. 2018. Introduction to: Individual Heterogeneity–the Causes and Consequences of a Fundamental Biological Process. Oikos 127(5):643-647.

Hamilton, W. 1966. The Moulding of Senescence by Natural Selection. Journal of Theoretical Biology 12(1):12-45.

Hartman, C., Ackerman, J., Eagles-Smith, C., Herzog, M. 2016. Differentiating Sex and Species of Western Grebes (*Aechmophorus occidentalis*) and Clark's Grebes (*Aechmophorus clarkii*) and Their Eggs Using External Morphometrics and Discriminant Function Analysis. Waterbirds 39: 13-26.

Hernández-Matías A., Real J., Pradel R. 2011. Quick Methods for Evaluating Survival of Age-Characterizable Long-Lived Territorial Birds. The Journal of Wildlife Management 75:856–866.

Hijmans, R. 2021. Raster: Geographic Data Analysis and Modeling. R package v3.4-10.

Hobbs, R. Higgs, E., Hall, C., Bridgewater, P., Chapin III, F., Ellis, E., Ewel, J., Hallett, L., Harris, J., Hulvey, K., Jackson, S. 2014. Managing the Whole Landscape: Historical, Hybrid, and Novel Ecosystems. Frontiers in Ecology and the Environment 12(10):557-564.

Hooten, M., Hobbs, N. 2015. A Guide to Bayesian Model Selection for Ecologists. Ecological Monographs 85(1):3-28.

Hoy, S., MacNulty, D., Smith, D., Stahler, D., Lambin, X., Peterson, R., Ruprecht, J., Vucetich, J. 2020. Fluctuations in Age Structure and Their Variable Influence on Population Growth. Functional Ecology 34(1):203-216.

Hull J., Pitzer S., Fish A., Ernest H., Hull A. 2012. Differential Migration in Five Species of Raptors in Central Coastal California. Journal of Raptor Research 46:50–56.

Hunt, G. 1998. Raptor Floaters at Moffat's Equilibrium. Oikos 82:191–197.

Inselman, W., Datta, S., Jenks, J., Klaver, R., Grovenburg, T. 2016. Spatial Ecology and Survival of Swainson's Hawks (*Buteo swainsoni*) in the Northern Great Plains. Journal of Raptor Research 50(4):338-350.

Jarek S. 2015. Mvnormtest: Normality Test for Multivariate Variables.

Jenouvrier, S., Aubry, L., Barbraud, C., Weimerskirch, H., Caswell, H. 2018. Interacting Effects of Unobserved Heterogeneity and Individual Stochasticity in the Life History of the Southern Fulmar. Journal of Animal Ecology 87(1):212-222.

Jenouvrier, S., Aubry, L., Van Daalen, S., Barbraud, C., Weimerskirch, H., Caswell, H. 2022. When the Going Gets Tough, the Tough Get Going: Effect of Extreme Climate on an Antarctic Seabird's Life History. Ecology Letters 00:1-12.

Jenouvrier, S., Péron, C., Weimerskirch, H. 2015. Extreme Climate Events and Individual Heterogeneity Shape Life-History Traits and Population Dynamics. Ecological Monographs 85:605–623.

Kane, S., Vennum, C., Woodbridge, B., Collopy, M., Bloom, P., Briggs, C. 2020. Age Distribution and Longevity in a Breeding Population of Swainson's Hawks, (*Buteo swainsoni*). Journal of Ornithology 161(3):885-891.

Karreth, J., Scogin, S., Williams, R., Beger, A. 2021. BayesPostEst: Generate Post Estimation Quantities for Bayesian MCMC Estimation. R package version 0.3.2.

Keitt, T., Bjornstad, O., Dixon, P., Citron-Pousty, S. 2002. Accounting for Spatial Pattern When Modeling Organism-Environment Interactions. Ecography 25(5):616–625.

Kendall, W. 2004. Coping With Unobservable and Mis–classified States in Capture–Recapture Studies. Animal biodiversity and Conservation 27(1):97-107.

Kendall, W. 2009. One Size Does Not Fit All: Adapting Mark-Recapture and Occupancy Models for State Uncertainty. In: Modeling demographic processes in marked populations (pp. 765-780). Springer, Boston, MA.

Kendall, W., Hines, J., Nichols, J. 2003. Adjusting Multistate Capture–Recapture Models For Misclassification Bias: Manatee Breeding Proportions. Ecology 84(4):1058-1066.

Kery, M., Schaub, M. 2012. Bayesian Population Analysis Using WinBUGS: A Hierarchical Perspective. Elsevier.

King, R. 2012. A Review of Bayesian State-Space Modelling of Capture–Recapture–Recovery Data. Interface Focus 2(2):190-204.

Klaassen R., Hake M., Strandberg R., Koks B., Exo K-M., Bairlein F., Alerstam T. 2014. When and Where Does Mortality Occur in Migratory Birds? Direct Evidence from Long-Term Satellite Tracking of Raptors. Journal of Animal Ecology 83:176–184.

Knight, R. 1999. Private Lands: the Neglected Geography. Conservation Biology 13(2):223-224.

Koch H., Blohm-Sievers E., Liedvogel M. 2019. Rapid Sex Determination of a Wild Passerine Species Using Loop-Mediated Isothermal Amplification (LAMP). Ecology and Evolution 9:5849–5858.

Kochert M., Mckinley J. 2008. Use of Body Mass , Footpad Length , and Wing Chord to Determine Sex in Swainson's Hawks. Journal of Raptor Research 42:138–141.

Kremen, C., Merenlender, A. 2018. Landscapes That Work for Biodiversity and People. Science 362(6412):6020.

Kross, S., Tylianakis, J., Nelson, X. 2012. Effects of Introducing Threatened Falcons into Vineyards on Abundance of Passeriformes and Bird Damage to Grapes. Conservation Biology 26(1):142-149.

Krüger O. 2005. The Evolution of Reversed Sexual Size Dimorphism in Hawks, Falcons and Owls: A Comparative Study. Evolutionary Ecology 19:467–486.

Krüger, O. 2005. Age at First Breeding and Fitness in Goshawk (*Accipiter gentilis*). Journal of Animal Ecology 74(2):266-273.

Lawson, J. 2014. Design and Analysis of Experiments with *R* (Vol. 115). CRC press.

Lebreton, J., Cefe, R. 2002. Multistate Recapture Models: Modelling Incomplete Individual Histories. Journal of Applied Statistics 29(1-4):353-369.

Lewis, S., Maslin, M. 2015. Defining the Anthropocene. Nature 519.7542: 171-180.

Lindberg, M., Sedinger, J., Derksen, D., Rockwell, R. 1998. Natal And Breeding Philopatry In A Black Brant Metapopulation. Ecology 79:1839–1904.

López-López P., Gil J., Alcantara M. 2011. Morphometrics and Sex Determination In The Endangered Bearded Vulture (*Gypaetus barbatus*). Journal of Raptor Research 45:361–366.

Magrath R. 1991. Nestling Weight and Juvenile Survival in the Blackbird, (*Turdus merula*). Journal of Animal Ecology 60:335–351.

McClintock, B., Langrock, R., Gimenez, O., Cam, E., Borchers, D., Glennie, R., Patterson, T. 2020. Uncovering Ecological State Dynamics with Hidden Markov Models. Ecology Letters 23(12):1878-1903.

McClure C., Schulwitz S., Anderson D., Robinson B., Mojica E., Therrien J-F., Oleyar M., Johnshon J. 2019. Commentary: Defining Raptors And Birds of Prey. Journal of Raptor Research 53:419–430.

McDonald P. 2003. Nestling Growth and Development in the Brown Falcon, (*Falco berigora*): an Improved Ageing Formula and Field-Based Method of Sex Determination. Wildlife Research 30:411–418.

McDonald P., Olsen P., Cockburn A. 2005. Sex Allocation and Nestling Survival in a Dimorphic Raptor: Does Size Matter? Behavioral Ecology 16:922–930.

Moss D. 1979. Growth of Nestling Sparrowhawks. Journal of Zoology 187:297–314.

Moyes, K., Coulson, T., Morgan, B., Donald, A., Morris, S., Clutton-Brock, T. 2006. Cumulative Reproduction and Survival Costs in Female Red Deer. Oikos, 115(2):241-252.

Muriel R., Casado E., Schmidt D., Calabuig C., Ferrer M. 2010. Morphometric Sex Determination of Young Ospreys (*Pandion haliaetus*) Using Discriminant Analysis. Bird Study 57:336–343.

Newton I. 1978. Feeding and Development of Sparrowhawk (*Accipiter nisus*) Nestlings. Journal of Zoology 184:465–487.

Newton, I. 1989. Lifetime Reproduction in Birds, 1st Edition. Academic Press, New York.

Newton I. 2001. Causes and Consequences of Breeding Dispersal in the Sparrowhawk (*Accipiter nisus*). Ardea 1:143–154.

Newton I., Marquiss M. 1983. Dispersal of Sparrowhawks Between Birthplace and Breeding Place. The Journal of Animal Ecology 52:463–477.

Newton I., Mcgrady M., Oli M. 2016. A Review of Survival Estimates for Raptors and Owls. Ibis 158:227–248.

Nichols, J., Kendall, W., Hines, J., Spendelow, J. 2004. Estimation of Sex-Specific Survival From Capture–Recapture Data When Sex is Not Always Known. Ecology 85(12):3192-3201.

Northrup, J., Gerber, B. 2018. A Comment on Priors for Bayesian Occupancy Models. PloS one 13(2):e0192819.

Oli, M., Dobson, F. 2003. The Relative Importance of Life-History Variables to Population Growth Rate in Mammals: Cole's Prediction Revisited. The American Naturalist 161:422–440.

Orians, G., Nolan E. 1979. On the Theory of Central Place Foraging. Analysis of Ecological Systems. Ohio State University Press, Columbus 2: 155-177.

Orloff, S. 1997. Intermountain Alfalfa Management (Vol. 3366). UCANR Publications.

Paini, D., Sheppard, A., Cook, D., De Barro, P., Worner, S., Thomas, M. 2016. Global Threat to Agriculture from Invasive Species. Proceedings of the National Academy of Sciences 113(27): 7575-7579.

Pay J., Katzner T., Wiersma J., Brown W., Hawkins C., Proft K., Cameron E. 2021. Morphometric Sex Identification of Nestling and Free-Flying Tasmanian Wedge-Tailed Eagles (*Aquila audax fleayi*). Journal of Raptor Research 55:539–551.

Phalan, B., Onial, M., Balmford, A., Green, R. 2011. Reconciling Food Production and Biodiversity Conservation: Land Sharing and Land Sparing Compared. Science 333:1289–1291.

Polasky, S., Nelson, E., Lonsdorf, E., Fackler, P., Starfield, A. 2005. Conserving Species in A Working Landscape: Land Use with Biological and Economic Objectives. Ecological Applications, 15(4):1387-1401.

Pradel, R. 2005. Multievent: An Extension of Multistate Capture-Recapture Models to Uncertain States. Biometrics 61:442–447.

Pradel, R., Lebreton, J. 1999. Comparison of Different Approaches to the Study of Local Recruitment of Breeders. Bird Study 46:S74–S81.

Pradel, R., Maurin-Bernier, L., Gimenez, O., Genovart, M., Choquet, R. Oro, D. 2008. Estimation of Sex-Specific Survival with Uncertainty in Sex Assessment. Canadian Journal of Statistics 36(1):29-42.

Putnam, D., Russelle, M., Orloff, S., Kuhn, J., Fitzhugh, L., Godfrey, L., Kiess, A., Long, R. 2001. Alfalfa, Wildlife and the Environment. The importance and benefits of alfalfa in the 21st century.

R Core Team 2021. R: A language and Environment for Statistical Computing. R Foundation for Statistical Computing, Vienna, Austria.

Ramankutty, N., Evan, A., Monfreda, C., Foley, J. 2008. Farming the Planet: 1. Geographic Distribution of Global Agricultural Lands in the year 2000. Global Biogeochemical Cycles 22:1–19.

Reynolds, R., Lambert, J., Kay, S., Sanderlin, J., Bird, B. 2019. Factors Affecting Lifetime Reproduction, Long-Term Territory-Specific Reproduction, and Estimation of Habitat Quality in Northern Goshawks. PloS one, 14(5):e0215841.

Ricklefs, R. 1968. Patterns of Growth in Birds. Ibis 110(4):419-451.

Roever C., Raabe N., Luebke K., Ligges U., Szepannek G., Zent-graf M., Meyer D. 2022. klaR: Classification and Visualization. R package version 1.7-0

Sæther, B., Coulson, T., Grøtan, V., Engen, S., Altwegg, R., Armitage, K., Barbraud, C., Becker, P., Blumstein, D., Dobson, F., Festa-Bianchet, M. 2013. How Life History Influences Population Dynamics in Fluctuating Environments. The American Naturalist 182(6):743-759.

Sarasola J., Negro J. 2004. Gender Determination In The Swainson's Hawk (*Buteo swainsoni*) Using Molecular Procedures and Discriminant Function Analysis. Journal of Raptor Research 38:357–361.

Sarasola, J., Bustamante, J., Negro, J., Travaini, A. 2008. Where do Swainson's hawks winter? Satellite Images Used to Identify Potential Habitat. Diversity and distributions 14(5):742-753.

Scott, J., Davis, F., McGhi, R., Wrigh, R., Groves, C., Estes, J. 2001. Nature Reserves: Do They Capture The Full Range of America's Biological Diversity? Ecological Applications 11:999–1007.

Sedinger J., Flint P., Lindberg M. 1995. Environmental Influence on Life-History Traits: Growth, Survival, and Fecundity in Black Brant (*Branta Bernicla*). Ecology 76:2404–2414.

Sedinger, J., Chelgren, N., Ward, D., Lindberg, M. 2008. Fidelity and Breeding Probability Related to Population Density and Individual Quality in Black Brent Geese (*Branta bernicla nigricans*). Journal of Animal Ecology 77:702–712.

Sergio, F., Blas, J., Baos, R., Forero, M., Donázar, J., Hiraldo, F. 2009. Short- and Long-term Consequences of Individual and Territory Quality in a Long-Lived Bird. Oecologia 160:507–514.

Sergio, F., Tavecchia, G., Blas, J., López, L., Tanferna, A., Hiraldo, F. 2011. Variation in Age-Structured Vital Rates of a Long-Lived Raptor: Implications for Population Growth. Basic and Applied Ecology 12:107–115.

Shave, M., Shwiff, S., Elser, J., Lindell, C. 2018. Falcons Using Orchard Nest Boxes Reduce Fruit-Eating Bird Abundances and Provide Economic Benefits for a Fruit-Growing Region. Journal of Applied Ecology 55(5):2451-2460.

Sheldon B. 1998. Recent Studies of Avian Sex Ratios. Heredity 80:397–402.

Snyder, R., Ellner, S. 2018. Pluck or Luck: Does Trait Variation or Chance Drive Variation in Lifetime Reproductive Success? The American Naturalist 191(4):E90–E107.

Stahl. J., Oli, M. 2006. Relative Importance of Avian Life-History Variables to Population Growth Rate. Ecological Modelling 198:23–39.

Stearns, S. 1976. Life-History Tactics: A Review of the Ideas. The Quarterly Review of Biology 51:3–47.

Steenhof K. 1987. Assessing Raptor Reproductive Success and Productivity. Pg. 157–170 in B. Pendleton, B. Millsap, K. Cline, and D. Bird, editors. Raptor Management Techniques Manual. National Wildlife Federation, Washington D.C.

Steiner, U., Tuljapurkar, S. 2012. Neutral Theory For Life Histories and Individual Variability in Fitness Components. Proceedings of the National Academy of Sciences 109(12):4684-4689.

Strobl C., Malley J., Tutz G. 2009. An Introduction to Recursive Partitioning: Rationale, Application and Characteristics of Classification and Regression Trees, Bagging and Random Forests. Psychological Methods 14:323–348.

Stuber, E., Gruber, L., Fontaine, J. 2017. A Bayesian Method for Assessing Multi-Scale Species-Habitat Relationships. Landscape Ecology 32(12):2365-2381.

Therneau T., Atkinson B. 2019. rpart: Recursive Partitioning and Regression Trees. R package version 4.1-15.

Tilman, D., Cassman, K., Matson, P., Naylor, R., Polasky, S. 2002. Agricultural Sustainability and Intensive Production Practices. Nature 418:671–677.

Tilman, D., Fargione, J., Wolff, B., D'antonio, C., Dobson, A., Howarth, R., Schindler, D., Schlesinger, W., Simberloff, D., Swackhamer, D. 2001. Forecasting Agriculturally Driven Global Environmental Change. Science, 292(5515): 281-284

Trivers R., Willard D. 1973. Natural Selection of Parental Ability to Vary the Sex Ratio of Offspring. Science 179:90–92.

Tuljapurkar, S., Zuo, W., Coulson, T., Horvitz, C., Gaillard, J. 2020. Skewed Distributions of Lifetime Reproductive Success: Beyond Mean and Variance. Ecology Letters 23:748–756.

USDA National Agricultural Statistics Service Cropland Data Layer. 2022. Published Crop-Specific Data Layer [Online]. https://www.nass.usda.gov

Van De Pol M., Bruinzeel L., Heg D., Van Der Jeugd H., Verhulst S. 2006. A silver spoon for a golden future: Long-term effects of natal origin on fitness prospects of oystercatchers (Haematopus ostralegus). Journal of Animal Ecology 75:616–626.

Vennum, C. 2017. Ecoimmunology and demography of recruitment in Swainson's Hawks. MS Thesis. University of Nevada, Reno.

Watanabe, S. 2013. A Widely Applicable Bayesian Information Criterion. Journal of Machine Learning Research 14:867–897.

Watson K. 2021. A Bird of Two Hemispheres: an Examination of Swainson's hawk (*Buteo swainsoni*) Ecology Across a Landscape of Increasing Wind Energy Development. Dissertation. Texas Tech University.

Weeks B., Willard D., Zimova M., Ellis A., Witynski M., Hennen M., Winger B. 2020. Shared Morphological Consequences of Global Warming in North American Migratory Birds. Ecology Letters 23:316–325.

Weimerskirch, H. 1992. Reproductive Effort in Long-Lived Birds: Age-Specific Patterns of Condition, Reproduction and Survival in the Wandering Albatross. Oikos 64(3):464-473.

Whisson, D., Orloff, S., Lancaster, D. 1999. Alfalfa Yield Loss from Belding's Ground Squirrels in Northeastern California. Wildlife Society Bulletin 27:178–183.

Williams, B., Nichols, J., Conroy, M. 2002. Analysis and Management of Animal Populations. Academic Press.

Wilson, S., Mitchell, G., Pasher, J., McGovern, M., Hudson, M., Fahrig, L. 2017. Influence of Crop Type, Heterogeneity and Woody Structure on Avian Biodiversity in Agricultural Landscapes. Ecological Indicators (83)218-226.

Woodbridge B. 1991. Habitat Selection by Nesting Swainson's Hawk: A hierarchical Approach. MS Thesis. Oregon State University.

Woolaver L., Nichols R., Morton E., Stutchbury B. 2013. Nestling Sex Ratio in a Critically Endangered Dimorphic Raptor, Ridgway's Hawk (*Buteo ridgwayi*). Journal of Raptor Research 47:117–126.

APPENDICES

Chapter 1 Appendices

Appendix A

Development Index

This index represents an informed hatch order, where younger siblings are assigned a value in reference to the oldest sibling in the nest. All nestlings are aged (days) based on feather development using a photographic guide (Gossett & Makela 2005). The oldest nestling is assigned an index value of zero. The index value of younger nestlings is calculated by subtracting age, in days, from the oldest nestling age. We assumed that all siblings hatched in close proximity to each other, so large index differences reflect stunted growth, not actual age differences. For example, the sibling on the right (oldest; 38d old at sampling), the second oldest sibling (far left feather development equal to 34d old), and youngest nestling (middle, feather development equivalent of 26d). Resulting in index scores of 0, -4, and -12. This example provides an exaggerated case, compared to most nests.

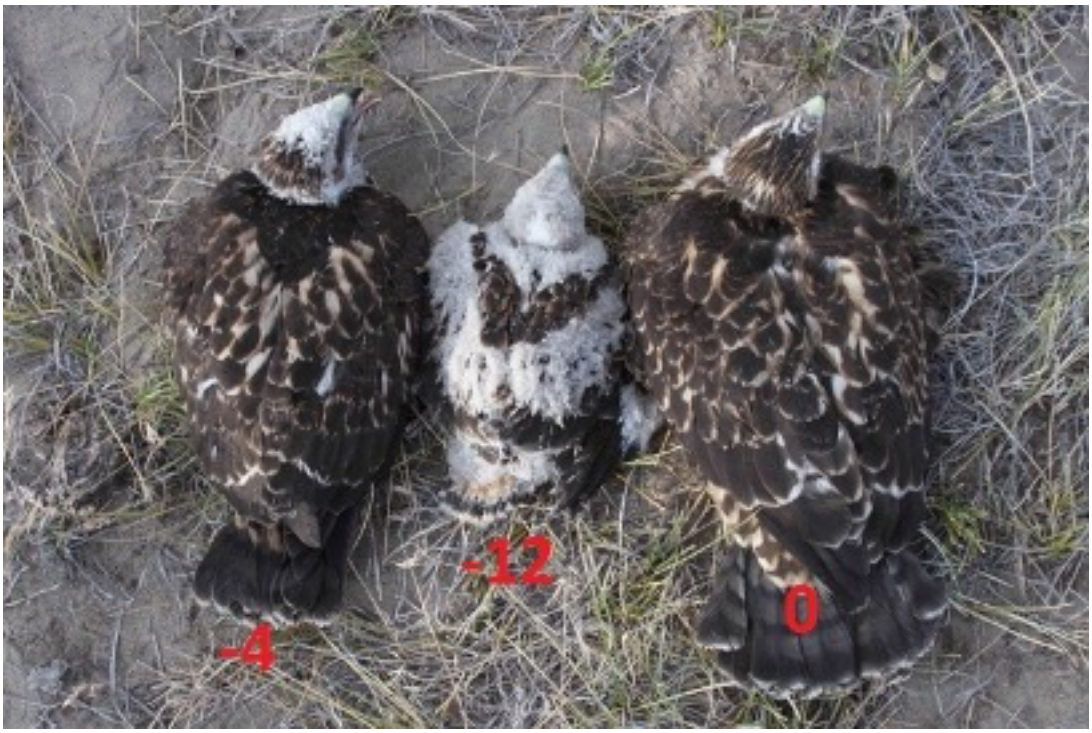

Appendix B

Graphics illustrating the lack of discriminator power for determining sex in nestling SWHA based on soft structures (i.e., feather measurements). Red points and trend line represent females, with blue points and trend line representing males.

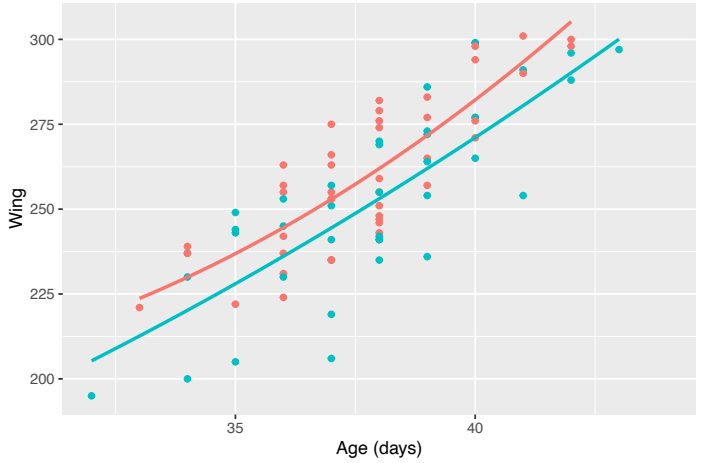

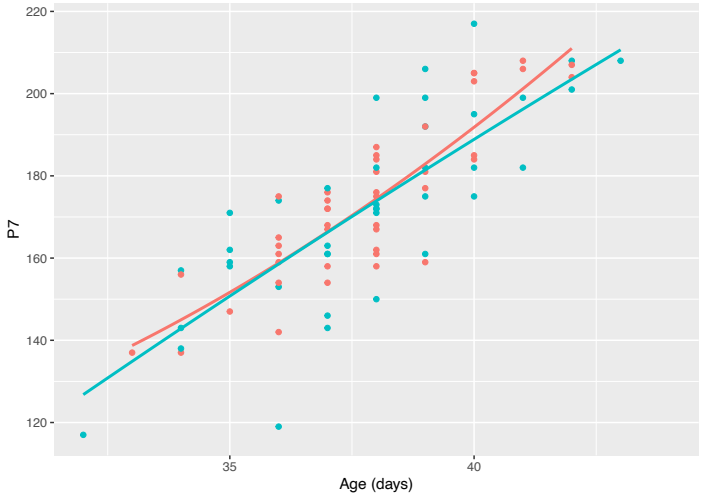

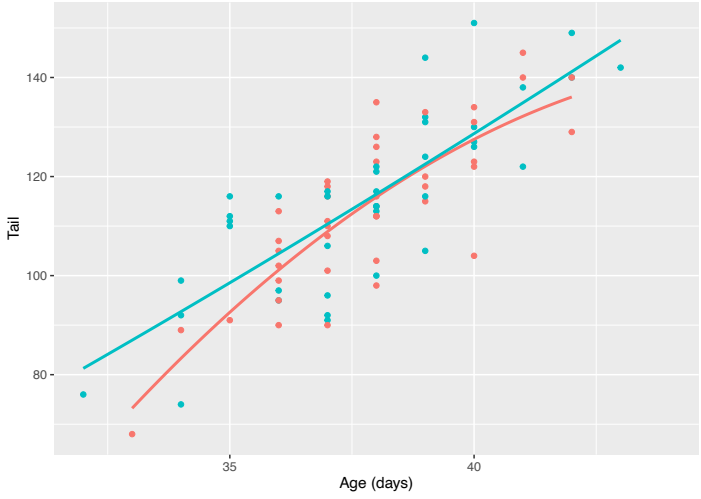

Appendix C

Growth trajectories of mass and tarsus width, separated by sex. Red points and trend line represent females, with blue dots and trend line representing males.

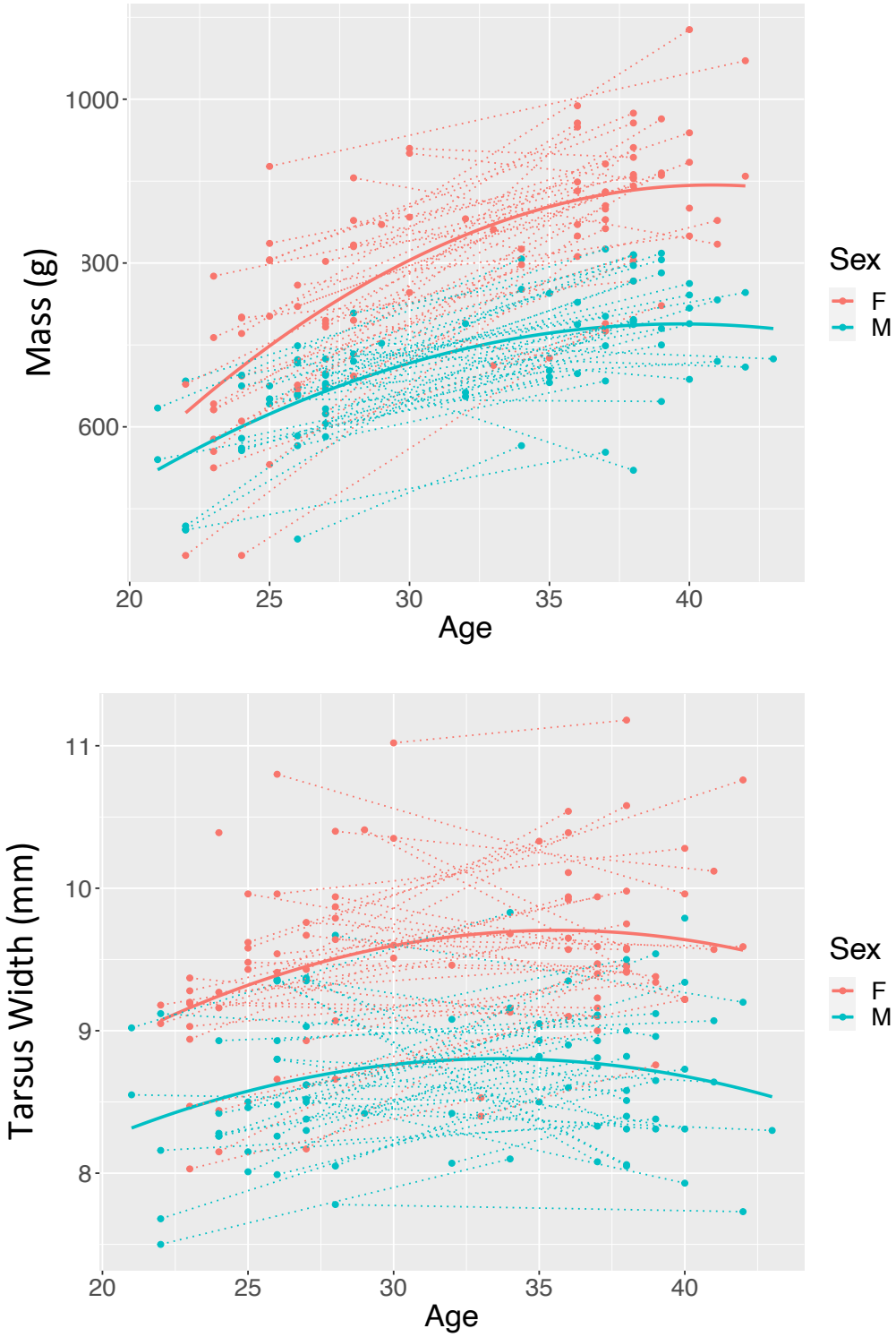

Chapter 3 Appendices

Appendix A

Sex-specific survival probabilities with 95% Bayesian credible intervals of adult Swainson's hawks. Males are triangles and females' circles. Survival for both sexes was generally high and similar to previous work on this population and other studies of SWHA.

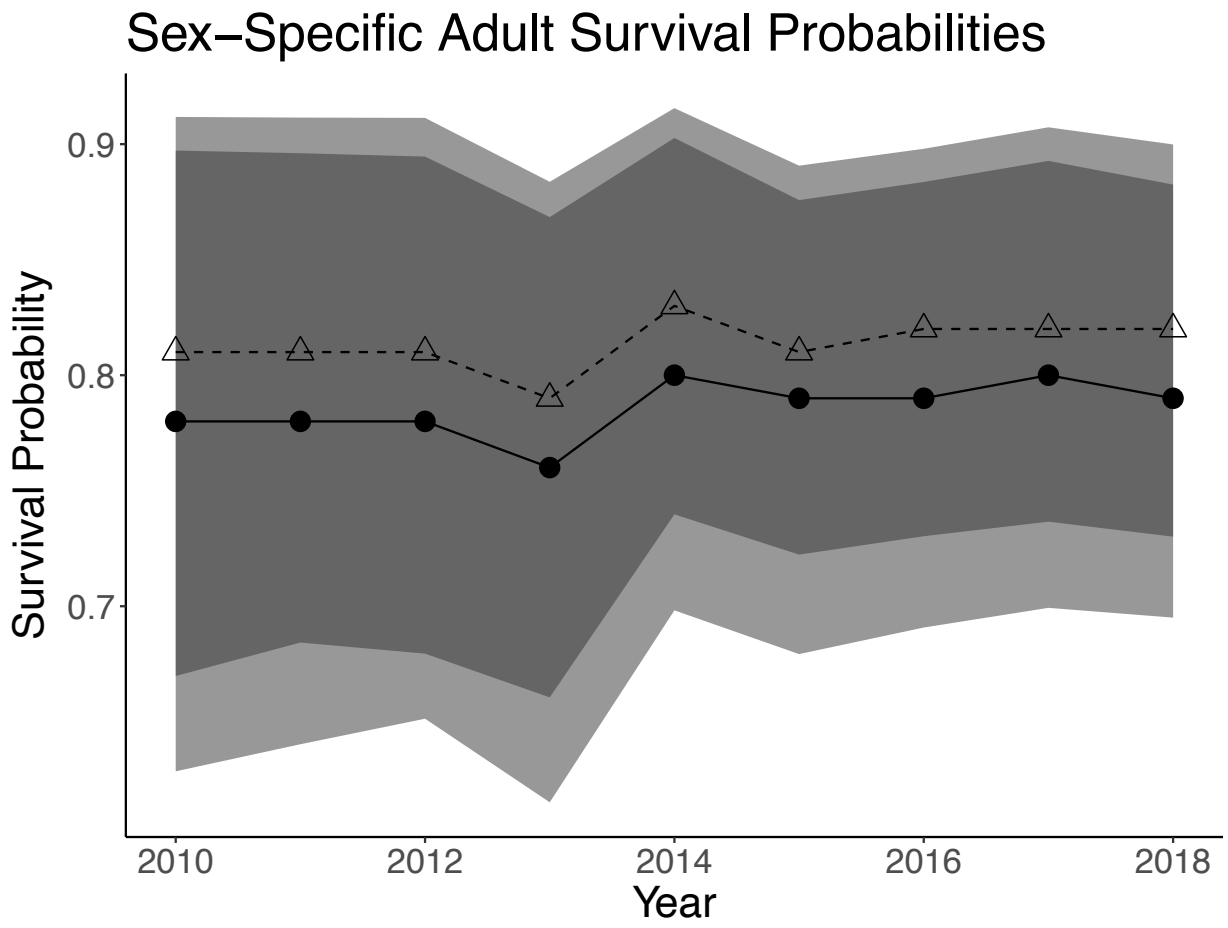

Appendix B

Annual detection probabilities with 95% Bayesian credible intervals (2011-2018). As the initial year of this model was 2009, the earliest a female could recruit and thus inform detection probabilities was 2011.The earliest a male could recruit in this analysis was 2012.

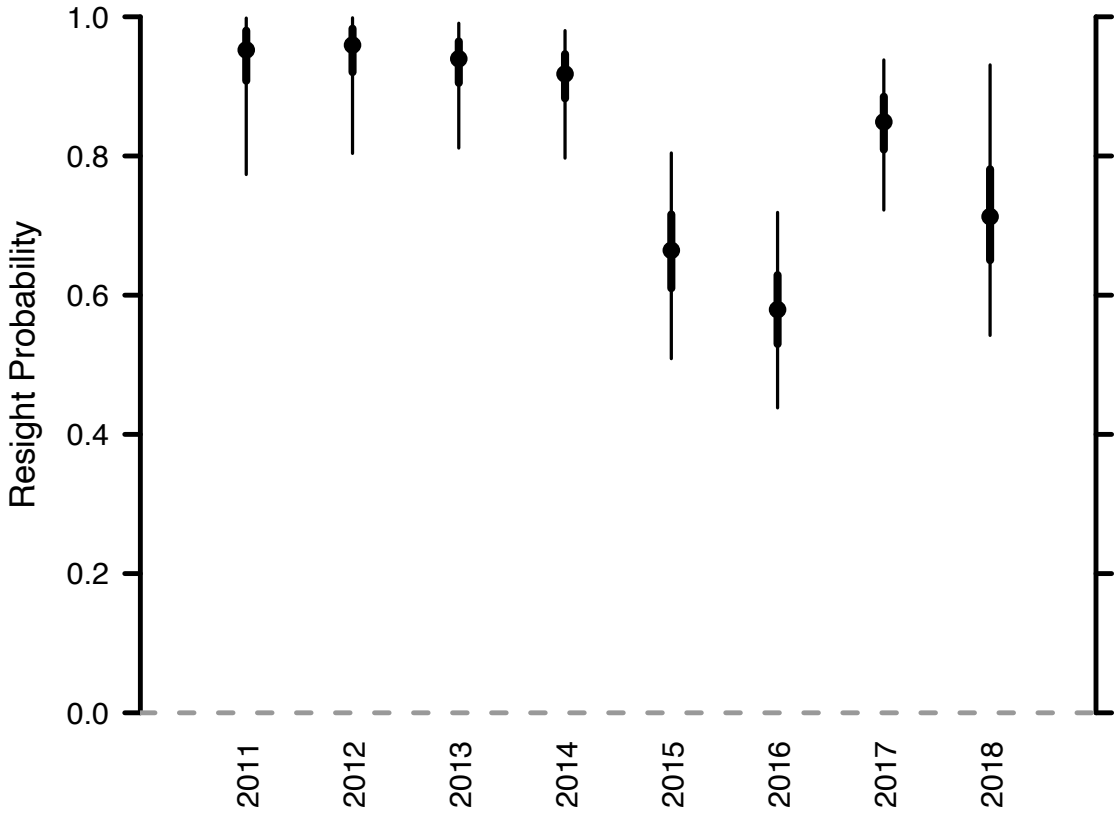

Appendix C

Table A. Result summaries for single variable models of different habitat types considered. A "Prop. Type" refers to the habitat composition of a territory. A "Proximity" model is the distance from nest tree to nearest field type. WAIC results illustrate a lack of model separation for habitat variables.

Model	ΔW_{aic}	W_{aic}	W_{aic} (SE)	K n.eff	K n.eff (SE)	ELPD	ELPD (SE)
Prop. Grassland	0	418.4	38.0	77.5	5.4	-209.2	19.0
Prop. Alfalfa	0.8	419.2	38.1	77.6	5.4	-209.6	19.0
Prop. Row Crop	1	419.4	38.2	77.4	5.5	-209.7	19.1
Prop. Dryland Hay	1.1	419.5	38.2	77.5	5.5	-209.7	19.1
Proximity to Row Crop	1.3	419.7	38.1	77.6	5.4	-209.8	19.1
Proximity to Alfalfa	1.5	419.9	38.2	77.6	5.5	-209.9	19.1

Chapter 4 Appendix

Table 1. Using a model selection approach with the WAIC scoring statistic, we built models that classified individuals into two age groups (prime-age vs. old). By estimating survival probabilities, conditioned on current reproductive state (year t), we found that classifying individuals < 10 years old as prime-aged, and individuals ≥ 10 as older, fit our data best. This age distinction was applied across all models.

Age (yr)	ΔWaic	Waic	K n.eff
7	6	3749	144
8	7	3750	144
9	7	3750	144
10	**0**	**3743**	143
11	3	3746	144
12	2	3745	143
13	1	3744	142